INSTITUTE OF TECHNOLOGY

AIR UNIVERSITY

UNITED STATES AIR FORCE

SCHOOL OF ENGINEERING

THESIS

WRIGHT-PATTERSON AIR FORCE BASE, OHIO

AF-WP-S-SEP 60 500

A PHASE STUDY OF A SELECTED PORTION OF THE Ti-Al-Zr TERNARY SYSTEM INCLUDING LATTICE PARAMETER DETERMINATIONS FOR THE Ti-Al γ PHASE

THESIS

Presented to the Faculty of the School of Engineering of
the Institute of Technology
Air University
in Partial Fulfillment of the
Requirements for the Degree of
Master of Science

By
Doral Randolph Sandlin
Capt. USAF
and
Henry Albaum Klung, Jr.
1st Lt. USAF

Graduate Air Weapons
August 1961

Preface

This report presents the results of two concurrent investigations of titanium-aluminum-zirconium alloys. The first investigation involved the determination of the effects of zirconium addition on the titanium-aluminum γ phase lattice parameters. The second part of the study was the determination of the phases present in the 50 atomic precent aluminum region of the Ti-Al-Zr ternary system. The lattice parameter determination and experimental procedures for the titanium rich portion of the phase study were performed by Captain Sandlin, whereas the experimental procedures of the zirconium rich portions of the phase study were performed by Lieutenant Klung. The conclusions based upon the data, however, are a joint effort.

We wish to express our thanks to Mr. J. R. Holland of Materials Central, ASD, for his advice and his aid in getting the specimens prepared and analyzed, and to Mr. H. J. Garrett of the Aeronautical Research Laboratory for his demonstration of the technique for preparing the glass tubing used in taking the Debye-Scherrer photographs. And, we are especially indebted to Captain Edward J. Myers, our thesis advisor, for the guidance, encouragement, and patience shown to us throughout the course of the investigation.

To our wives, for their forbearance, we express our deepest appreciation.

D.R.S. and H.A.K.

Contents

	Page
Preface	ii
List of Figures	v
List of Tables	vi
Abstract	vii
I. Introduction	1
II. Alloy Preparation	4
III. X-ray Procedures	10
IV. Metallography	15
V. γ Phase Precise Lattice Parameter Determinations	17
Discussion and Results	17
Accuracy	20
VI. Phase Determinations	21
VII. Conclusions and Recommendations	28
Bibliography	30
Appendix A: Chemical Analyses of Alloys	32
Appendix B: Diffractometer Patterns of Ti-Al-Zr Alloys Used in Determination of Phases	40
Appendix C: Tabulation of Diffraction Data and Calculated Values for Graphical Determination of Lattice Parameters	51
Appendix D: Graphical Solutions for the Determination of Lattice Parameters	62
Appendix E: Tabulation of 2θ Angles, Intensities and Identities of Peaks Recorded From Diffractometer Patterns of Fifteen Titanium-Rich Specimens	73
Appendix F: Photomicrographs of Ti-Al-Zr Alloys	83

Contents

		Page
Appendix G:	Debye-Scherrer Camera Techniques	100
Appendix H:	Tabulated 2θ Angles and Intensities of Lines Recorded from Debye-Scherrer Photographs for Twelve Zirconium-Rich Alloys	106

List of Figures

Figure		Page
1	Ti-Al Phase Diagram	1
2	Y Phase Crystal Structure	2
3	Nominal Compositions of Alloys	3
4	X-Ray Diffraction Equipment	10
5	Diffractometer Calibration Correction	12
6	Comparison of the Variation of c/a Ratio with Zirconium for Ti-50Al as Obtained by Davies and by Sandlin	19
7	Zr-Al Phase Diagram	24
8	Phases Present in Selected Ti-Al-Zr Alloys	28
9-11	Diffractometer Patterns	42-50
12-21	Graphical Solutions for Determination of Lattice Parameters, Specimens OB through 20C	63-72
22-51	Photomicrographs of Ti-Al-Zr Alloys	84-98
52	Debye-Scherrer Camera	100
53	Breaking Glass Tubing	102
54	Example of Debye-Scherrer Photographs	104

List of Tables

Table		Page
I	Impurities Found in Alloying Elements . . .	5
II	Homogenizing Heat Treatment of Alloys . . .	9
III	Stress-relief Treatment of Powders	11
IV	Etching Solutions	15
V	γ Phase Lattice Parameters	18
VI	Comparison of Nominal and Actual Compositions of Alloys	33
VII-XII	Results of Chemical Analyses for all Specimens	35-39
XIII-XXII	Tabulation of Diffraction Data and Calculated Values for Graphical Determination of Lattice Parameters	52-61
XXIII-XXXI	Tabulation of 2θ Angles, Intensities and Identities of Peaks Recorded From Diffractometer Patterns of Fifteen Titanium-Rich Specimens	74-82
XXXII-XLI	Tabulated 2θ Angles and Intensities of Lines Recorded From Debye-Scherrer Photographs Twelve Zirconium-Rich Alloys	108-119

Abstract

The γ phase of the Ti-Al binary system is of interest because it exists as a single phase up to its melting temperature (1460°C) and has been shown by the Armour Research Foundation to have good strength to very high temperatures. However, the brittleness of the γ phase, which is believed to be caused by its ordered face-centered tetragonal crystal structure, has discouraged its development as an elevated temperature material. It is believed that if the c/a ratio of the crystal structure could be lowered and the ordering destroyed, the brittleness would be reduced. Previous investigators have reported a lowering of the c/a ratio to 1.006 at 15% zirconium and predicted a c/a ratio of unity at 20% zirconium in the γ phase.

This investigation was conducted to determine if the c/a ratio of unity could be obtained. Data obtained are compared with data from F.C. Davies' report in which the c/a ratio of unity was predicted. The conclusions that are drawn from this comparison are that the c/a ratio of unity can not be obtained as predicted, and that phases other than the γ phase are present in alloys at which his prediction was made.

Coincident with the lattice parameter determinations, a study was made of the presence of phases in the region of the Ti-Al-Zr ternary system between 45 and 55 atomic percent aluminum. Two, and possibly three, new phases are observed, but their identification was not undertaken. The results of the phase investigation are available within the report.

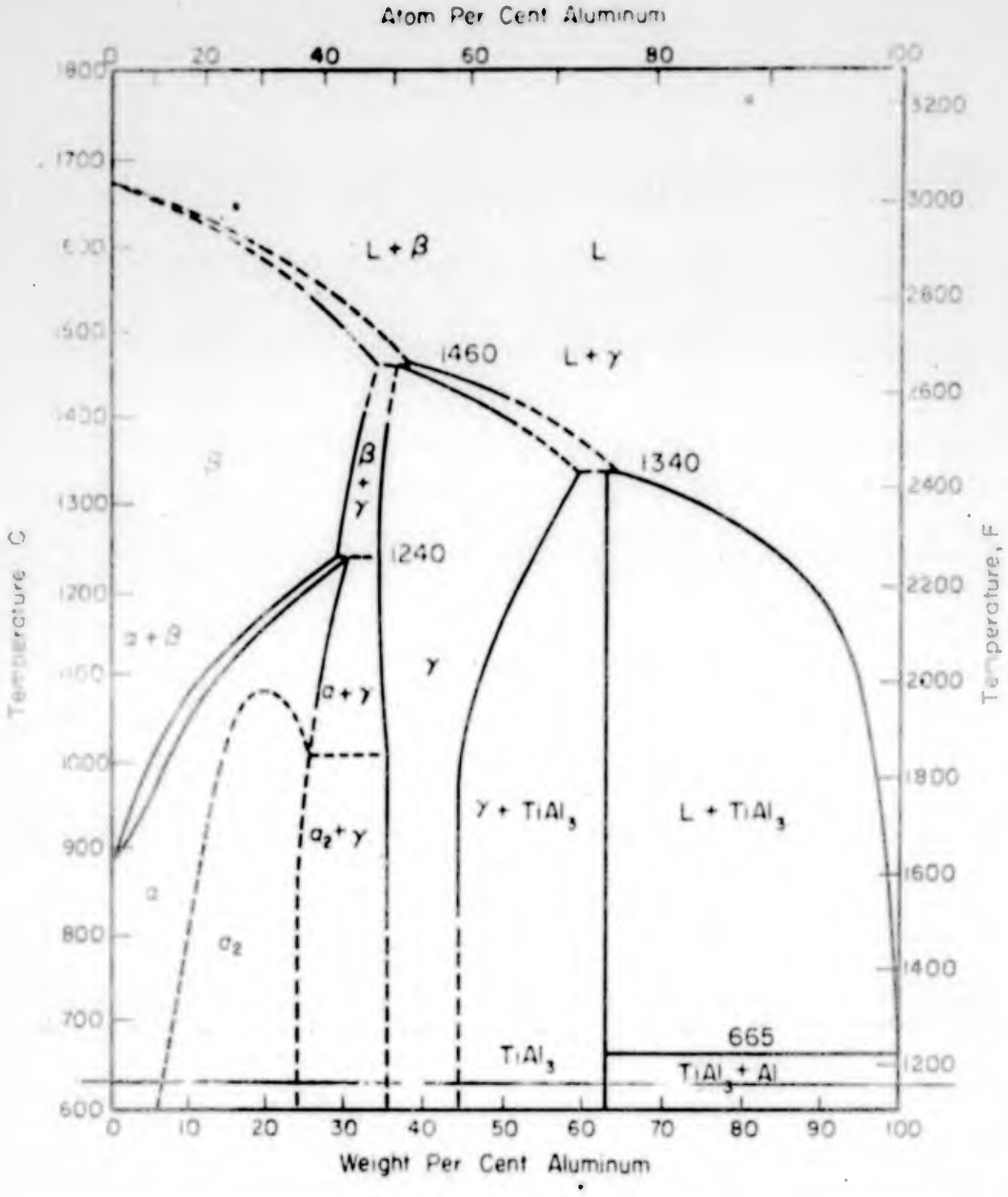

NOTE: Corrections to the Ti-Al Phase Diagram contained in Ref 4:Fig 4 affecting the α and α_2 phase regions have not been indicated on this figure. (Ref 7:12)

Fig. 1

Tentative Ti-Al Phase Diagram

A PHASE STUDY OF A SELECTED PORTION OF THE Ti-Al-Zr TERNARY SYSTEM INCLUDING LATTICE PARAMETER DETERMINATIONS FOR THE Ti-Al γ PHASE

1. Introduction

The γ phase of aluminum titanium base alloys is of interest due to its existence as a single phase up to its melting temperature (Fig. 1). The crystal structure of this phase is face-centered tetragonal (c/a ratio equal to 1.020) with (001) planes of aluminum atoms alternating with like planes of titanium atoms (Fig. 2). This ordering has been shown to persist throughout the temperature range of the γ phase (Ref 5).

The lack of an allotropic phase transformation is an asset in alloys used in structural applications; however, the γ phase also exhibits a lack of ductility at and above room temperatures. This brittleness is attributed to the face-centered tetragonal crystal structure. If the c/a ratio could be reduced to unity and the atomic arrangement could be disordered, the ductility of the γ phase would probably be improved. Kessler and McAndrew and Franklin Case Davies have investigated the possibility of lowering the c/a ratio. With a composition of 50% aluminum, 40% titanium and 10% zirconium, Kessler and McAndrew were able to lower the c/a ratio to 1.012 (Ref 5). (All compositions in this report will be expressed as atomic percentages unless

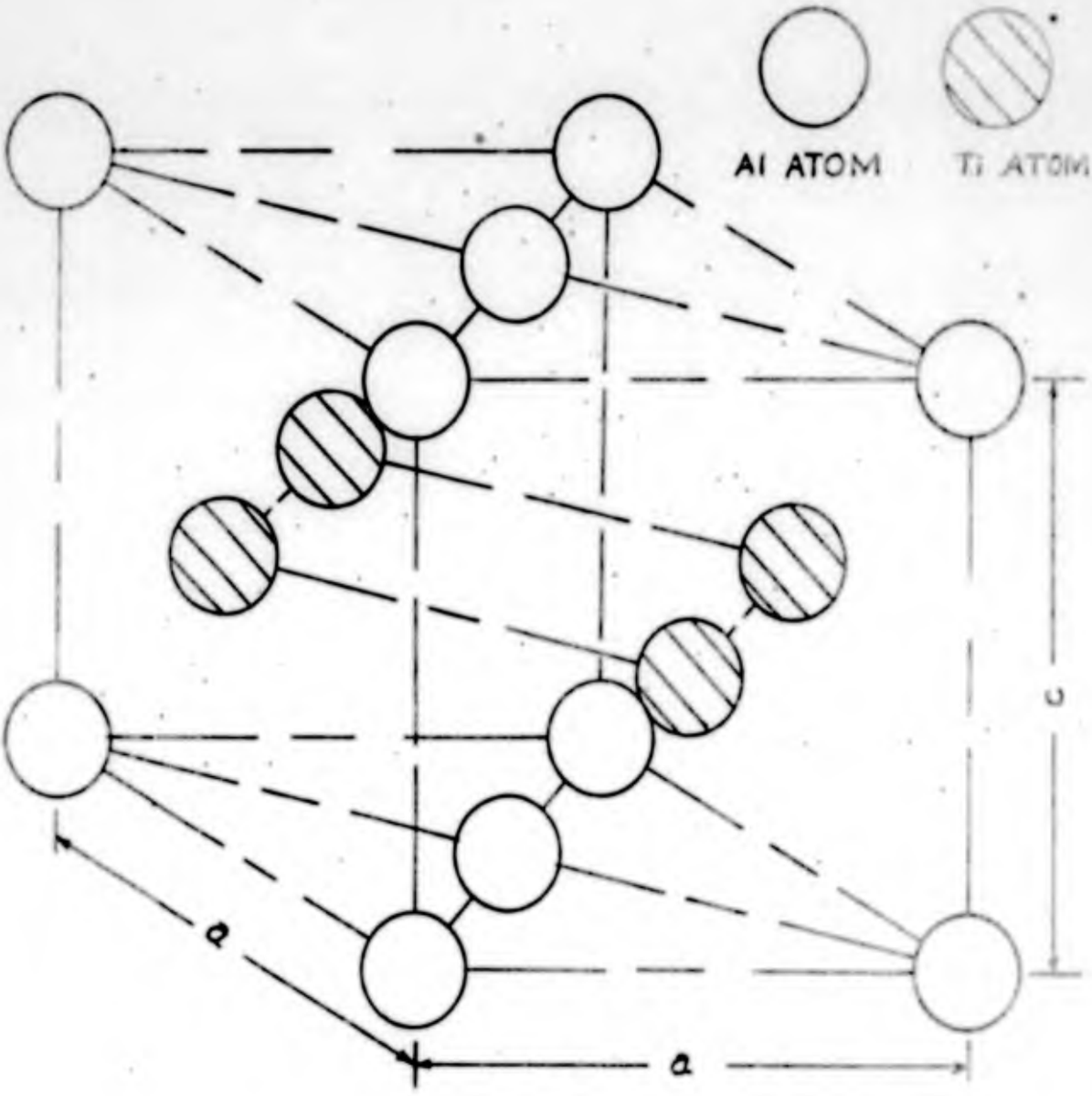

Fig. 2
Diagramatic Representation of the Crystal Structure of TiAl Showing the Paremeters c and a.

otherwise stated.) Davies stated that he was able to further reduce the c/a ratio to 1.006 with a composition of 50% aluminum 35% titanium and 15% zirconium (Ref 2:26). By extrapolation of his data, Davies predicted a c/a ratio of unity with a composition of 50% aluminum, 30% titanium, and 20% zirconium (Ref 2:34). Davies did not determine the number of phases present in his alloy samples.

The purposes of this investigation were:

1) to determine if the c/a ratio of the face-centered tetragonal crystal structure of the γ phase of Ti-Al base alloys could be reduced to unity as predicted by Davies;

2) to determine the number and, if possible the identity of phases present in twenty eight specimens from a selected region of the Al-Ti-Zr system (Fig. 3).

This particular range of the aluminum, titanium, and zirconium system was selected: 1) to include the compositions investigated by Kessler and McAndrew and by Davies, 2) to include the composition at which Davies predicted a c/a ratio of unity, and 3) to permit determination of the extent of the γ phase in the ternary system. After preparation of the specimens selected, x-ray and metallographic data were taken. The conclusions of this investigation are based primarily on the x-ray data. The metallographic data were used only as a secondary source of data.

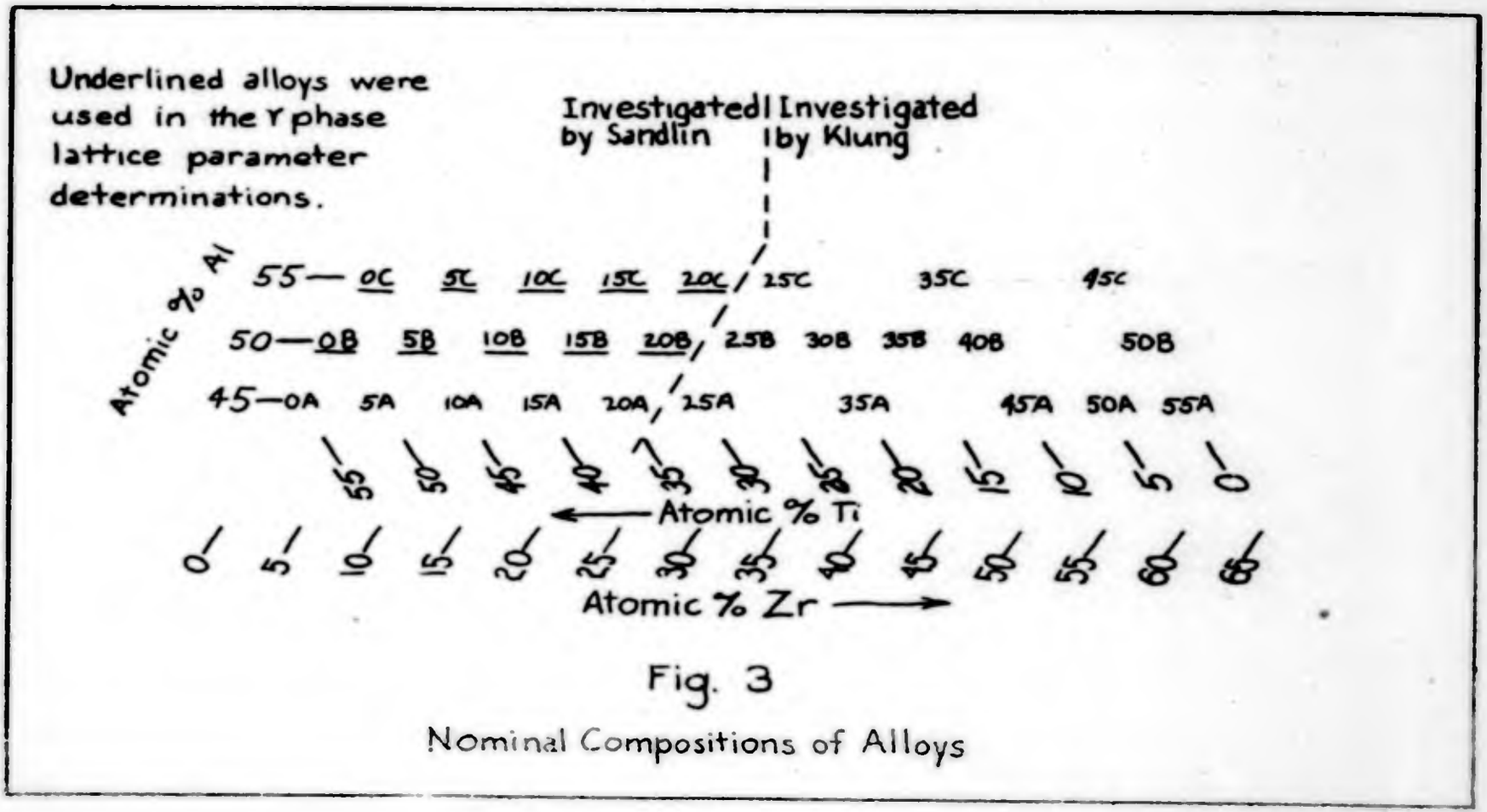

Fig. 3

Nominal Compositions of Alloys

This report will be divided into six major parts: 1) preparation of alloys, 2) x-ray procedures, 3) metallography, 4) determination of c/a ratios of crystal structure within the γ phase, 5) examination of phases, 6) conclusions and recommendations.

II. Alloy Preparation

At this point, it would be well to discuss the system used in numbering the specimens. For convenience, a system was chosen such that specimen numbers yielded the nominal compositions. Each specimen designation consisted partly of either one or two letters. The first letter denotes the aluminum content: A being 45% aluminum, B is 50%, and C- 55%. A second letter of A indicates an as-cast specimen, and an E is used for one specimen to indicate a special heat treatment. The number preceding the letters indicates the percentage zirconium content. For example, 45BA indicates an as-cast specimen of 45% zirconium and 50% aluminum; the remainder of the alloy is titanium.

From the compositions shown in Fig. 3, the weights of the pure materials necessary to prepare an alloy button weighing approximately 62 grams were calculated. (The weight of 62 grams is the amount of alloying material necessary to adequately fill the crucibles of the Zak furnace.) The pig form aluminum was obtained from the Aluminum Company of America, the sponge titanium from the U. S. Bureau of Mines, and the chunklets of zirconium from the Reactive Metals Corporation. Table I lists the impurities found in these metals by a spectrographic analysis performed by the Bowser-Morner Testing Laboratories, Inc. of Dayton, Ohio.

Table I

Impurities Found in Alloying Metals

NOTE: Figures are in weight percent

	Al	Ti	Zr
Silicon	.01	<.01	<.01
Manganese	<.003	.02	<.01
Copper	.002	<.01	<.01
Iron	.02	<.01	<.01
Magnesium	<.002	<.01	<.01
Titanium	<.005	-	-
Nickel	<.01	<.01	<.01
Aluminum	-	<.01	<.01
Calcium	-	<.001	-
Hafnium	-	-	.21

Melting of alloys was accomplished in a Zak Button Furnace at the Research Institute of the University of Dayton. The Zak Button Furnace is an arc furnace with a cylindrical wall and a copper hearth on its floor. Both the hearth and the wall are water cooled. The furnace is powered by a 30-volt D.C. generator, the amperage of which is variable up to 600 amps. Melting is accomplished with a water-cooled, tungsten tipped, non-consumable electrode which is fitted through a ball joint at the top of the furnace. The ball joint fitting permits movement of the electrode by the operator.

The measured constituents of each alloy were placed in four of the five water-cooled, copper crucibles in the hearth of the furnace. Titanium sponge with a Brinell Hardness Number (BHN) of 75 was placed in the fifth crucible. The furnace was sealed and evacuated to a pressure of one micron and then flushed with a helium-argon mixture up to a pressure of one atmosphere. The chamber was evacuated and flushed several times to insure the removal of all reactive gases. The final pressure of the helium-argon atmosphere in the chamber was 380 mm Hg.

After the flushing operation, an arc was struck between the electrode and a button of tungsten which sits on the hearth (30 volts and 600 amps were used in the melting operation). The electrode was then held three quarters of an inch above the surface of the crucibles, and the alloys were melted when the electrode was slowly moved over their surface. The pure titanium was melted first in order to purify the atmosphere within the furnace. Each of the remaining alloys was melted a total of four times, twice from each side, in order to obtain homogeneity. The furnace was then shut off, the melted specimens removed, and an unmelted set of specimens placed in the crucibles. During shut-down the hardness of the pure titanium button was checked

and in all cases found not to exceed 70 BHN. Since hardness of titanium is a function of the impurities within, this check indicated that the helium-argon atmosphere in which the alloys were melted was relatively free of impurities. Therefore, the assumption was made that the alloys were not contaminated during the melting process.

Spectrographic analyses were performed on portions of each specimen because a) the pressure between the arc and the melt forced some material from the crucibles and b) the zirconium rich alloys were so brittle that they shattered when the arc was quickly removed from the melt and small pieces of the shattered buttons flew from the crucibles. The results of the spectrographic analyses, contained in Appendix A, reveal that most of the alloys have a higher percentage of aluminum and lower percentages of titanium and zirconium in the actual compositions than in the nominal compositions. The form of the unmelted elements accounts for this fact. The initial pressure between the arc and unmelted materials forced more of the smaller, lighter pieces of titanium and zirconium from the crucibles than the larger, heavier aluminum pieces.

After melting, the buttons were broken into small pieces by use of either a hammer or a hydraulic press. The specimens with greater than 20% zirconium content were relatively easy to break and were broken with a hammer. (Although the 55A(46.2Al-53.8Zr)

button was also broken with a hammer, it exhibited a marked increase in toughness over the other zirconium-rich alloys.) The Ti-Al binaries and these buttons containing a small percentage of zirconium were very difficult to break and a hydraulic press was used to fracture these alloys. Small pieces of each specimen were encapsulated in Vycor under a pressure less than 0.1 micron to prevent the specimens from reacting with the atmosphere at elevated temperatures. The encapsulated specimens were then homogenized in an electric furnace. Table II indicates for each specimen the time, temperature, and method of cooling used during homogenizing heat treatment. Some of the specimens had an oxide coating which had formed during the heat treatments. This coating was removed by pickling in the solution indicated in Table II.

Table II

Homogenizing Heat Treatment of Alloys

NOTE: 1) The alloys were immersed in a solution of 5% HF, 50% HNO_3 and 45% H_2O to remove a thin oxide coating which formed during annealing.

2) All specimens were annealed at 2000° F.

3) Specimen 50BH was a portion of specimen 50B which was given additional heat treatment at 2192° F for six hours.

Specimen	Annealing Time	Cooling
0A	39 hrs	Still air
5A	39 hrs	Still air
10A	39 hrs	Still air
15A	39 hrs	Still air
20A	39 hrs	Still air
25A	48 hrs	Water quenched
35A	48 hrs	Water quenched
45A	48 hrs	Water quenched
50A	48 hrs	Water quenched
55A	48 hrs	Water quenched
0B	39 hrs	Still air
5B	39 hrs	Still air
10B	40½ hrs	Still air
15B	40½ hrs	Still air
20B	40½ hrs	Still air
25B	48 hrs	Water quenched
30B	48 hrs	Water quenched
35B	48 hrs	Water quenched
40B	48 hrs	Water quenched
50B	48 hrs	Water quenched
0C	39 hrs	Still air
5C	39 hrs	Still air
10C	39 hrs	Still air
20C	39 hrs	Still air
25C	48 hrs	Water quenched
35C	48 hrs	Water quenched
45C	48 hrs	Water quenched

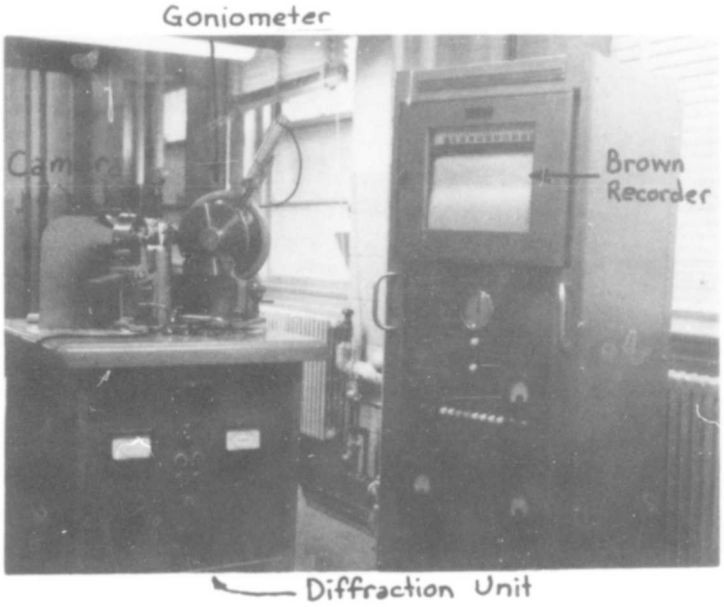

Fig. 4

X-Ray Diffraction Equipment

III. X-ray Procedures

Preparation of Powders

In the preparation for x-ray analyses, small portions of each of the annealed specimens were ground to powder with a mortar and pestle. The powder was made fine enough to pass through a 325 mesh screen in order to obtain random grain orientations. After grinding, some of the powdered specimens were wrapped in molybdenum or tantalum foil, encapsulated in Vycor under 0.1 micron pressure, and given a heat treatment to relieve stresses induced while grinding. (No difference was detected in the x-ray patterns of the powders wrapped in the two different foils.) Some of the specimens were reduced to powder so easily that it was not necessary to stress-relieve by heat treating. (Generally, these specimens were of a high zirconium content.) Table III indicates those specimens that were stress-relieved and the time and temperature of the stress-relief treatment given each specimen.

X-ray Diffractometer Procedures

A North American Philips X-ray Diffractometer (Fig. 4) composed of 1) a water-cooled x-ray diffraction unit, 2) a wide-range goniometer, and 3) a Brown strip chart recorder, was used to obtain diffraction patterns of all samples. The

Table III

Stress Relief Treatment of Powders

NOTE: 1) All powders were wrapped in molybdenum or tantalum foil and encased in V gear under a pressure of 0.1 micron.

2) Differences in annealing times had no significant effect on diffraction peak intensities.

Specimen	Temperature (°F)	Time at Temperature
0A	2200	30 min
5A	2000	45 min
10A	2000	30 min
15A	2000	30 min
20A	2000	30 min
25A	2000	30 min
35A	2000	30 min
40A	2000	30 min
50A	2000	30 min
55AA	4572	1 hour
0B	1950	30 min
5B	2000	30 min
10B	2000	30 min
15B	2000	30 min
20B	2000	15 min
30B	2000	40 min
35B	2000	40 min
50B	2000	40 min
0C	2000	30 min
5C	2000	30 min
10C	2000	30 min
15C	2000	30 min
20C	2000	30 min
35C	2000	40 min

Table III

Stress Relief Treatment of Powders

NOTE: 1) All powders were wrapped in molybdenum or tantalum foil and sealed in Vycor under a pressure of 1.1 micron.

2) Differences in annealing times had no significant effect on diffraction peak intensities.

Specimen	Temperature (°F)	Time at Temperature
0..	2000	30 min
5..	2000	45 min
10..	2000	60 min
15..	2000	90 min
20..	2000	120 min
25..	2000	10 min
30..	2000	20 min
40..	2000	40 min
50..	2000	60 min
75..	2000	1 hour
80	1900	30 min
85	2000	30 min
100	2000	30 min
1 5	2000	30 min
200	2000	15 min
300	2000	40 min
350	2000	10 min
500	2000	40 min
00	2000	30 min
50	2000	30 min
100	2000	30 min
150	2000	30 min
200	2000	30 min
350	2000	40 min

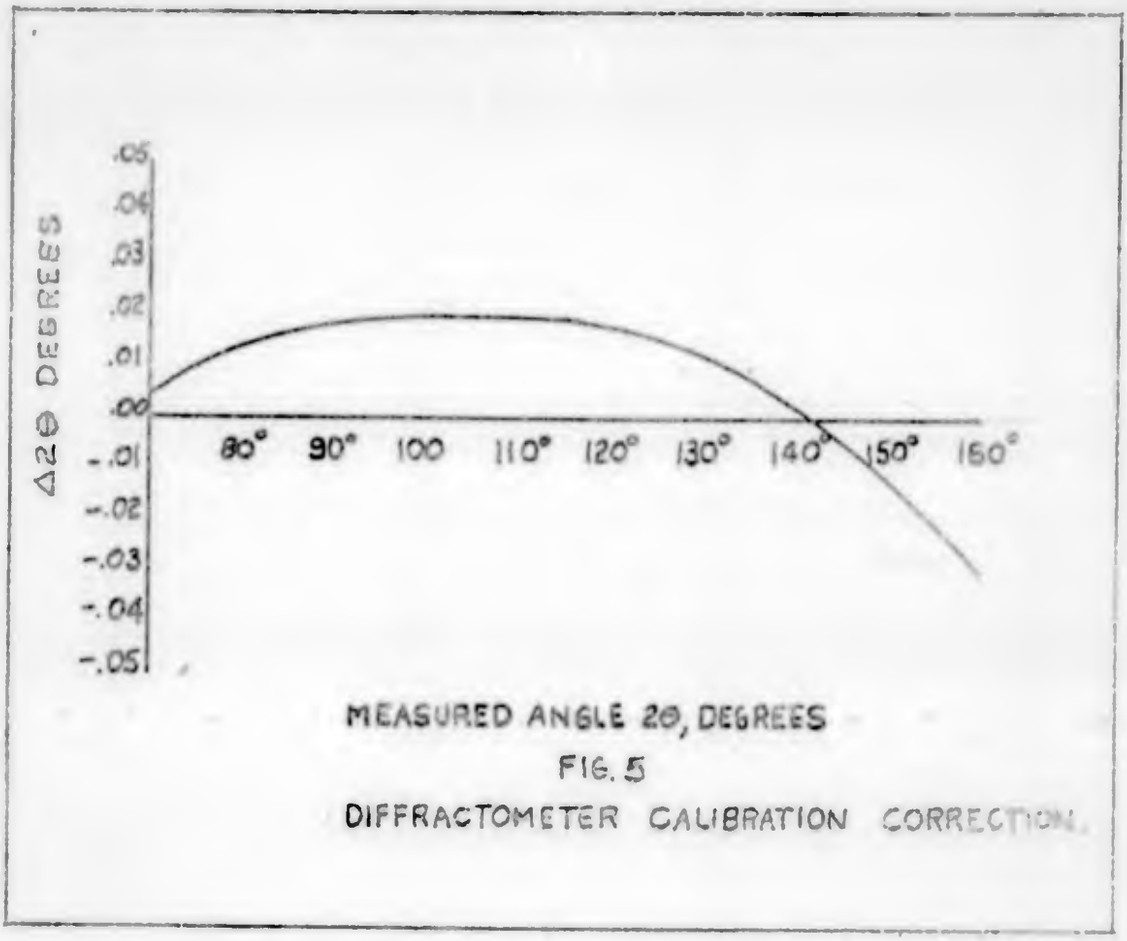

FIG. 5

DIFFRACTOMETER CALIBRATION CORRECTION.

x-rays from a copper target tube in the diffractometer unit are focused on the powdered specimen located at the center of the wide-range goniometer. The diffracted x-rays are detected by a Geiger tube which rotates at constant speed. Connected electronically to the Geiger tube is the Brown recorder which records a graphical plot of intensity of reflected beam versus 2θ (two times the angle of reflection).

Before any data were taken, the goniometer was aligned with the diffraction unit in accordance with the instructions furnished by the manufacturer. After alignment, the unit was calibrated by scanning the peaks of a silicon standard specimen, observing the 2θ angles at which these peaks were obtained, and then comparing the published values of 2θ with the observed values. The results of the calibration are included in Fig. 5. (Values below 70 degrees 2θ are not indicated in this figure because these angles were not used in the lattice parameter determinations.) Periodically during the investigation the alignment was rechecked by rescanning the peaks of the silicon standard specimen.

Each powdered specimen was packed in an aluminum holder and placed in the proper position on the goniometer. Fifteen titanium rich specimens were scanned at the rate of one degree per minute through a range of 2θ from 10 to 160 degrees. Tabulated

in Appendix E are the corrected values of 2θ, the relative intensities and, in most cases, the identity of peaks recorded for these fifteen specimens. Subsequently, all the specimens were scanned at the rate of two degrees per minute through the range of 2θ from 10 to 160 degrees. For the phase determination portion of this study only a range of 2θ between 18 and 48 degrees was used because: 1) this range included the most intense peaks of all phases present; 2) a large number of indistinct peaks and zirconium fluorescence, which caused high background intensities, made analysing of data above 90 degrees 2θ particularly difficult; 3) in most cases only one peak was reflected in the range of 2θ between 0 and 18 degrees; 4) only a few weak peaks were reflected in the range of 2θ between 48 and 90 degrees; and 5) in some cases cards of the X-ray Powder Data File (ASTM cards) used for identifying and indexing peaks did not list those peaks above 45 degrees. Appendix B includes pictures of diffractometer patterns of all specimens in the range of 2θ between 18 and 48 degrees.

In order to obtain more accurate measurements of 2θ angles to be used in the determination of precise lattice parameters of the crystal structure of alloys in the γ phase region, selected peaks of ten specimens (indicated in Fig. 3) were scanned at a goniometer speed of one half degree per minute. This rate coupled with the recorder speed of one half inch per minute permitted accurate readings of 2θ angles to 0.05 degrees with estimations to

0.01 degrees. Only those peaks that were to be used in calculating the lattice parameters were scanned. In the selection of peaks to be used, an attempt was made to use a large number of peaks in the range of 2θ above 90 degrees since both random and systematic errors approach zero as 2θ approaches 180 degrees (Ref 6:441). Peaks and data used for lattice parameter determination are available in Appendix C.

The Debye-Scherrer cameras were used to take powder photographs of the x-ray patterns of thirteen zirconium rich specimens. Appendix G describes techniques developed and used while using these cameras. The 2θ values corrected for film shrinkage and relative intensities of line from the films are tabulated in Appendix H. Data obtained with the use of the Debye-Scherrer cameras were not used in this report because: 1) the large number of lines present on the film made these data difficult to analyze and 2) goniometer patterns of titanium-rich alloys were difficult to correlate with camera patterns of the zirconium-rich alloys.

IV. Metallography

For ease in handling, portions of each of the annealed alloys were mounted in bakelite. A flat surface was ground on each specimen by use of a belt grinder. These surfaces were then polished with successively finer grits of paper down to 4/0 grit. Successively finer grades of polishing alumina were applied by electrically driven turntables for further polishing; the final polishing was done on the vibrating table of an automatic polisher, in which 1552 AB Gamma Polishing Alumina # 3 was used as the abrasive.

After polishing, the specimens were swab etched with the solutions indicated in Table IV. The etchant was applied for about two seconds, rinsed off with water, then alcohol, which was evaporated by use of a cold air blower.

Table IV

Etchants Used on Al-Ti-Zr Alloys

Specimens	Etchant Composition (Percent by Volume)
0A through 20A 0B through 15B 0C through 20C	6% HNO_3, 3% HF, 91% H_2O (Kroll's Etch)
25A through 55A 20B through 50B 25C through 45C	20% HNO_3, 20% HF, 60% glycerin

To augment the x-ray data, photomicrographs were taken of each specimen at varying magnifications. Some pictures were taken with photographic plates and the remainder with Polaroid film. These photomicrographs are in Appendix F.

V. γ Phase Precise Lattice Parameters Determination

Discussion and Results

The specimens selected for precise lattice parameter determination include: 1) specimens 0B through 20B (these specimens were chosen to include the range of Ti-Al-Zr compositions investigated by Davies and the composition at which Davies predicted a c/a ratio of unity; and 2) specimens 0C through 20C (these specimens were chosen since their range also started in the single phase γ region). Diffraction patterns were taken of these specimens, as described in Chapter III. Eight peaks in the higher ranges of 2θ angles could be clearly distinguished and accurately read from the x-ray patterns of group C specimens while only seven peaks in the higher ranges of 2θ angles were usable from group B specimens.

Peaks of each specimen were scanned at the rate of one half degree per minute. All peaks were scanned in only the forward direction of 2θ, with particular care being taken that the x-ray unit and Brown recorder were started in exactly the same manner for each run. This insured that any error being induced would be constant and would go to zero when values of angles were extrapolated to 90 degrees. The values of 2θ angles for each peak were recorded, and the calibration correction described in Chapter III was added.

All peaks were indexed by converting their corrected 2θ angles to d spacings with the use of a table of d spacings furnished by the manufacturer of the x-ray equipment. These d spacings were then compared to published values of d spacings for the γ phase that are available in the ASTM card file (Ref 14). Myers and Davies' graphical method of precise lattice parameter determination (Ref 9) was used to analyze all data of this phase of the investigation.

Diffraction data for the ten selected specimens and the computed values necessary for the graphical determination of lattice parameters are given in tabular form in Appendix C. Appendix D contains the graphs that were drawn from these data. Table V lists the specimens that were analyzed and the values of c, a, and c/a ratio determined from the graphical plots.

Table V

γ Phase Lattice Parameters

	Composition (Atomic %)			Lattice Parameters (A)		c/a
Specimen No.	Al	Ti	Zr	c	a	
0B	51.3	48.7	0.0	4.079	3.997	1.021
5B	52.5	42.7	4.8	4.097	4.020	1.019
10B	52.2	38.6	9.2	4.105	4.042	1.016
15B	52.5	33.6	13.9	4.109	4.049	1.015
20B	52.5	29.1	18.4	4.105	4.042	1.016
0C	58.2	41.8	0.0	4.078	3.988	1.022
5C	57.8	37.6	4.5	4.078	3.986	1.022
10C	56.3	34.6	9.1	4.113	4.033	1.020
15C	56.9	28.9	14.1	4.113	4.040	1.018
20C	57.8	23.4	18.8	4.115	4.046	1.017

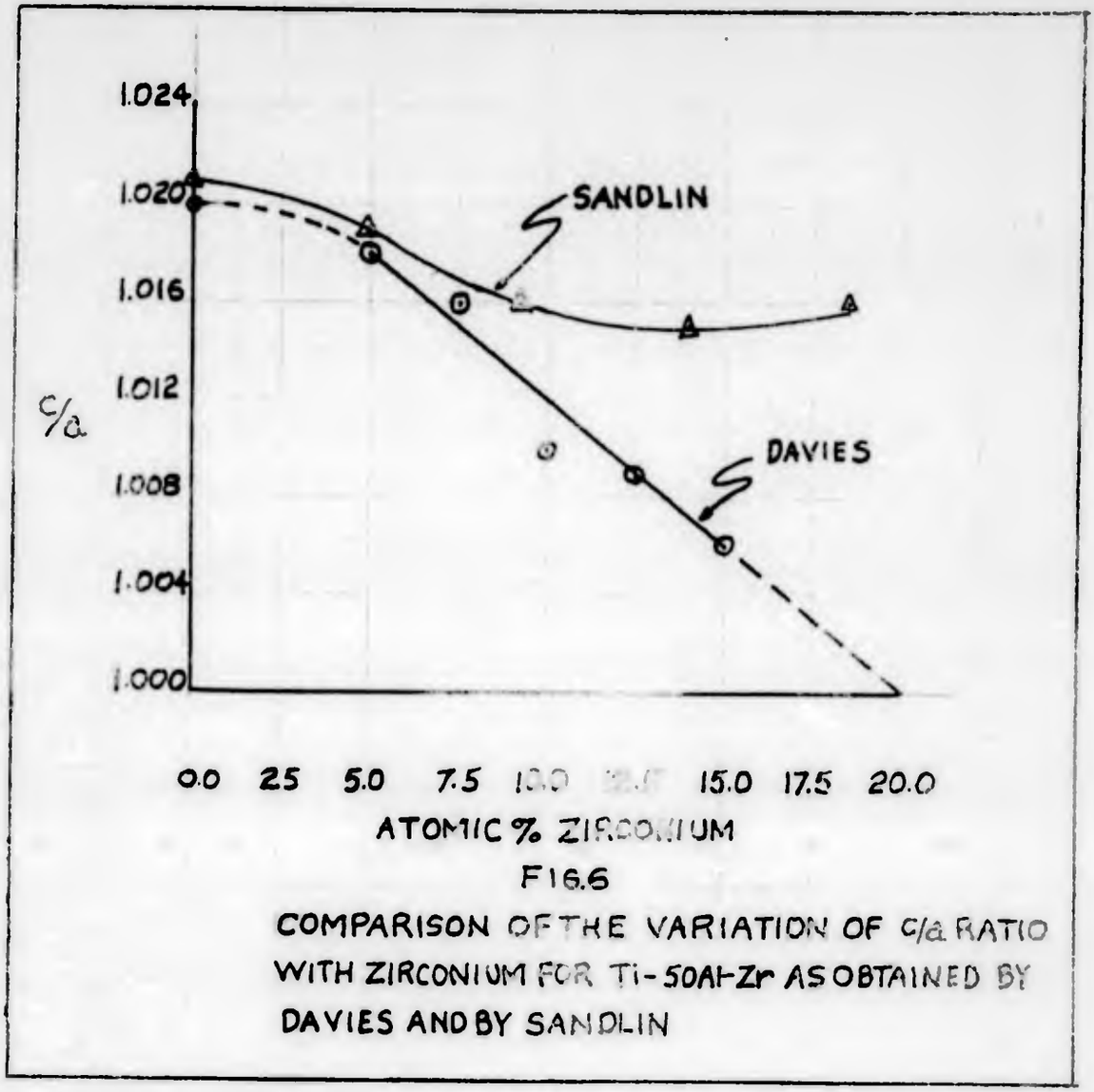

FIG.6

COMPARISON OF THE VARIATION OF c/a RATIO WITH ZIRCONIUM FOR Ti-50At-Zr AS OBTAINED BY DAVIES AND BY SANDLIN

Figure 6 compares Davies' plot of c/a versus zirconium content with a similar plot of values determined by this investigation. The variation between the nominal and actual compositions of specimens offers a possible explanation for the differences in results obtained in the range of 0% zirconium to 5% zirconium content. Duwez and Taylor show the c/a ratio in the binary γ phase increasing almost linearly with increasing percent of aluminum. (Ref 3:71) Since the actual compositions examined in this study contain more aluminum than the nominal compositions, an increase in the c/a ratio would be expected in the lower ranges of zirconium content. However, in the range of zirconium content greater than 5% the differences in results are too large to attributed to increase in aluminum content. The only explanation for the differences in this range which can be offered is the different manner with which the specimens were handled in the two investigations. Davies did not encapsulate his alloys to prevent oxidation during the homogenizing heat treatment. Consequently, a thick oxide scale, which had to be machined away, formed on the surface of his specimens. Also, for stress-relief, Davies encapsulated his powders in Pyrex tubes and annealed them for one hour at 660 degrees Centigrade. The possibility exists that the treatment given Davies' specimens was not careful enough to eliminate reaction with impurities such as hydrogen, nitrogen, and oxygen,

and that the stress-relief temperature was not high enough to sufficiently sharpen the high angle peaks. The latter premise is corroborated by the fact that Davies used only five angles for specimens with 10 and 15 percent zirconium in his lattice parameter determinations, whereas, at least seven lines were useable in the present investigation.

Evidence of the ordering of the tetragonal crystal structure of the γ phase was detected by the appearance of two weak peaks ($\gamma(201)$ and $\gamma(112)$). These peaks would not be present in the pattern of a face-centered tetragonal structure if the crystal was not ordered (Ref 6:349). Both these peaks were not present in the specimens with a zirconium content of 20% or greater. Their absence could be caused by either: 1) disordering of the crystal structure or 2) by the decrease in percent of the γ phase causing a decrease in peak intensity and therefore, a disappearance of weak peaks. The latter explanation seems most likely.

Accuracy

As stated in Chapter III, goniometer speed and chart speed permitted estimated reading of 2θ angles to 0.01 degrees. All computations were performed on a desk calculator permitting accuracy to the fifth decimal place. Five place trigonometric tables were used to convert 2θ angles to $\sin^2\theta$ values. Accuracy of lines plotted in the graphical solution was to four significant figures, and values of lattice parameters determined were rounded off to the nearest 0.001Å.

VI. Phase Determinations

The x-ray patterns included in Appendix B were used to determine the number of phases present in each specimen. The patterns of the aluminum-titanium binaries were selected as starting points in this phase of the investigation since the crystal structures of the phases in this region are available in the literature.

All of the peaks of the Ti-Al binary compositions were indexed by use of the information contained for the respective phases in the ASTM card files (Ref 14). As expected, only the peaks of the γ and $\alpha_2(Ti_3Al)$ phases were present in the pattern of specimen 0A(51.4Ti-48.6Al). All but two peaks of specimen 0B(48.7Ti-51.3Al) were identified as peaks of the γ phase. One peak at 40.10 degrees 2θ, identified as the most intense peak of α-titanium, appeared in specimen 0B and was not present in any of the succeeding 50% Al specimens. Its presence indicates a lack of equilibrium and could probably have been eliminated by longer annealing time. Another peak at 12.80 degrees 2θ appearing in specimens 0B(48.7Ti-51.3Al), 15B(33.6Ti-52.5Al-13.9Zr), and 20B(29.1Ti-52.5Al-18.4Zr) was not of the γ phase and could not be identified (nor could it be attributed to tungsten contamination of the copper target in the x-ray tube). Specimen 0C(41.8Ti-58.2Al) was found to be single phase γ.

The next step in the investigation was to compare the binary patterns with those of specimens having succeedingly greater

zirconium content. This comparison was made by juxtaposing patterns of succeeding specimens as shown in Appendix B. Thus the known peaks of the binaries could be traced into the ternary system. Figure 9 contains the diffractometer patterns of the specimens composed of 45% aluminum. The patterns of this series indicate the following:

1) a new phase $\emptyset$ is formed between 5 and 10% zirconium and extends to between 20 and 25% zirconium;

2) the α_2 phase is replaced by a new phase ϵ between 15 and 20% zirconium;

3) the ϵ phase extends to between 45 and 50% zirconium;

4) the γ phase extends to between 35 and 45% zirconium; and

5) possibly a new phase δ was detected at 25% zirconium.

The δ phase was hypothesised on the basis of the one strong peak of pattern 25A(30.2Ti-46.2Al-23.6Zr) that otherwise could not be identified, and on the basis of metallographic data (Fig. 26) which indicates that possibly three phases exist in this specimen. Peaks of pattern 35A(19.5Ti-46.1Al-34.4Zr) show that the δ phase could also possibly exist in this specimen; however, the investigators feel that it does not exist because metallographic examination (Fig. 27) indicates the presence of only two phases in this specimen.

The patterns of 50% aluminum alloys are contained in Fig. 10. These patterns indicate the following:

1) the $\emptyset$ phase is present from between 5 and 10% zirconium

to between 25 and 30% zirconium;

2) the ϵ phase starts between 10 and 15% zirconium and extends to between 40 and 50% zirconium; and

3) the γ phase extends to between 30 and 35% zirconium.

An anomaly exists in the patterns and metallography of specimen 30B(19.6Ti-51.3Al-29.1Zr). Weak unknown peaks exist in this pattern that can be either: a) weaker peaks of the ϵ phase that appear because a larger percentage of this phase is present in this specimen than in the preceding specimen, or b) peaks of a new phase. The former hypothesis is supported by the increased intensities of the ϵ peaks over the same peaks in the other specimens of the B series (50% Al) the latter hypothesis is supported by metallographic data (Fig. 38) which indicates that three phases exist in this specimen.

In pattern 35B(13.8Ti-51.6Al-34.6Zr) the ϵ phase exists along with either one, or possibly two other phases. If one other phase exists, it is different from all other phases detected. If two other phases exist, one phase is possibly Zr_2Al_3 (two peaks of this phase could be traced from specimens 40B to 35B), and the other phase is an unknown phase. Metallographic data (Fig. 39) does not clearly indicate whether two or three phases exist in this specimen.

The patterns of the 55% aluminum specimens contained in Fig. 11 indicate the following:

1) the γ phase extends to between 25 and 35% zirconium;

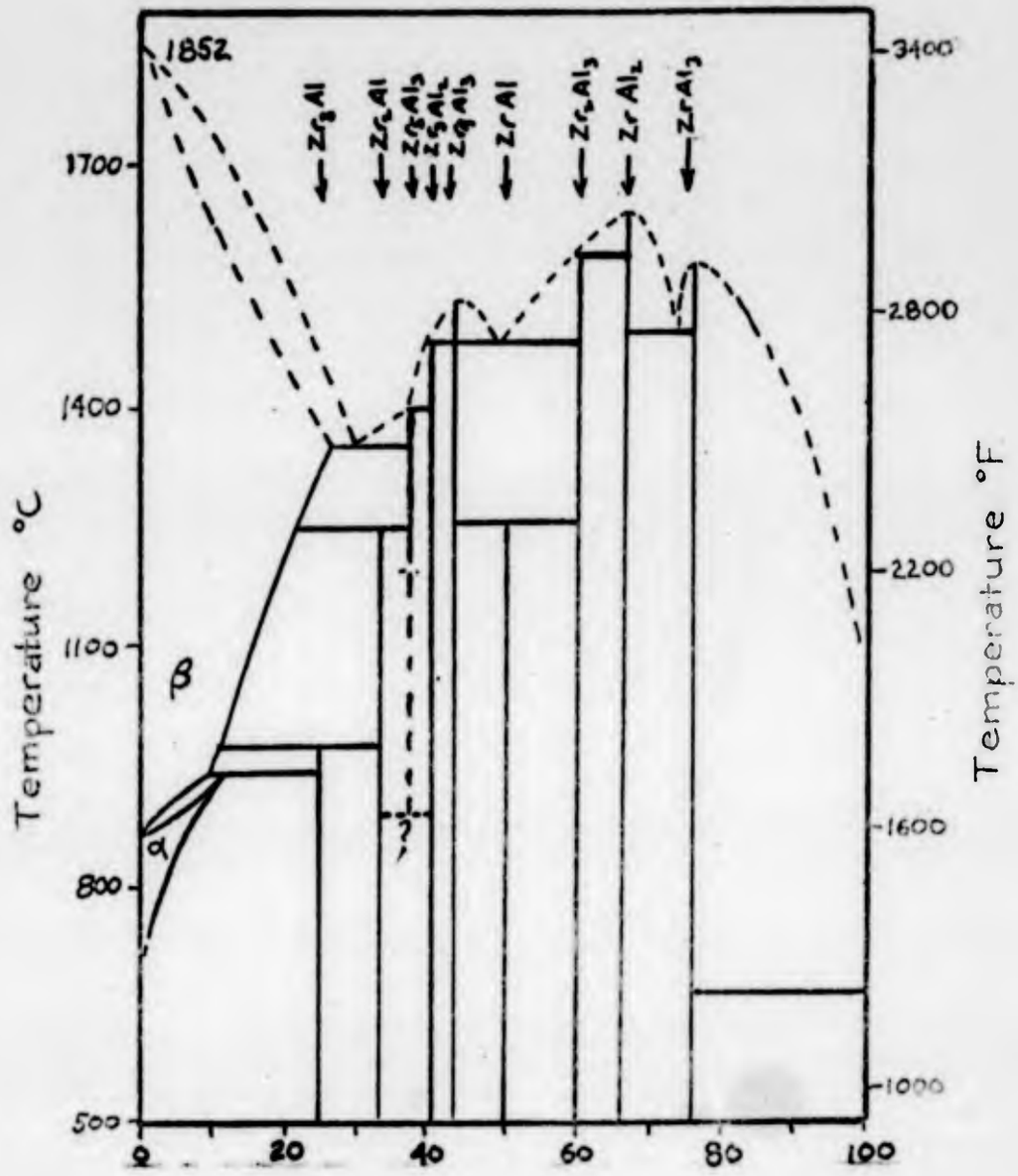

(Ref8:153)

Fig. 7

Zirconium-Aluminum Equilibrium Diagram

2) the ϕ phase was not present; and

3) the ϵ phase extends from between 5 and 10% zirconium to between 35 and 40% zirconium.

Attempts were made to index the peaks of the ϵ and ϕ phases by the use of published crystal structure data of the various Ti-Al and Zr-Al phases. No agreement was found between the ϕ phase and any of the other phases. The pattern of the ϵ phase corresponded closely with the pattern of $ZrAl_2$; however, it appears unlikely that an intermetallic compound so near to the aluminum side of the Zr-Al binary phase diagram would extend this far into the ternary system.

After the information obtained from the Ti-Al binary compositions had been extended as far as possible into the ternary system, a new approach was taken. Attempts were made to identify phases in the Zr-Al binary compositions and to extend this information into the ternary diagram.

Since the Zr-Al phase diagram (Fig. 7) indicates that only Zr_2Al_3 and Zr_4Al_3 should be present in the patterns of the as-cast binary specimens, 45CA(56.0Al-44.0Zr), 50BA(51.4Al-48.6Zr), and 55A(46.2Al-53.8Zr) (Figs. 11(c), 10(c), and 9(c)), an attempt was made to index all peaks present in the diffraction patterns of these specimens with the published crystal structure data of these phases (Ref 10 and 12). Many peaks in the binary, as-cast patterns could not be identified as Zr_4Al_3 and Zr_2Al_3 but could be identified as peaks of other Zr-Al intermetallics and α-

zirconium. The presence of these latter phases in these particular binaries indicated that equilibrium had not been obtained in the melting operation.

Comparison of the patterns of the above as-cast specimens with those of the annealed binary specimens allowed the indexing of a large number of peaks in the latter patterns.

The appearance of Zr_2Al_3 and α- zirconium in specimen 55A(46.2Al-53.8Zr) indicated a lack of equilibrium; therefore, the possibility existed that specimens 50B(51.4Al-48.6Zr) and 45C(56.0Al-44.0Ti) were also not in equilibrium. Specimen 50B was selected for further annealing at 1200 degrees Centigrade for six hours in an attempt to reach equilibrium. This specimen, number 50BH(51.4Al-48.6Zr), was ground to powder and an x-ray pattern taken (Fig. 10(c)).

A comparison of patterns 50BH, which was assumed to be in equilibrium, and 50B indicates a sharpening of the detail in the former, but no gross changes. Thus it was assumed that specimen 50B was in equilibrium as possibly was specimen 45C(56Al-44.0Ti).

At equilibrium only Zr_2Al_3 and ZrAl phases exist in specimen 50B(51.4Al-48.6Zr); therefore, all peaks not identified as Zr_2Al_3 in the pattern for this specimen are peaks of ZrAl, which has a previously unreported crystal structure. Pattern 50B was compared to the patterns of the other binaries, 45C(56.0Al-44.0Zr) and 55A(46.2Al-53.8Zr), and the peaks of the ZrAl phase were identified. This permitted identification of all major

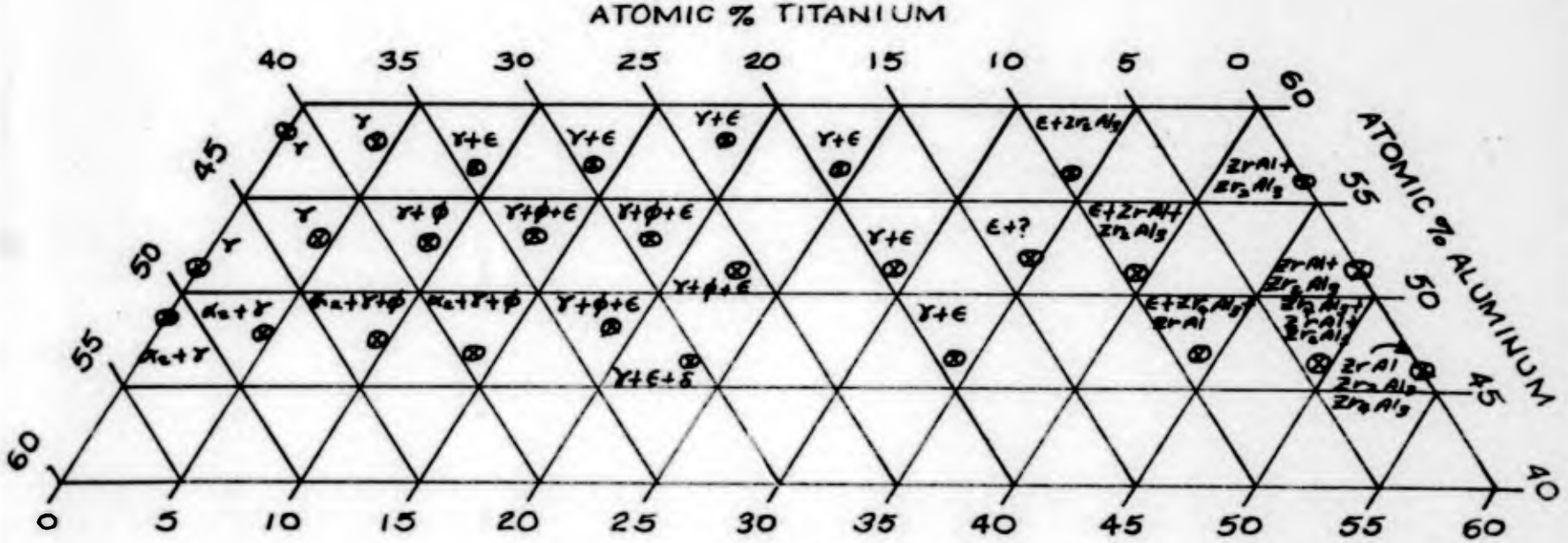

FIG. 8

PHASES PRESENT IN POWDER SPECIMENS
AT 2000°F

peaks of the binaries as peaks of Zr_2Al_3, Zr_4Al_3, ZrAl and α-zirconium. A few peaks still could not be identified.

The following conclusions were drawn concerning the extent of the Zr-Al intermetallic phases into the ternary system:

1) for the 55% aluminum specimens (Fig. 11) the Zr-Al existed to between 35 and 45% zirconium, while the Zr_2Al_3 extended to between 25 and 35% zirconium;

2) for the 50% aluminum specimen (Fig. 10) both ZrAl and Zr_2Al_3 extended to between 35 and 40% zirconium;and

3) for the 45% aluminum series (Fig. 9) Zr_2Al_3, ZrAl, and Zr_4Al_3 all extended to between 35 and 45% zirconium.

Figure 8 summarizes the presence of phases in each specimen and also indicates exact, rather than nominal composition of the specimens, by the location of points marked ⊗.

The extension of this information to the formulation of a ternary equilibrium diagram was not feasible since the rules elaborated by Rhines (Ref 11:207-209) could not be adhered to. Two reasons for this are offered.

1. There is not enough information available from the data taken to make a determination of the phase relationships. Such information as the compositions and crystal structures of the phases $\emptyset$, ϵ , and δ would be extremely helpful. Also in some cases, more alloys need to be prepared in certain areas and analyzed in order to give needed information about phase relationships.

2. Phase δ was predicated on inconclusive x-ray and metallographic data. More information is needed to definitely determine if this phase exists.

There is a disagreement between the x-ray data and the Zr-Al equilibrium diagram. The phase diagram indicates that a large percentage of the as-cast specimens 45CA(56.0Al-44.0Zr), 50BA(51.4Al-48.6Zr), 55AA(46.2Al-53.8Zr) and annealed specimen 45C should be Zr_4Al_3. If a large percentage of a phase is present in an alloy, the intensities of some of the peaks from that phase would normally be strong. However, in the patterns of these binary specimens, the peaks of Zr_4Al_3 were weak and in some cases did not appear. The investigators can offer no explanation for this disagreement. A closer investigation of this area of the phase diagram should prove fruitful.

Generally, the conclusioas drawn from the diffraction patterns concerning number of phases present in any one specimen were supported by the metallographic data included in Appendix F.

VII. Conclusions and Recommendations

1. The c/a ratio of the face-centered tetragonal crystal structure of the γ phase of Ti-Al base alloys can not be reduced to unity as predicted by Davies. The lowest value of the c/a ratio obtained was 1.015 at a composition of 50% Al, 35% Ti, and 15% Zr.

2. Figure 8 indicates the phases found to be present in the Ti-Al-Zr system at 1100 degrees Centigrade. Two phases (ϵ and $\emptyset$), and possibly a third phase (δ), were detected which were previously unreported. The crystal structures and compositions of these phases were not determined.

The following areas are recommended for further investigation.

1) The region of the Ti-Al-Zr ternary system between 45 and 55 atomic percent aluminum and greater than 20% zirconium should be further studied with particular attention given to the equilibrium heat treatments. The study should consider alloys having small composition differences in order that boundaries of multiple phase regions may be established. The proposed study should also determine if the δ phase exists.

2) A study should be conducted to determine the composition and crystal structure of the ϵ and $\emptyset$ phases.

3) Since x-ray data of the as-cast binaries of aluminum and zirconium were not in agreement with the appropriate portion of the binary phase diagram, a study should be conducted in which x-ray analysis is employed to verify the Zr-Al phase diagram in

the range of 40 to 60 atomic percent aluminum.

4) A study should be conducted to determine the remainder of the Ti-Al-Zr ternary phase diagram.

Bibliography

1. Cullity, B.D. Elements of X-ray Diffraction. Reading, Massachusetts: Addison-Wesley Publishing Co., Inc. 1956.

2. Davies, Franklin C. The Effects of Ternary Additions On Lattice Parameters In the γ Phase of Titanium-Aluminum Alloy Systems. Master's Thesis, Institute of Technology (Air University), Wright-Patterson Air Force Base, Ohio September 1959.

3. Duwez, P. and J. L. Taylor, "Crystal Structure of Ti-Al" Journal of Metals, 4:70-71(1952).

4. Ence, E. and H. Margolin. The Titanium Aluminum Phase Diagram. Report New York University, July 1959.

5. Kessler, H.D. and J.B. McAndrew. Investigation of the Metallurgical Characteristics of the 36% Aluminum Titanium-Base Alloy. WADC Tech. Report 53-182, July 1953.

6. Klug, Harold C. and Leroy E. Alexander. X-ray Diffraction Procedures. New York: John Wiley and Sons, Inc. 1954.

7. Maykuth, D.J. et al. The Effects of Alloying Elements in Titanium. Columbus, Ohio: Defense Metals Information Center, Battelle Memorial Institute, September 15, 1960.

8. McPherson, J.D. and M. Hansen. "The System Zirconium-Aluminum." Transactions of the American Society for Metals, 46:354-374(1954).

9. Myers, Edward J. and Franklin C. Davies. "A Direct Graphical Method for the Precise Determination of Lattice Parameters of Tetragonal or Hexagonal Crystals." Acta Crystallographica, 14:194-197(1961).

10. Renouf, T. J. and C.A. Beevers. "The Crystal Structure of Zr_2Al_3." Acta Crystallographica, 14:469-472(1961).

11. Rhines, Frederick N. Phase Diagrams in Metallurgy. New York: McGraw-Hill Book Company, Inc., 1956.

12. Wilson, C.G., et al. "The Crystal Structure of Zr_4Al_3." Acta Crystallographica, 13:56-57(1960).

13. Wilson, C.G. and F. J. Spooner. "The Crystal Structure of Zr_3Al_2." Acta Crystallographica, 13:358-359(1960).

14. _____. X-Ray Powder Data File (Eighth Set). Philadelphia: American Society for Testing Materials, 1958.

Appendix A

Chemical Analyses of Alloys

Table VI contains a comparison of the nominal and actual compositions of the alloys investigated in this study. The weight percent figures were taken from Tables VII through XII. The actual atomic percentages were calculated from the actual weight percentages by neglecting the impurities. The sums of the atomic percentages for a given alloy should add to 100.0%, but in some cases they do not due to losses in rounding off the figures to the first decimal place.

The chemical analyses of all of the alloys studied are contained in Tables VII through XII. The amounts of all constituents were determined by spectrographic analysis; those marked by an asterisk (*) were determined by wet chemistry. All figures are in weight percent except the impurities in Tables X through XII which are indicated as parts per million (ppm).

The symbol $\angle$ means "less than."

Table	Specimen No.	Page
VI	Comparison of all specimens	33
VII	0A, 5A, 10A, 15A, 20A	35
VIII	0B, 5B, 10B, 15B, 20B	36
IX	0C, 5C, 10C, 15C, 20C	36
X	25A, 35A, 45A, 50A, 55A	37
XI	25B, 30B, 35B, 40B, 50B	38
XII	25C, 35C, 45C	39

TABLE VI

Comparison of Nominal and Actual Compositions of Alloys

Specimen No.	Actual Weight %			Actual Atomic %			Nominal Atomic %		
	Al	Ti	Zr	Al	Ti	Zr	Al	Ti	Zr
0A	34.40	65.07	0.02	48.6	51.4	0.0	45.0	55.0	0.0
5A	32.15	57.30	10.30	47.6	47.8	4.5	45.0	50.0	5.0
10A	29.92	48.80	20.34	47.2	43.3	9.5	45.0	45.0	10.0
15A	28.53	42.20	28.90	46.9	39.0	14.1	45.0	40.0	15.0
20A	27.85	34.25	37.01	48.0	33.2	18.8	45.0	35.0	20.0
0B	36.90	62.75	0.02	51.3	48.7	0.0	50.0	50.0	0.0
5B	36.91	52.35	11.25	52.5	42.7	4.8	50.0	45.0	5.0
10B	34.30	45.05	20.42	52.2	38.6	9.2	50.0	40.0	10.0
15B	32.89	37.40	29.40	52.5	33.6	13.9	50.0	35.0	15.0
20B	31.35	30.80	37.15	52.5	29.1	18.4	50.0	30.0	20.0
0C	43.75	55.70	0.01	58.2	41.8	0.0	55.0	45.0	0.0
5C	41.03	47.40	10.90	57.8	37.6	4.5	55.0	40.0	5.0
10C	37.71	41.15	20.55	56.3	34.6	9.1	55.0	35.0	10.0
15C	36.23	32.60	30.55	56.9	28.9	14.1	55.0	30.0	15.0
20C	35.20	25.35	38.70	57.8	23.4	18.8	55.0	25.0	20.0

TABLE VI (Continued)

Comparison of Nominal and Actual Compositions of Alloys

Specimen No.	Actual Weight % Al	Ti	Zr	Actual Atomic % Al	Ti	Zr	Nominal Atomic % Al	Ti	Zr
25A	25.70	29.78	44.46	46.2	30.2	23.6	45.0	30.0	25.0
35A	23.38	17.58	59.01	46.1	19.5	34.4	45.0	20.0	35.0
45A	21.76	7.48	70.74	46.6	9.0	44.4	45.0	10.0	45.0
50A	20.97	3.17	75.79	46.4	4.0	49.6	45.0	5.0	50.0
55A	20.21	0.02	79.63	46.2	0.0	53.8	45.0	0.0	55.0
25B	29.11	26.68	44.14	50.9	26.3	22.8	50.0	25.0	25.0
30B	27.81	18.87	53.26	51.3	19.6	29.1	50.0	20.0	30.0
35B	26.68	12.68	50.58	51.6	13.8	34.6	50.0	15.0	35.0
40B	25.27	8.18	66.50	51.0	9.3	39.7	50.0	10.0	40.0
50B	23.81	0.01	76.10	51.4	0.0	48.6	50.0	0.0	50.0
25C	32.65	19.20	48.09	56.6	18.7	24.7	55.0	20.0	25.0
35C	29.69	9.05	61.21	56.1	9.6	34.2	55.0	10.0	35.0
45C	27.32	0.02	72.62	56.0	0.0	44.0	55.0	0.0	45.0

TABLE VII

Chemical Analyses for Specimens 0A through 20A

Element	Specimen Number 0A	5A	10A	15A	20A
Al	34.40*	32.15*	29.92*	28.53*	27.85*
Ti	65.07*	57.30*	48.80*	42.20*	34.25*
Zr	.02*	10.30*	20.34*	28.90*	37.01*
Fe	.06	.10	.06	.07	.07
Si	.06	.05	.06	.03	.03
Cu	.06	.02	.02	.05	.02
Mn	.009	.008	.009	.01	.008
Ni	<.01	<.01	<.01	<.01	<.01
Mg	Trace	Trace	Trace	Trace	Trace
Hf	-	Trace	Trace	Trace	Trace

Analyses were performed by Bowser-Morner Testing Laboratories, Inc., Dayton, Ohio

TABLE VIII

Chemical Analyses of Specimens 0B through 20B

Element	Specimen Number 0B	5B	10B	15B	20B
Al	36.90*	36.31*	34.30*	32.89*	31.35*
Ti	62.75*	52.35*	45.05*	37.40*	30.80*
Zr	.02*	11.25*	20.42*	29.40*	37.15*
Fe	.09	.08	.07	.07	.07
Si	.04	.03	.03	.06	.03
Cu	.05	.03	.03	.05	.01
Mn	.009	.009	.008	.007	.008
Ni	<.01	<.01	<.01	<.01	<.01
Mg	Trace	Trace	Trace	Trace	Trace
Hf	-	Trace	Trace	Trace	Trace

Analyses were performed by Bowser-Morner Testing Laboratories, Inc., Dayton, Ohio

TABLE IX

Chemical Analyses of Specimens 0C through 20C

Element	Specimen Number 0C	5C	10C	15C	20C
Al	43.75*	41.03*	37.71*	36.23*	35.20*
Ti	55.70*	47.40*	41.15*	32.60*	25.35*
Zr	.01*	10.9 *	20.55*	30.55*	38.70*
Fe	.07	.07	.07	.07	.07
Si	.03	.01	.02	.03	.03
Cu	.01	.02	.02	.01	.01
Mn	.008	.009	.008	.009	.009
Ni	<.01	<.01	<.01	<.01	<.01
Mg	Trace	Trace	Trace	Trace	Trace
Hf	-	Trace	Trace	Trace	Trace

Analyses were performed by Bowser-Morner Testing Laboratories, Inc., Dayton, Ohio

TABLE X

Chemical Analyses of Specimens 25A through 55A

Element	Specimen Number 25A	35A	45A	50A	55A
Al	25.70	23.38	21.76	20.97	20.21
Ti	29.78	17.58	7.48	3.17	160ppm
Zr	44.46	59.01	70.74	75.79	79.63
Si (ppm)	20	26	24	80	30
Fe (ppm)	100	95	60	100	120
Cu (ppm)	88	25	45	47	25
Ni (ppm)	/10	/10	/10	/10	/10
Cr (ppm)	/20	/20	/20	55	/20
V (ppm)	15	/10	/10	35	/10
Mn (ppm)	45	/20	/20	/20	/20
Ca (ppm)	/10	/10	/10	/10	/10
Mg (ppm)	/10	/10	/10	/10	/10
Bi (ppm)	/10	/10	/10	/10	/10
Mo (ppm)	/20	/20	/20	/20	/20
Pb (ppm)	/10	/10	/10	/10	/10
Sn (ppm)	/10	/10	/10	/10	/10
Ag (ppm)	/10	/10	/10	/10	/10
Co (ppm)	/10	/10	/10	250	/10
B (ppm)	/1	1	1	/1	/1
Zn (ppm)	/20	/20	/20	/20	700
Ba (ppm)	/10	/10	/10	/10	/10
Na (ppm)	/10	/10	/10	/10	/10
K (ppm)	/10	/10	/10	/10	/10
Li (ppm)	/1	/1	/1	/1	/1
Cd (ppm)	/5	/5	/5	/5	/5

Analyses performed by National Spectrographic Laboratories, Inc., Cleveland, Ohio

TABLE XI

Chemical Analyses of Specimens 25B through 50B

Element	Specimen Number 25B	30B	35B	40B	50B
Al	29.11	27.81	26.68	25.27	23.81
Ti	26.68	18.87	12.68	8.18	130 ppm
Zr	44.14	53.26	50.58	66.50	76.10
Si (ppm)	40	30	120	30	40
Fe (ppm)	50	50	90	50	50
Cu (ppm)	36	60	68	22	21
Ni (ppm)	<10	<10	<10	<10	<10
Cr (ppm)	<20	36	34	<20	<20
V (ppm)	<10	15	15	<10	<10
Mn (ppm)	<20	50	50	<20	<20
Ca (ppm)	<10	<10	20	<10	<10
Mg (ppm)	<10	<10	<10	<10	<10
Bi (ppm)	<10	<10	<10	<10	<10
Mo (ppm)	<20	<20	<20	<20	<20
Pb (ppm)	<10	<10	<10	<10	<10
Sn (ppm)	<10	<10	<10	<10	<10
Ag (ppm)	<10	<10	<10	<10	<10
Co (ppm)	<10	80	70	<10	<10
B (ppm)	<1	<1	<1	<1	<1
Zn (ppm)	<20	<20	120	<20	<20
Ba (ppm)	<10	<10	<10	<10	<10
Na (ppm)	<10	<10	<10	<10	<10
K (ppm)	<10	<10	<10	<10	<10
Li (ppm)	<1	<1	<1	<1	<1
Cd (ppm)	<5	<5	<5	<5	<5

Analyses performed by National Spectrographic Laboratories, Inc., Cleveland, Ohio

TABLE XII

Chemical Analyses of Specimens 25C through 45C

Element	Specimen Number 25C	35C	45C
Al	32.65	29.69	27.32
Ti	19.20	9.05	200 ppm
Zr	48.09	61.21	72.62
Si (ppm)	30	43	35
Fe (ppm)	90	65	70
Cu (ppm)	70	21	35
Ni (ppm)	<10	<10	<10
Cr (ppm)	<20	<20	<20
V (ppm)	15	<10	<10
Mn (ppm)	38	<20	<20
Ca (ppm)	20	<10	<10
Mg (ppm)	<10	<10	<10
Bi (ppm)	<10	<10	<10
Mo (ppm)	<20	<20	<20
Pb (ppm)	<10	<10	<10
Sn (ppm)	<10	<10	<10
Ag (ppm)	<10	<10	<10
Co (ppm)	<10	<10	<10
B (ppm)	<1	1	<1
Zn (ppm)	<20	<20	<20
Ba (ppm)	<10	<10	<10
Na (ppm)	<10	<10	<10
K (ppm)	<10	<10	<10
Li (ppm)	<1	<1	<1
Cd (ppm)	<5	<5	<5

Analyses performed by National Spectrographic Laboratories, Inc., Cleveland, Ohio

Appendix B

Diffractometer Patterns

This appendix contains the diffractometer patterns which were used in the phase determination portion of the present study. All of the patterns were recorded under the following conditions:

X-ray tube - copper

filter - nickel

tube voltage - 50 kv

tube current - 20 ma

divergent slit - 1°

receiving slit - 0.003 in.

scatter slit - 1°

multiplier - 1

time constant

all specimens except 50B - 4 sec.

specimen 50B - 8 sec.

scale factor - 4

chart speed - 30 inches per hour

goniometer speed

Specimens	0A - 20A 0B - 20B 0C - 20C	2° per minute
Specimens	20A - 55A 20B - 50B 20C - 45C	1° per minute

Figure	Specimen No.	Page
9(a)	0A, 5A, 10A, 15A, 20A	42
9(b)	20A, 25A, 35A, 45A	43
9(c)	50A, 55A, 55AA	44
10(a)	0B, 5B, 10B, 15B, 20B	45
10(b)	20B, 25B, 30B, 35B	46
10(c)	40B, 50B, 50BA, 50BH	47
11(a)	0C, 5C, 10C, 15C, 20C	48
11(b)	20C, 25C, 35C	49
11(c)	45C, 45CA	50

GAW/Mech 61-6

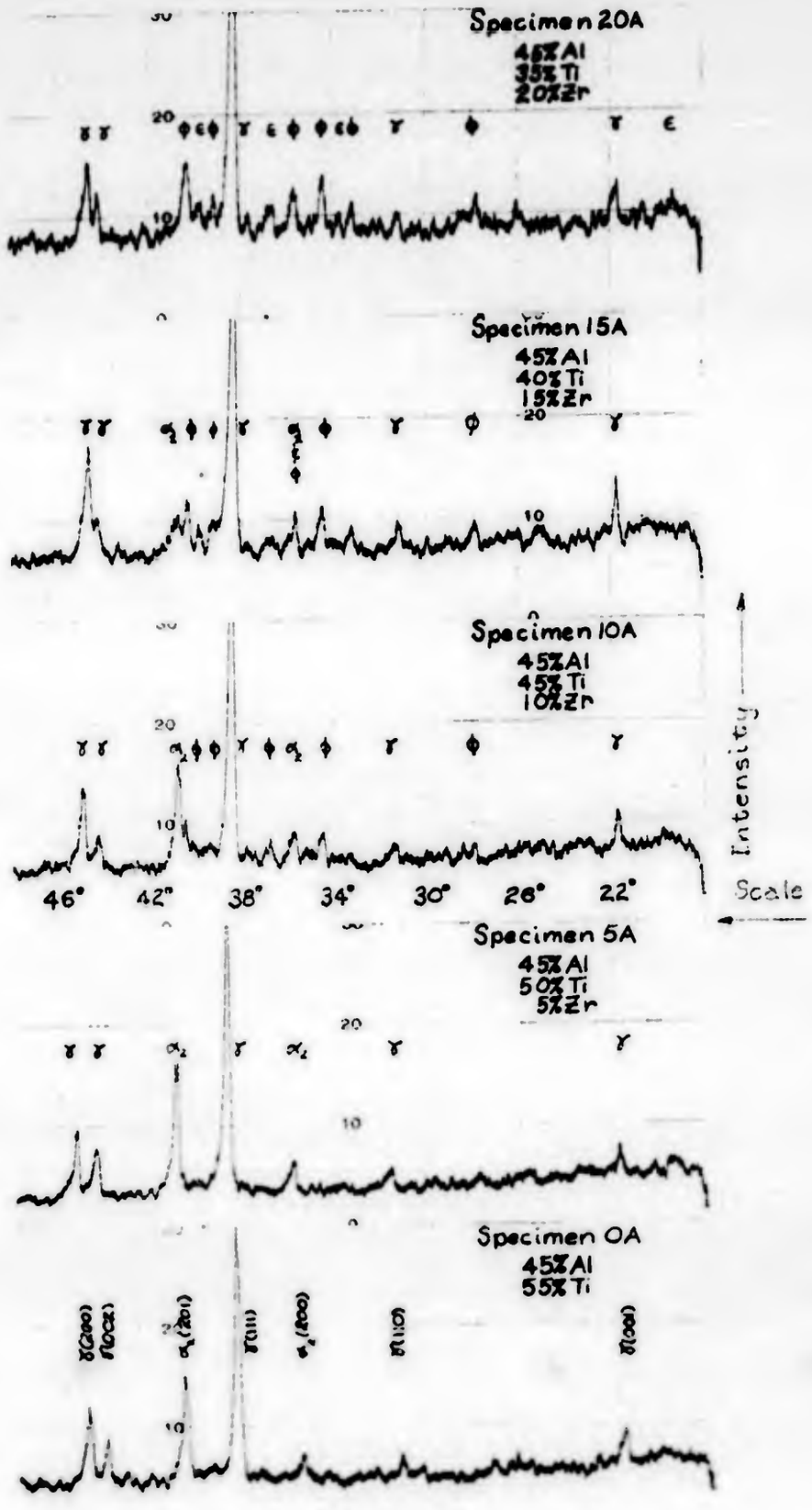

Fig. 9(a)

GEW/Mech 61-6

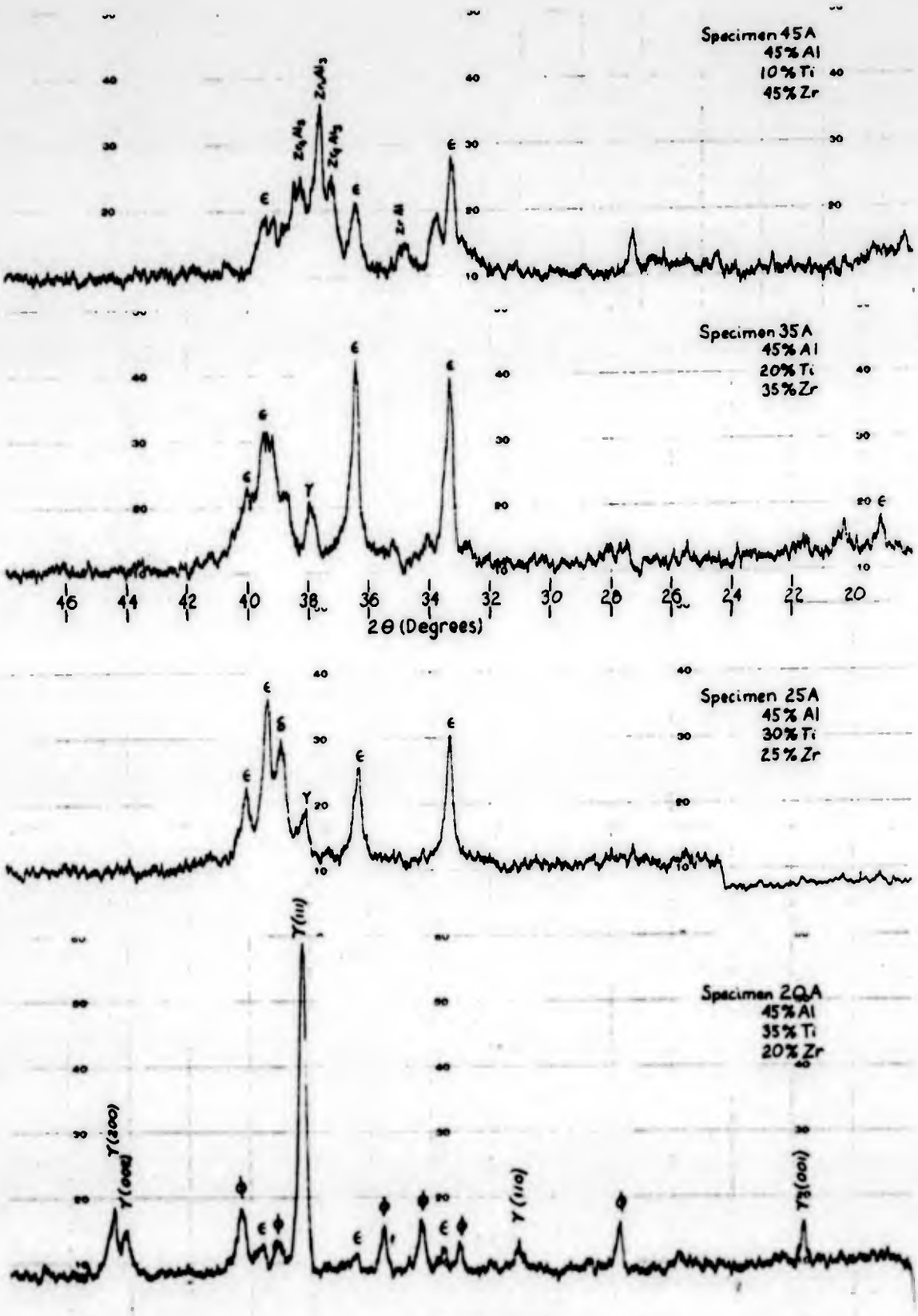

Fig. 9(b)

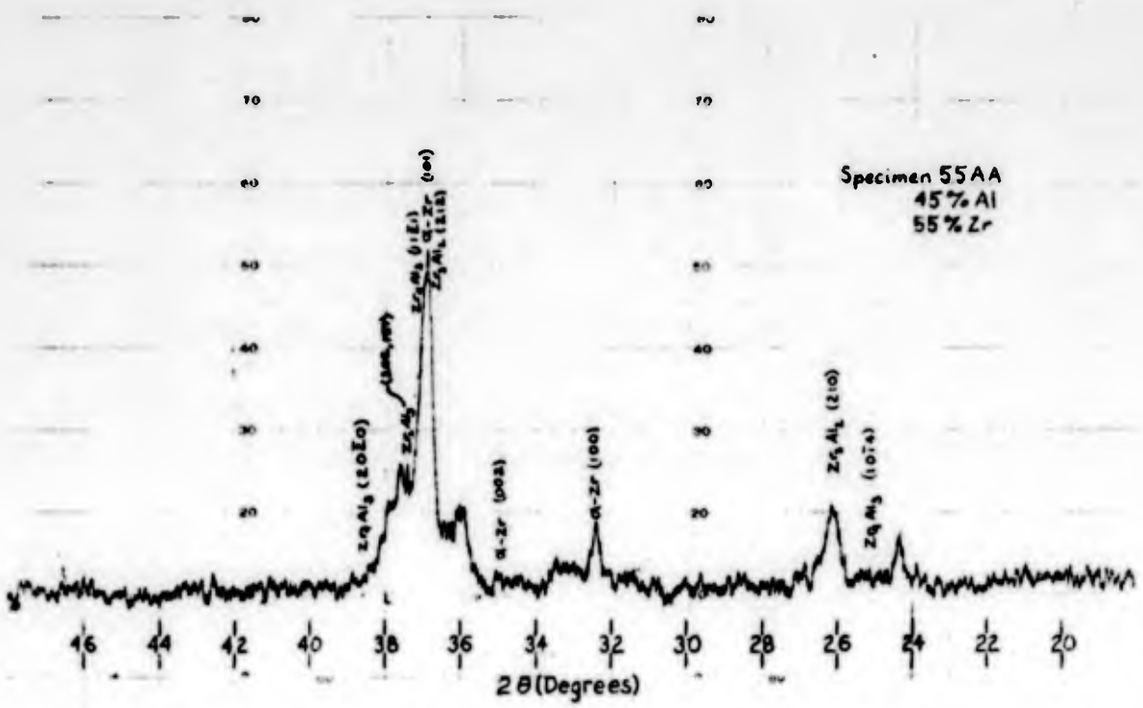
Specimen 55AA
45% Al
55% Zr
Intensity
Scale
2θ(Degrees)
46 44 42 40 38 36 34 32 30 28 26 24 22 20

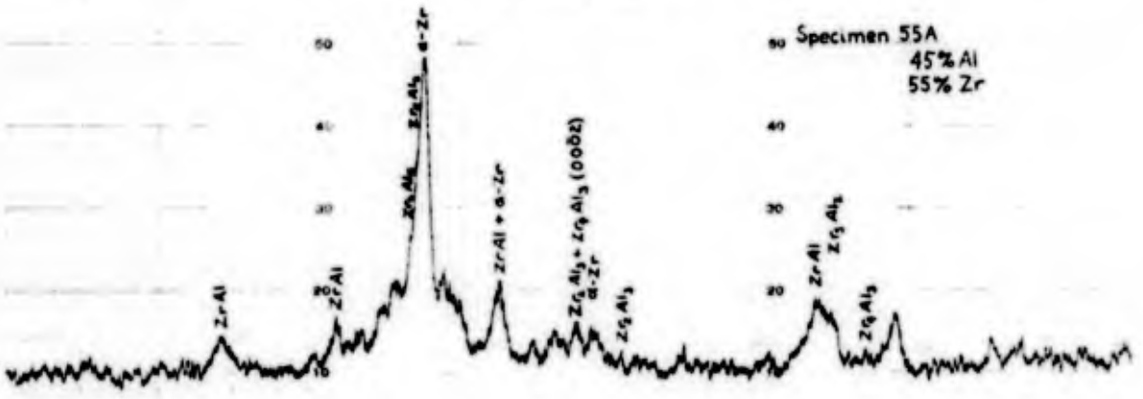
Specimen 55A
45% Al
55% Zr

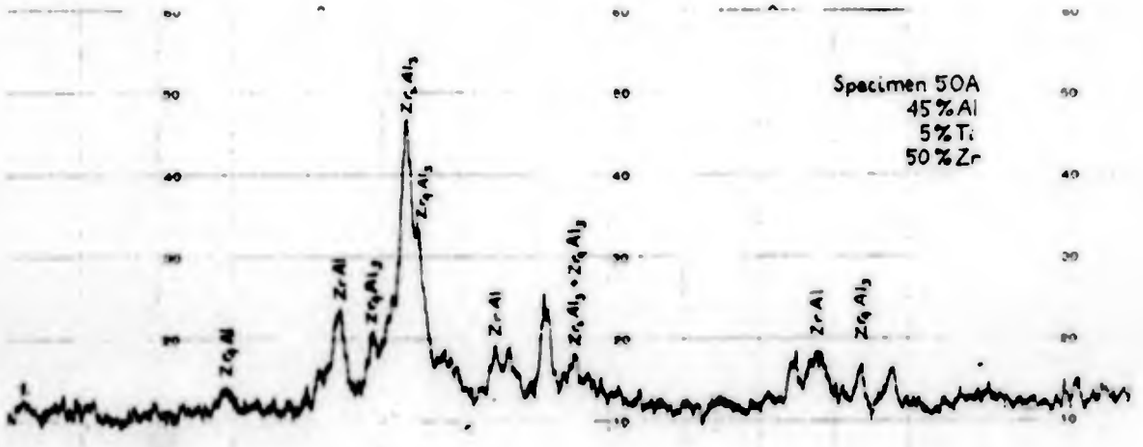
Specimen 50A
45% Al
5% Ti
50% Zr

Fig. 3(c)

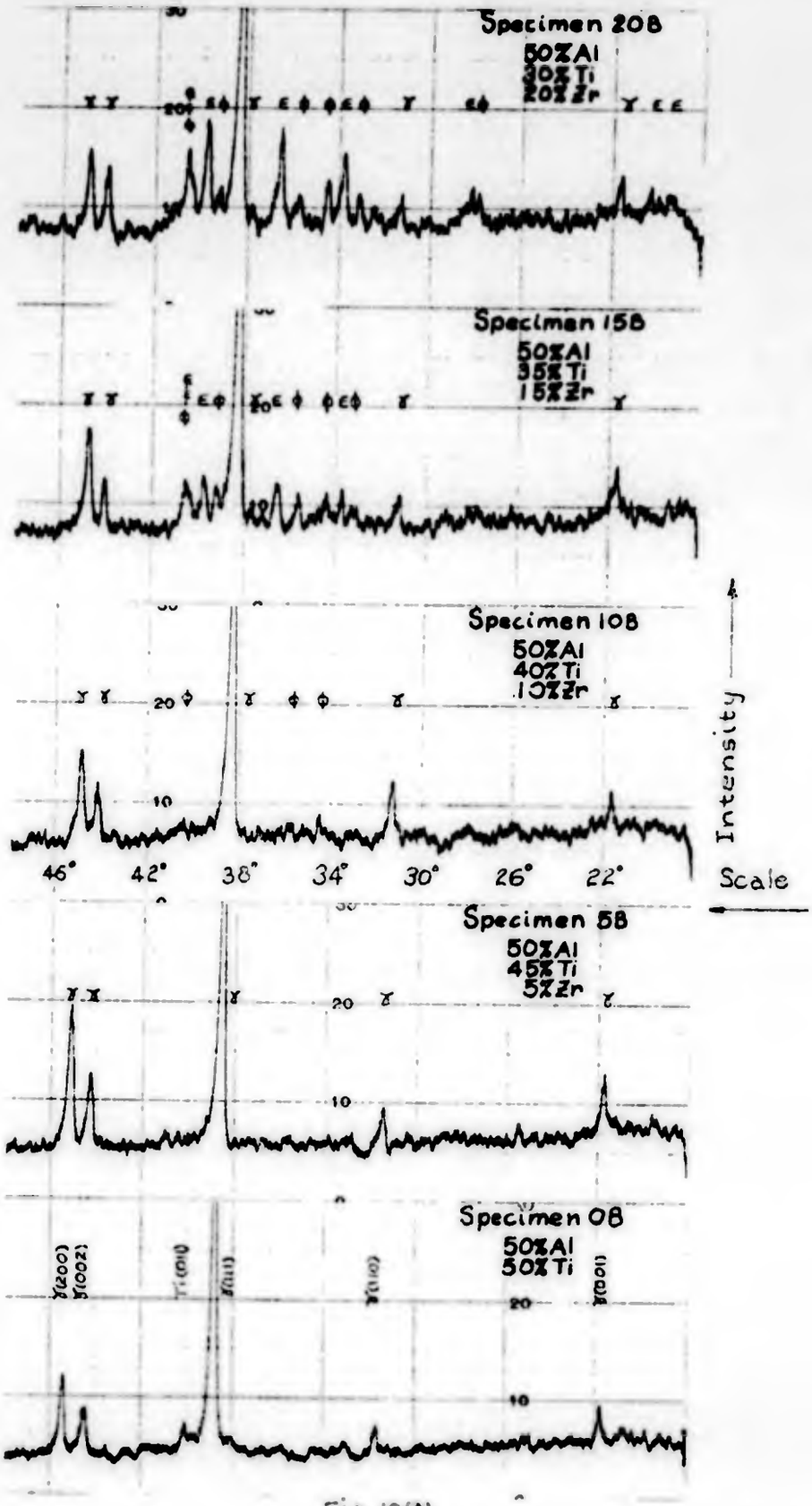
Specimen 208
50%Al
30%Ti
20%Zr
Specimen 158
50%Al
35%Ti
15%Zr
Specimen 108
50%Al
40%Ti
10%Zr
Specimen 58
50%Al
45%Ti
5%Zr
Specimen 08
50%Al
50%Ti
γ(200)
β(002)
Ti(011)
β(111)
γ(110)
γ(001)
Intensity
Scale
46°
42°
38°
34°
30°
26°
22°

Fig. 10(a)

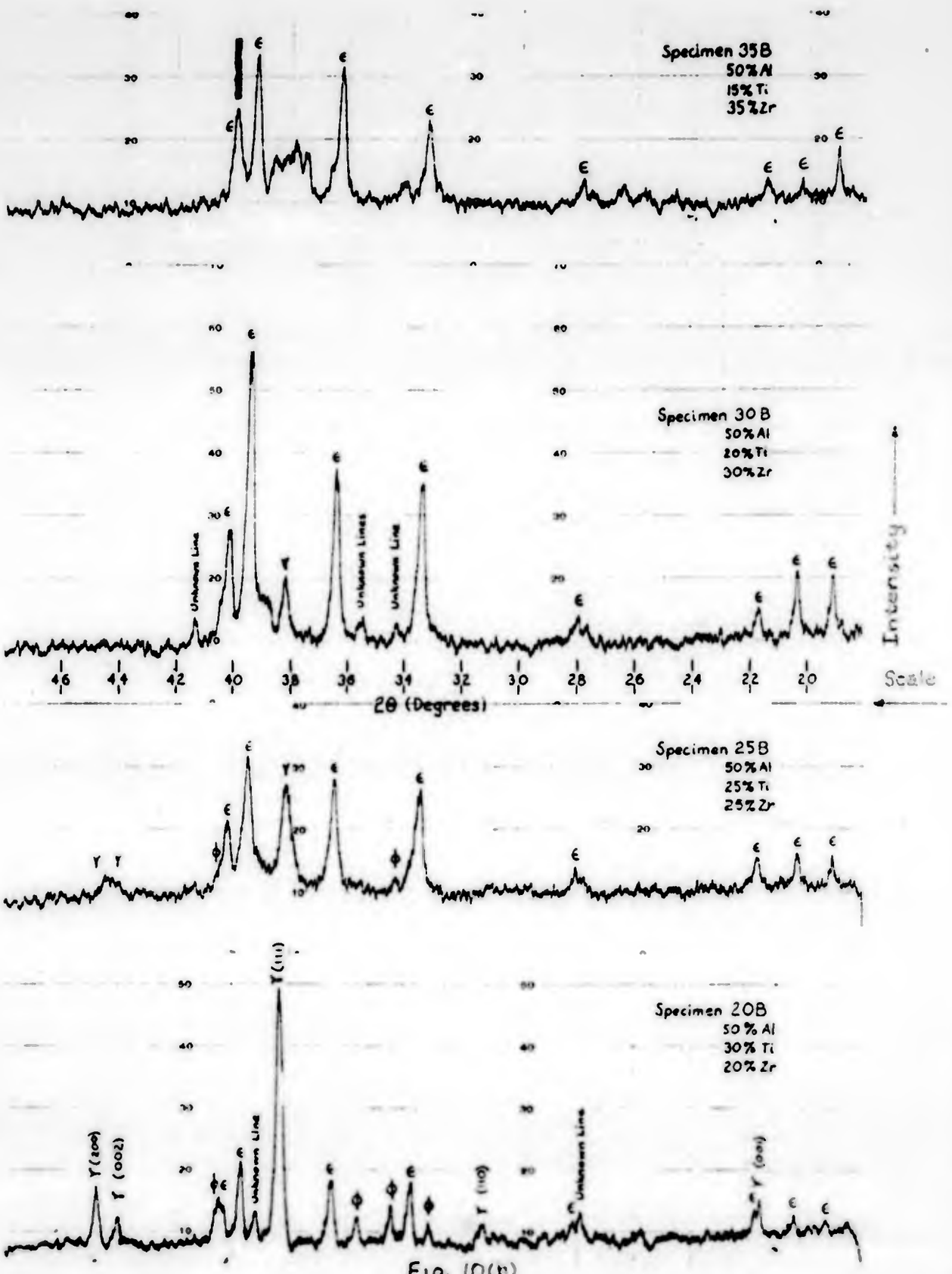
Specimen 35B
50% Al
15% Ti
35% Zr
Specimen 30B
50% Al
20% Ti
30% Zr
Unknown Line
Unknown Lines
Unknown Line
Intensity
Scale
4.6 4.4 4.2 4.0 3.8 3.6 3.4 3.2 3.0 2.8 2.6 2.4 2.2 2.0
2θ (Degrees)
Specimen 25B
50% Al
25% Ti
25% Zr
Specimen 20B
50% Al
30% Ti
20% Zr
γ(200)
γ (002)
Unknown Line
γ(111)
γ (110)
Unknown Line
γ (200)

Fig. 10(b)

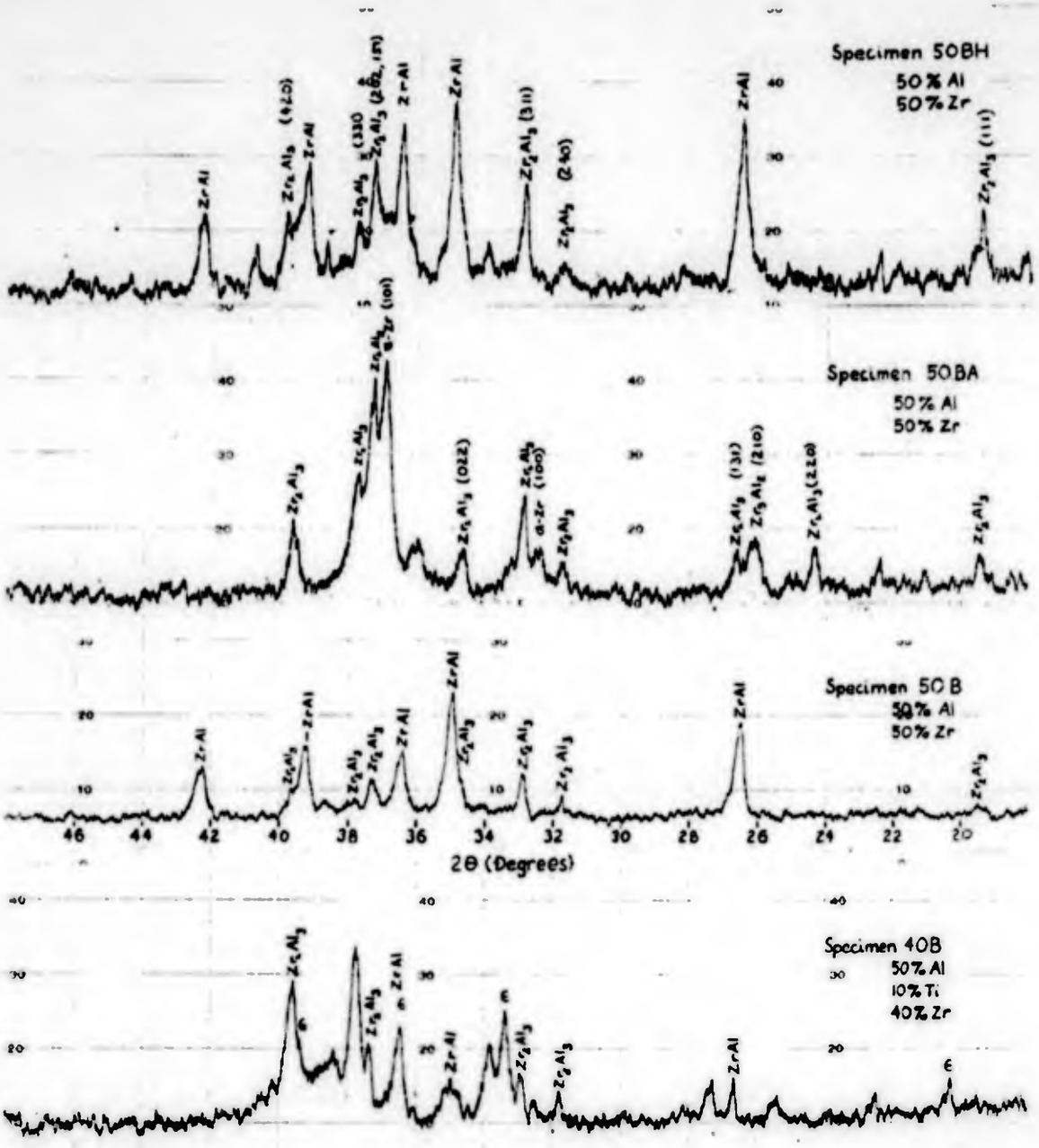
Specimen 50BH
50% Al
50% Zr
Specimen 50BA
50% Al
50% Zr
Specimen 50B
50% Al
50% Zr
Specimen 40B
50% Al
10% Ti
40% Zr
2θ (Degrees)
Intensity
Scale

Fig. 10(c)

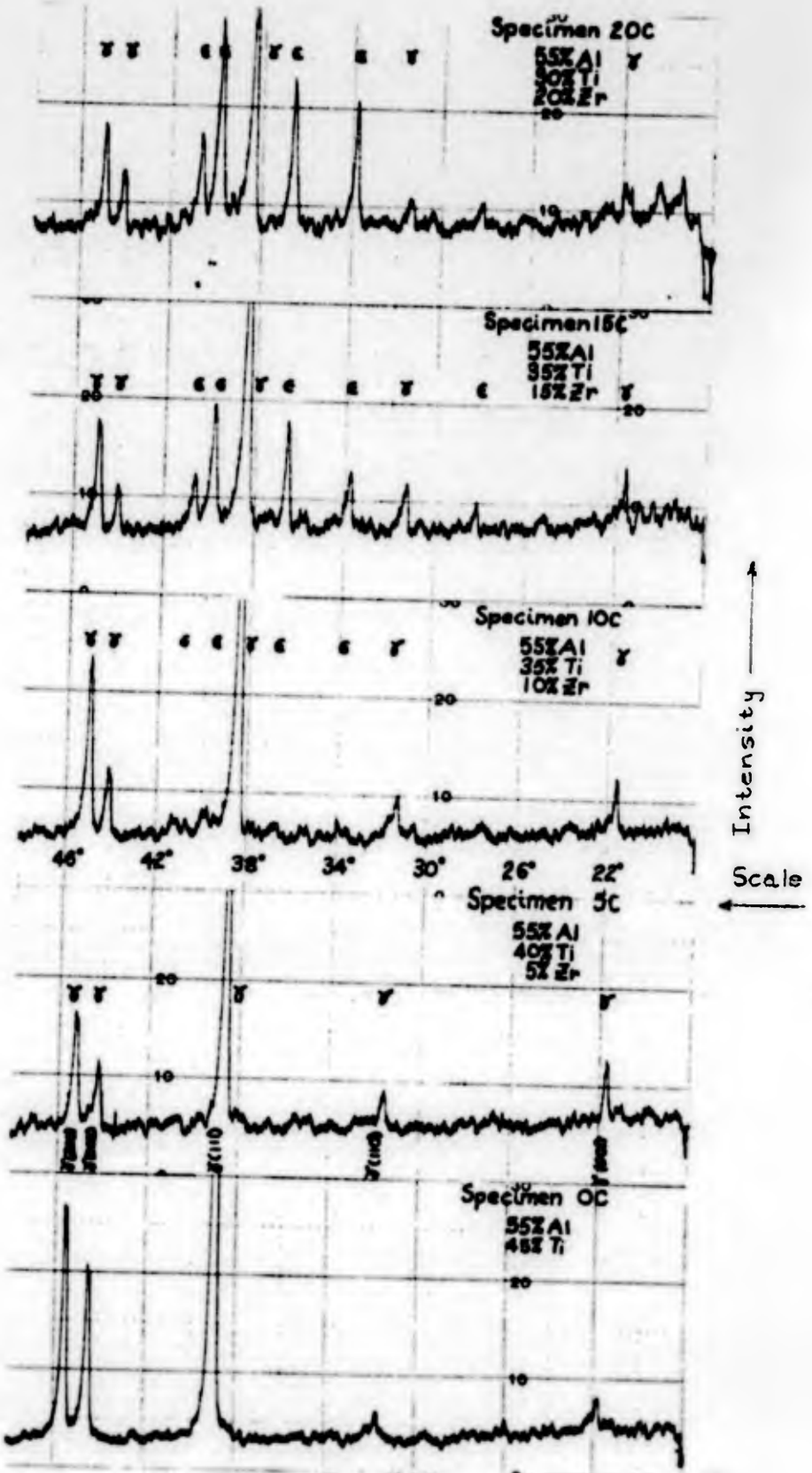
Specimen 20C
55%Al
30%Ti
20%Zr
Specimen 15C
55%Al
35%Ti
15%Zr
Specimen 10C
55%Al
35% Ti
10% Zr
Specimen 5C
55% Al
40% Ti
5% Zr
Specimen 0C
55% Al
45% Ti
46°
42°
38°
34°
30°
26°
22°
Intensity
Scale

Fig. 11(a)

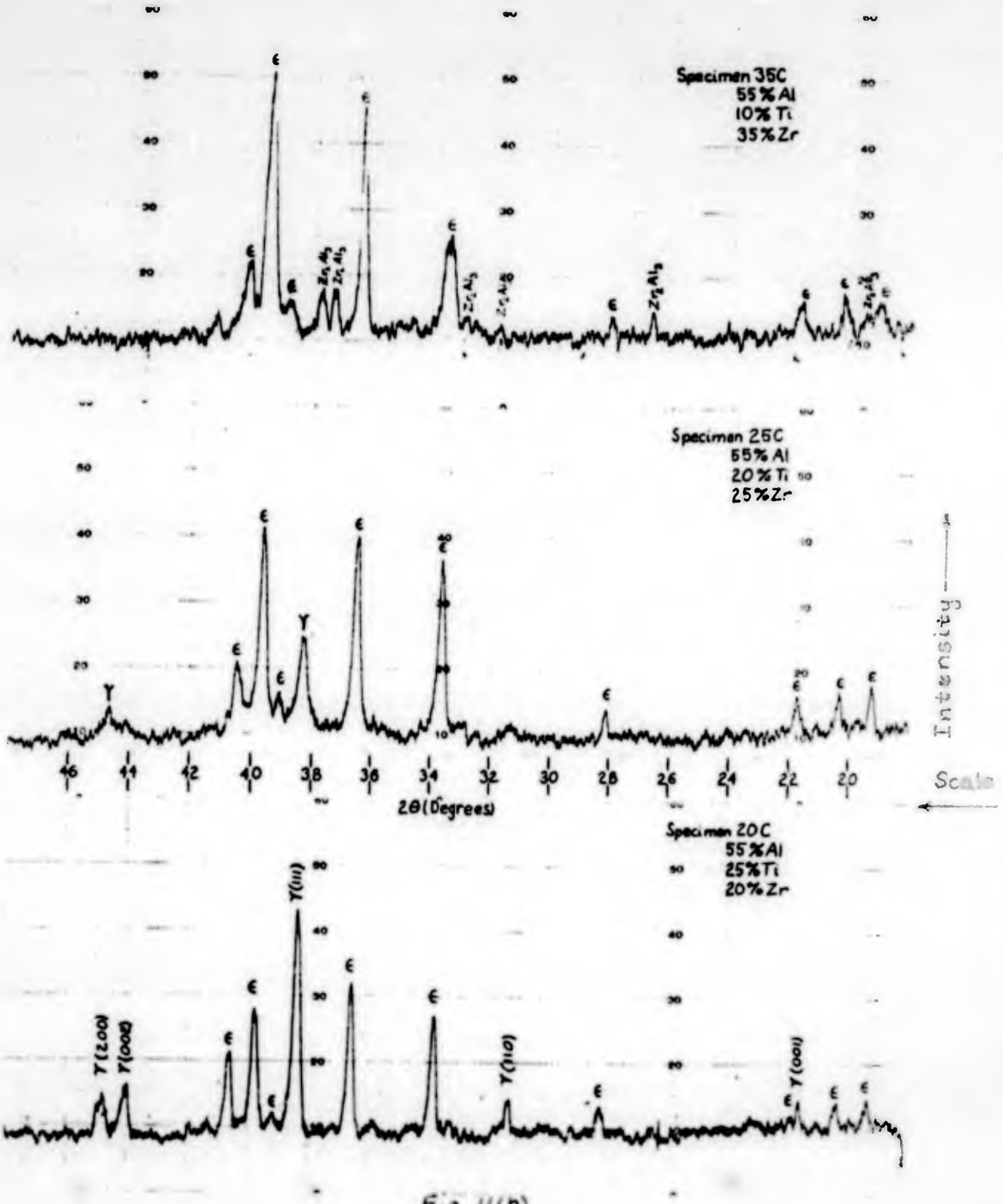
Specimen 35C
55% Al
10% Ti
35% Zr
Specimen 25C
55% Al
20% Ti
25% Zr
Specimen 20C
55% Al
25% Ti
20% Zr
Intensity
Scale
2θ(Degrees)
46
44
42
40
38
36
34
32
30
28
26
24
22
20
ε
γ
γ(111)
γ(200)
γ(002)
γ(110)
γ(001)

Fig. 11(b)

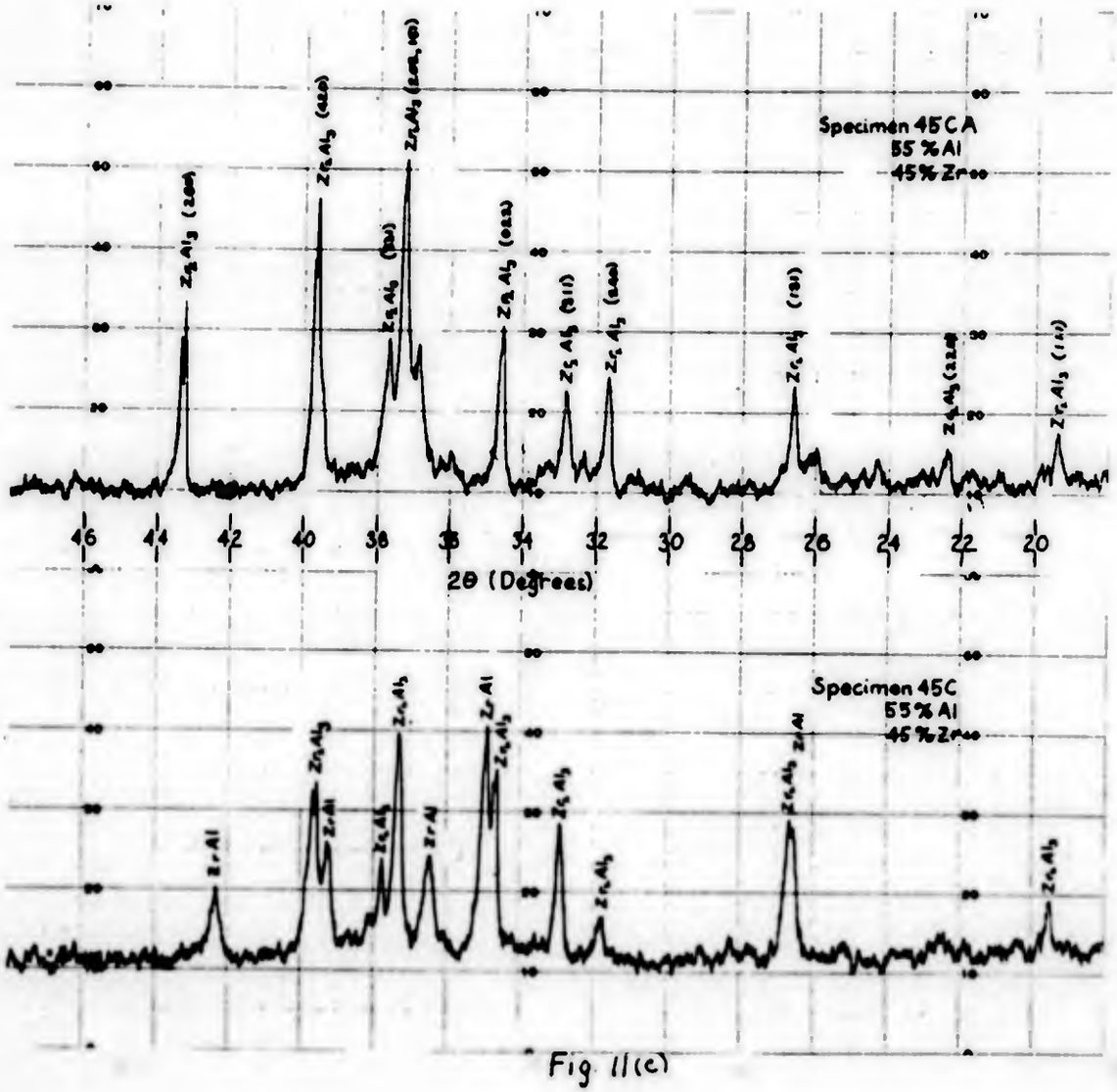
Specimen 45CA
55 %Al
45% Zr
Specimen 45C
55% Al
45% Zr
Intensity
Scale
2θ (Degrees)
46
44
42
40
38
36
34
32
30
28
26
24
22
20

Fig 11(c)

Appendix C

Tabulation of Diffraction Data and Calculated Values for Graphical Determination of Lattice Parameters

Table	Specimen No.	Compositions (atomic %)	Page
XIII	0B	48.7 Ti-51.3Al	52
XIV	5B	42.7 Ti-52.5Al-4.8Zr	53
XV	10B	38.6 Ti-52.2Al-9.2Zr	54
XVI	15B	33.6 Ti-52.5Al-13.9Zr	55
XVII	20B	29.1 Ti-52.5Al-18.4Zr	56
XVIII	0C	41.8 Ti-58.2Al	57
XIX	5C	37.6 Ti-57.8Al-4.5Zr	58
XX	10C	34.6 Ti-56.3Al-9.1Zr	59
XXI	15C	28.9 Ti-56.9Al-14.1Zr	60
XXII	20C	23.4 Ti-57.8Al-18.8Zr	61

Two values of $(a/c)^2$ and a^2 are calculated to permit the line of the equation to be drawn. Plots of lines are included in Appendix D.

TABLE XIII

Diffraction Data
and
Calculated Values for Graphical Determination of Lattice Parameters

Specimen OB
Composition
Al 51.3 Atomic %
Ti 48.7 Atomic %

Peak No.	Plane	Measured Angle 2θ	2θ Corr. For Calib.	θ (deg.)	$\sin^2\theta$	$\frac{4\sin^2\theta}{\lambda^2 \ell^2}$	$\frac{h^2+k^2}{\ell^2}$
1	202	65.32	65.32	32.660	.29126	.12273	1
2	113	77.91	77.92	38.960	.39532	.07403	2/9
3	131	79.30	79.31	39.655	.40724	.68640	10
4	313	112.61	112.63	56.315	.69236	.12966	10/9
5	204	115.97	115.99	57.995	.71912	.07515	1/4
6	402	118.29	118.31	59.155	.73713	.31060	4
7	422	140.46	140.46	70.236	.88563	.37318	5

Peak No.	Equation of Line	$(a/c)^2$	a^2	$(a/c)^2$	a^2
1	$(a/c)^2 = .12273a^2 - 1.00000$	.953	15.913	.967	16.027
2	$(a/c)^2 = .07403a^2 - .22222$	.953	15.875	.967	16.064
3	$(a/c)^2 = .68640a^2 - 10.00000$	.953	15.957	.967	15.978
4	$(a/c)^2 = .12966a^2 - 1.11111$	.953	15.919	.967	16.027
5	$(a/c)^2 = .07575a^2 - .25000$	.953	15.846	.967	16.066
6	$(a/c)^2 = .31060a^2 - 4.00000$	.953	15.947	.967	15.992
7	$(a/c)^2 = .37318a^2 - 5.00000$	.953	15.956	.967	15.990

TABLE XIV

Diffraction Data
and
Calculated Values for Graphical Determination of Lattice Parameters

Specimen 5B
Composition
Al 52.5 Atomic %
Ti 42.7 Atomic %
Zr 4.8 Atomic %

Peak No.	Plane	Measured Angle 2θ	2θ Corr. For Calib.	θ (deg.)	$\sin^2\theta$	$\frac{4\sin^2\theta}{\lambda^2 \ell^2}$	$\frac{h^2+k^2}{\ell^2}$
1	202	64.93	64.93	32.465	.28814	.12141	1
2	113	77.46	77.47	38.735	.39150	.07331	2/9
3	131	78.74	78.75	39.375	.40248	.67838	10
4	313	111.72	111.74	55.870	.68522	.12832	10/9
5	204	115.14	115.16	57.580	.71258	.07506	1/4
6	402	117.21	117.23	58.615	.72874	.30707	4
7	422	138.68	138.69	69.345	.87560	.36895	5

Peak No.	Equation of Line	$(a/c)^2$	a^2	$(a/c)^2$	a^2
1	$(a/c)^2 = .12141a^2 - 1.00000$	.956	15.913	.967	16.027
2	$(a/c)^2 = .07331a^2 - .22222$	.956	15.875	.967	16.064
3	$(a/c)^2 = .6838a^2 - 10.00000$	.956	15.957	.967	15.978
4	$(a/c)^2 = .12837a^2 - 1.11111$	.956	15.919	.967	16.029
5	$(a/c)^2 = .07506a^2 - .25000$	.956	15.846	.967	16.066
6	$(a/c)^2 = .30707a^2 - 4.00000$	.956	15.947	.967	15.992
7	$(a/c)^2 = .36895a^2 - 5.00000$	.956	15.956	.967	15.990

TABLE XV

Diffraction Data
and
Calculated Values for Graphical Determination of Lattice Parameters

Specimen 10B
Composition
Al 52.2 Atomic %
Ti 38.6 Atomic %
Zr 9.2 Atomic %

Peak No.	Plane	Measured Angle 2θ	2θ Corr. For Calib.	θ (deg.)	$\sin^2\theta$	$\frac{4\sin^2\theta}{\lambda^2 \ell^2}$	$\frac{h^2+k^2}{\ell^2}$
1	202	64.60	64.60	32.300	.28550	.12030	1
2	113	77.17	77.18	38.590	.38903	.07285	2/9
3	131	78.70	78.21	39.105	.39789	.67064	10
4	313	111.08	111.10	55.550	.68000	.12734	10/9
5	204	114.60	114.62	57.310	.70826	.07461	1/4
6	402	116.30	116.32	58.160	.72170	.30410	4
7	422	137.27	137.28	68.640	.86734	.36547	5

Peak No.	Equation of Line	$(a/c)^2$	a^2	$(a/c)^2$	a^2
1	$(a/c)^2 = .12030a^2 - 1.00000$	.962	16.309	.974	16.409
2	$(a/c)^2 = .07285a^2 - .22222$	.962	16.256	.974	16.420
3	$(a/c)^2 = .67064a^2 - 10.00000$	.962	16.346	.974	16.364
4	$(a/c)^2 = .12734a^2 - 1.11111$	.962	16.280	.974	16.374
5	$(a/c)^2 = .07461a^2 - .25000$	.962	16.245	.974	16.405
6	$(a/c)^2 = .30410a^2 - 4.00000$	.962	16.317	.974	16.357
7	$(a/c)^2 = .36547a^2 - 5.00000$	.962	16.313	.974	16.346

TABLE XVI

Diffraction Data
and
Calculated Values for Graphical Determination of Lattice Parameters

Specimen 15B
Composition
Al 52.5 Atomic %
Ti 33.6 Atomic %
Zr 13.9 Atomic %

Peak No.	Plane	Measured Angle 2θ	2θ Corr. For Calib.	θ (deg.)	$\sin^2\theta$	$\frac{4\sin^2\theta}{\lambda^2 \ell^2}$	$\frac{h^2+k^2}{\ell^2}$
1	202	64.55	64.55	32.275	.28513	.12014	1
2	113	77.12	77.13	38.565	.38861	.07278	2/9
3	131	78.12	78.13	39.065	.39717	.66942	10
4	313	110.85	110.87	55.435	.67816	.12700	10/9
5	204	114.45	114.47	57.235	.70713	.07449	1/4
6	402	116.15	116.17	58.085	.72056	.30362	4
7	422	136.75	136.76	68.380	.86426	.36417	5

Peak No.	Equation of Line	$(a/c)^2$	a^2	$(a/c)^2$	a^2
1	$(a/c)^2 = .12014a^2 - 1.00000$	.966	16.364	.980	16.481
2	$(a/c)^2 = .07278a^2 - .22222$	.966	16.326	.980	16.519
3	$(a/c)^2 = .66943a^2 - 10.00000$	.966	16.381	.980	16.402
4	$(a/c)^2 = .12700a^2 - 1.11111$	.966	16.355	.980	16.465
5	$(a/c)^2 = .07449a^2 - .25000$	.966	16.324	.980	16.512
6	$(a/c)^2 = .30362a^2 - 4.00000$	.966	16.356	.980	16.402
7	$(a/c)^2 = .36417a^2 - 5.00000$	.966	16.382	.980	16.421

TABLE XVII

Diffraction Data and Calculated Values for Graphical Determination of Lattice Parameters

Specimen 20B
Composition
Al 52.5 Atomic %
Ti 29.1 Atomic %
Zr 18.4 Atomic %

Peak No.	Plane	Measured Angle 2θ	2θ Corr. For Calib.	θ (deg.)	$\sin^2\theta$	$\frac{\Sigma \sin^2\theta}{\lambda^2 \ell^2}$	$\frac{h^2+k^2}{\ell^2}$
1	202	64.52	64.52	32.260	.28490	.12005	1
2	113	77.12	77.13	38.515	.38861	.07277	2/9
3	131	78.15	78.16	39.080	.39744	.66989	10
4	313	110.86	110.88	55.440	.67824	.12702	10/9
5	204	114.38	114.40	57.200	.70660	.07443	1/4
6	402	116.15	116.17	58.085	.72056	.30362	4
7	422	136.90	136.91	68.455	.86516	.36455	5

Peak No.	Equation of Line	$(a/c)^2$	a^2	$(a/c)^2$	a^2
1	$(a/c)^2 = .12005a^2 - 1.00000$	.963	16.358	.975	16.458
2	$(a/c)^2 = .07277a^2 - .22222$	.963	16.287	.975	16.452
3	$(a/c)^2 = .66989a^2 - 10.00000$	.963	16.365	.975	16.383
4	$(a/c)^2 = .12702a^2 - 1.11111$	.963	16.329	.975	16.458
5	$(a/c)^2 = .07443a^2 - .25000$	.963	16.297	.975	16.458
6	$(a/c)^2 = .30362a^2 - 4.00000$	.963	16.346	.975	16.386
7	$(a/c)^2 = .36455a^2 - 5.00000$	.963	16.357	.975	16.390

TABLE XVIII

Diffraction Data
and
Calculated Values for Graphical Determination of Lattice Parameters

Specimen # OC
Composition
Al 58.2 Atomic %
Ti 41.8 Atomic %

Peak No.	Plane	Measured Angle 2θ	2θ Corr. For Calib.	θ (deg.)	$\sin^2\theta$	$\frac{4\sin^2\theta}{\lambda^2 l^2}$	$\frac{h^2+k^2}{l^2}$
1	202	65.35	65.35	32.675	.29150	.12283	1
2	113	77.94	77.95	38.975	.39558	.07408	2/9
3	131	79.44	79.45	39.725	.40843	.68841	10
4	313	112.80	112.82	56.410	.69396	.12999	10/9
5	331	114.42	114.44	57.220	.70690	1.19149	18
6	204	116.07	116.09	58.045	.71992	.07584	1/4
7	402	118.58	118.60	59.300	.73930	.31153	4
8	422	141.01	141.01	70.505	.88866	.37446	5

Peak No.	Equation of Line	$(a/c)^2$	a^2	$(a/c)^2$	a^2
1	$(a/c)^2 = .12283a^2 - 1.00000$	.950	15.876	.962	15.973
2	$(a/c)^2 = .07408a^2 - .22222$	.950	15.824	.962	15.986
3	$(a/c)^2 = .68841a^2 - 10.00000$	.950	15.906	.962	15.924
4	$(a/c)^2 = .12997a^2 - 1.11111$	.950	15.858	.962	15.951
5	$(a/c)^2 = 1.19149a^2 - 18.00000$	.950	15.905	.962	15.915
6	$(a/c)^2 = .07584a^2 - .25000$	.950	15.823	.962	15.981
7	$(a/c)^2 = .31153a^2 - 4.00000$	.950	15.889	.962	15.928
8	$(a/c)^2 = .37446a^2 - 5.00000$	.950	15.890	.962	15.922

TABLE XIX

Diffraction Data
and
Calculated Values for Graphical Determination of Lattice Parameters

Specimen # 5C
Composition
Al 57.8 Atomic %
Ti 37.6 Atomic %
Zr 4.5 Atomic %

Peak No.	Plane	Measured Angle 2θ	2θ Corr. For Calib.	θ (deg.)	$\sin^2\theta$	$\frac{4\sin^2\theta}{\lambda^2\ell^2}$	$\frac{h^2+k^2}{\ell^2}$
1	202	64.88	64.88	32.440	.28774	.12125	1
2	113	77.30	77.31	38.655	.39014	.07307	2/9
3	131	78.84	78.85	39.425	.40333	.67982	10
4	313	111.75	111.77	55.885	.68546	.12837	10/9
5	331	113.35	113.37	56.685	.69836	1.17709	18
6	204	114.91	114.93	57.465	.71074	.07489	1/4
7	402	117.40	117.42	58.710	.73025	.30771	4
8	422	139.10	139.10	69.550	.87795	.36995	5

Peak No.	Equation of Line	$(a/c)^2$	a^2	$(a/c)^2$	a^2
1	$(a/c)^2 = .12125a^2 - 1.00000$	.952	16.099	.964	16.198
2	$(a/c)^2 = .07307a^2 - .22222$	.952	16.070	.964	16.234
3	$(a/c)^2 = .67982a^2 - 10.00000$	.952	16.110	.964	16.128
4	$(a/c)^2 = .12837a^2 - 1.11111$	.952	16.072	.964	16.165
5	$(a/c)^2 = 1.17709a^2 - 18.00000$	.952	16.101	.964	16.111
6	$(a/c)^2 = .07487a^2 - .25000$	.952	16.055	.964	16.215
7	$(a/c)^2 = .30771a^2 - 4.00000$	.952	16.093	.964	16.132
8	$(a/c)^2 = .36995a^2 - 5.00000$	.952	16.089	.964	16.121

TABLE XX

Diffraction Data
and
Calculated Values for Graphical Determination of Lattice Parameters

Specimen # 10C
Composition
Al 56.3 Atomic %
Ti 34.6 Atomic %
Zr 9.1 Atomic %

Peak No.	Plane	Measured Angle 2θ	2θ Corr. For Calib.	θ (deg.)	$\sin^2\theta$	$\frac{4\sin^2\theta}{\lambda^2\ell^2}$	$\frac{h^2+k^2}{\ell^2}$
1	202	64.68	64.68	32.340	.28614	.12057	1
2	113	77.11	77.12	38.560	.38852	.07276	2/9
3	131	78.41	78.42	39.210	.39967	.67365	10
4	313	111.15	111.17	55.585	.68056	.12746	10/9
5	331	112.50	112.52	56.260	.69146	1.16546	18
6	204	114.51	114.53	57.265	.70758	.07454	1/4
7	402	116.58	116.60	58.300	.72390	.30504	4
8	422	137.70	137.71	68.855	.86986	.36654	5

Peak No.	Equation of Line	$(a/c)^2$	a^2	$(a/c)^2$	a^2
1	$(a/c)^2 = .12057a^2 - 1.00000$	.956	16.223	.968	16.323
2	$(a/c)^2 = .07276a^2 - .22222$	.956	16.193	.968	16.358
3	$(a/c)^2 = .67365a^2 - 10.00000$	.956	16.264	.968	16.282
4	$(a/c)^2 = .12746a^2 - 1.11111$	.956	16.218	.968	16.312
5	$(a/c)^2 = 1.16546a^2 - 18.00000$	.956	16.265	.968	16.275
6	$(a/c)^2 = .07454a^2 - .25000$	.956	16.179	.968	16.340
7	$(a/c)^2 = .30504a^2 - 4.00000$	.956	16.247	.968	16.286
8	$(a/c)^2 = .36654a^2 - 5.00000$	.956	16.249	.968	16.282

TABLE XXI

Diffraction Data
and
Calculated Values for Graphical Determination of Lattice Parameters

Specimen # 15C
Composition
Al 56.9 Atomic %
Ti 28.9 Atomic %
Zr 14.1 Atomic %

Peak No.	Plane	Measured Angle 2θ	2θ Corr. For Calib.	θ (deg.)	$\sin^2\theta$	$\frac{4\sin^2\theta}{\lambda^2 \ell^2}$	$\frac{h^2+k^2}{\ell^2}$
1	202	64.63	64.63	32.315	.28574	.12041	1
2	113	77.08	77.09	38.545	.38827	.07272	2/9
3	131	78.31	78.32	39.160	.39882	.67222	10
4	313	110.99	111.01	55.505	.67928	.12722	10/9
5	331	112.25	112.27	56.135	.68946	1.16209	18
6	204	114.35	114.37	57.185	.70636	.07441	1/4
7	402	116.32	116.34	58.170	.72185	.30417	4
8	422	137.27	137.28	68.640	.86734	.36548	5

Peak No.	Equation of Line	$(a/c)^2$	a^2	$(a/c)^2$	a^2
1	$(a/c)^2 = .12041a^2 - 1.00000$	.958	16.261	.970	16.361
2	$(a/c)^2 = .07277a^2 - .22222$	.958	16.230	.970	16.395
3	$(a/c)^2 = .67222a^2 - 10.00000$	.958	16.301	.970	16.319
4	$(a/c)^2 = .12722a^2 - 1.11111$	.958	16.264	.970	16.358
5	$(a/c)^2 = 1.16209a^2 - 18.00000$	.958	16.314	.970	16.324
6	$(a/c)^2 = .07441a^2 - .25000$	.958	16.234	.970	16.396
7	$(a/c)^2 = .30417a^2 - 4.00000$	.958	16.300	.970	16.340
8	$(a/c)^2 = .36548a^2 - 5.00000$	.958	16.302	.970	16.335

TABLE XXII

Diffraction Data
and
Calculated Values for Graphical Determination of Lattice Parameters

Specimen # 20C
Composition
Al 57.8 Atomic %
Ti 23.4 Atomic %
Zr 18.8 Atomic %

Peak No.	Plane	Measured Angle 2θ	2θ Corr. For Calib.	θ (deg.)	$\sin^2\theta$	$\frac{4\sin^2\theta}{\lambda^2 \ell^2}$	$\frac{h^2+k^2}{\ell^2}$
1	202	64.45	64.45	32.225	.28438	.11983	1
2	113	77.00	77.01	38.505	.38759	.07259	2/9
3	131	78.12	78.13	39.065	.39612	.66766	10
4	313	110.79	110.81	55.405	.67768	.12692	10/9
5	331	111.98	112.00	56.000	.68730	1.15845	18
6	204	114.26	114.28	57.140	.70564	.07433	1/4
7	402	116.10	116.12	58.060	.72016	.30346	4
8	422	136.81	136.82	68.410	.86462	.36433	5

Peak No.	Equation of Line	$(a/c)^2$	a^2	$(a/c)^2$	a^2
1	$(a/c)^2 = .11983a^2 - 1.00000$	.960	16.357	.972	16.457
2	$(a/c)^2 = .07259a^2 - .22222$	.960	16.286	.972	16.452
3	$(a/c)^2 = .66766a^2 - 10.00000$	.960	16.416	.972	16.434
4	$(a/c)^2 = .12692a^2 - 1.11111$	.960	16.318	.972	16.413
5	$(a/c)^2 = 1.15845a^2 - 18.00000$	.960	16.367	.972	16.377
6	$(a/c)^2 = .07433a^2 - .25000$	.960	16.279	.972	16.440
7	$(a/c)^2 = .30346a^2 - 4.00000$	.960	16.345	.972	16.384
8	$(a/c)^2 = .36433a^2 - 5.00000$	.960	16.359	.972	16.392

Appendix D

Graphical Solutions for the Determination of Lattice Parameters

Figure	Specimen	Composition (Atomic %)	Page
12	0B	48.7Ti - 51.3Al	63
13	5B	42.7Ti - 52.5Al - 4.8Zr	64
14	10B	38.6Ti - 52.2Al - 9.2Zr	65
15	15B	33.6Ti - 52.5Al - 13.9Zr	66
16	20B	29.1Ti - 52.5Al - 18.4Zr	67
17	0C	41.8Ti - 58.2Al	68
18	5C	37.6Ti - 57.8Al - 4.5Zr	69
19	10C	34.6Ti - 56.3Al - 9.1Zr	70
20	15C	28.9Ti - 56.9Al - 14.1Zr	71
21	20C	23.4Ti - 57.8Al - 18.8Zr	72

Graphical Solution
for Determination of
Lattice Parameters

Specimen No. OB
Composition (at.%)
48.7Ti-51.3Al

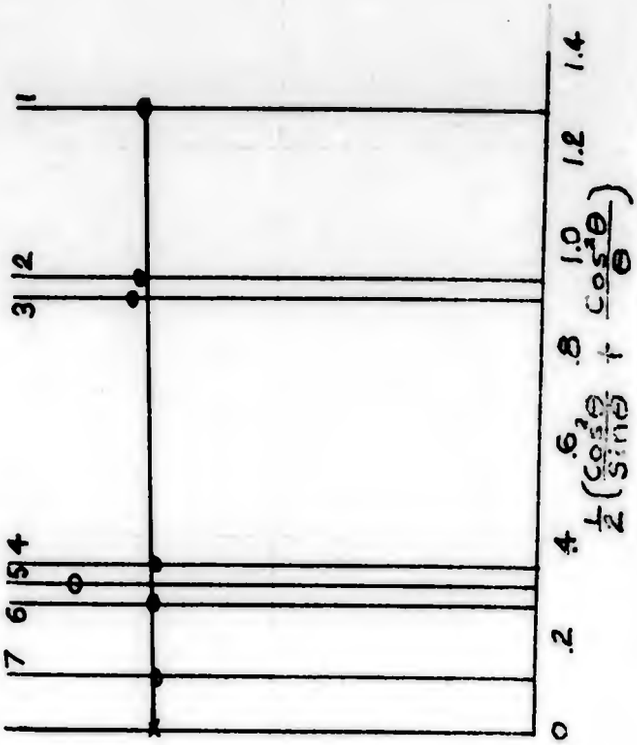

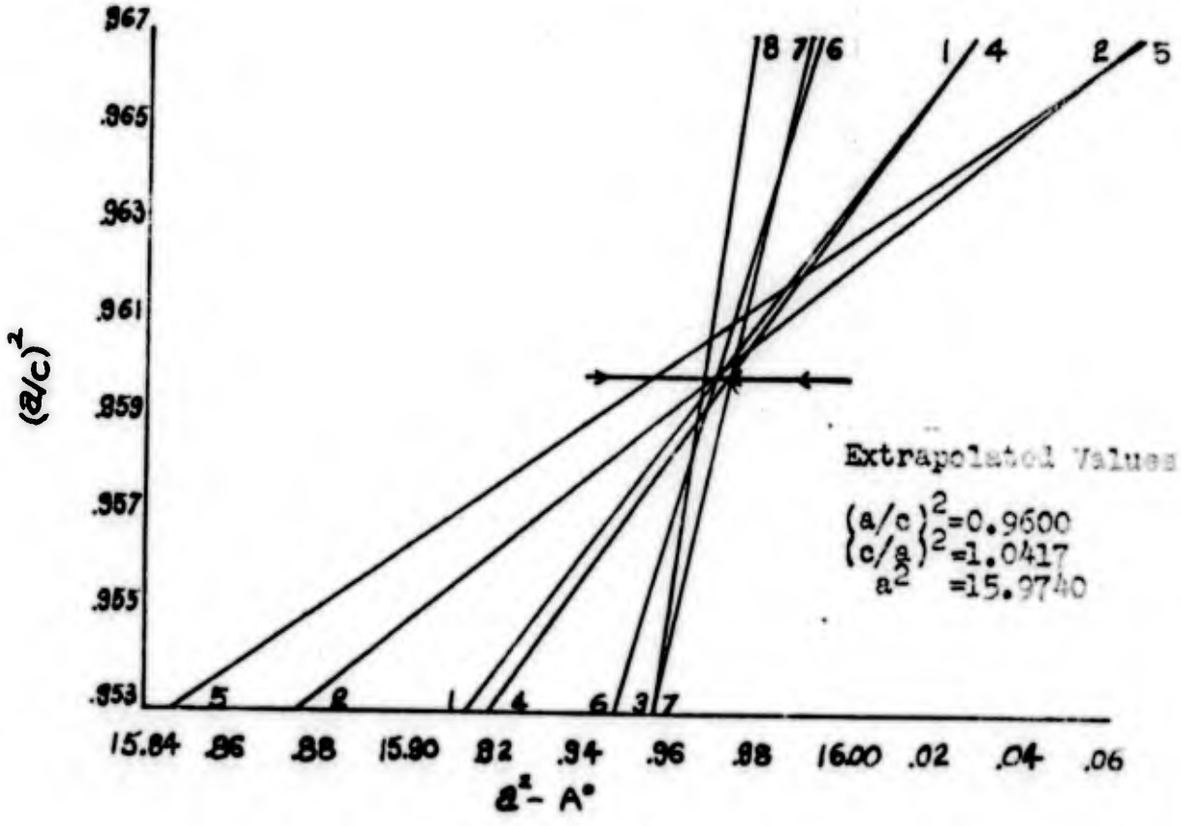

Fig. 12

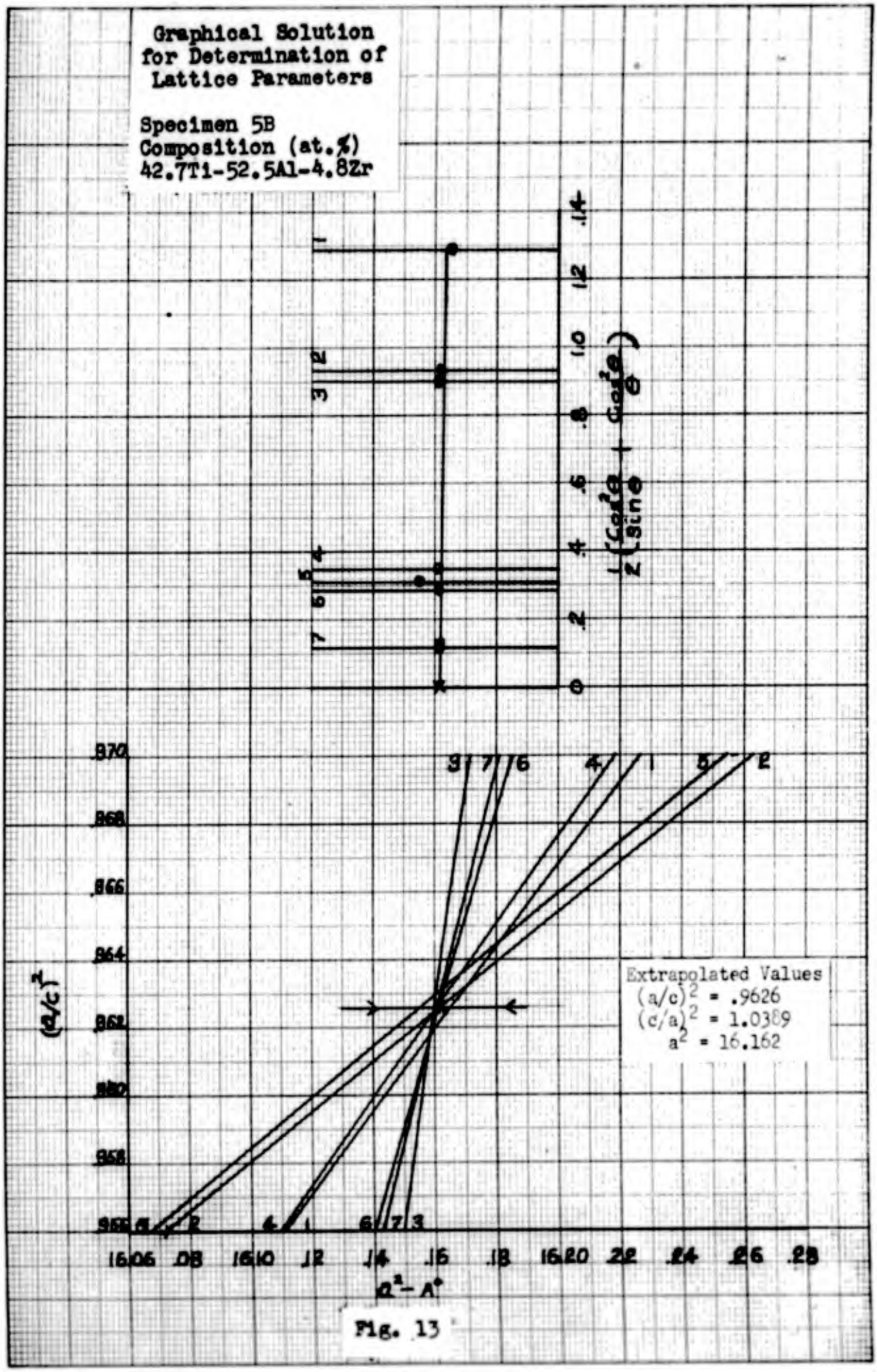
Graphical Solution
for Determination of
Lattice Parameters
Specimen 5B
Composition (at.%)
42.7Ti-52.5Al-4.8Zr
1
2
3
4
5
6
7
1/2(sinθ + tanθ/θ)
(a/c)²
(c/a)²
Extrapolated Values
(a/c)² = .9626
(c/a)² = 1.0389
a² = 16.162
Ω² - A*

Fig. 13

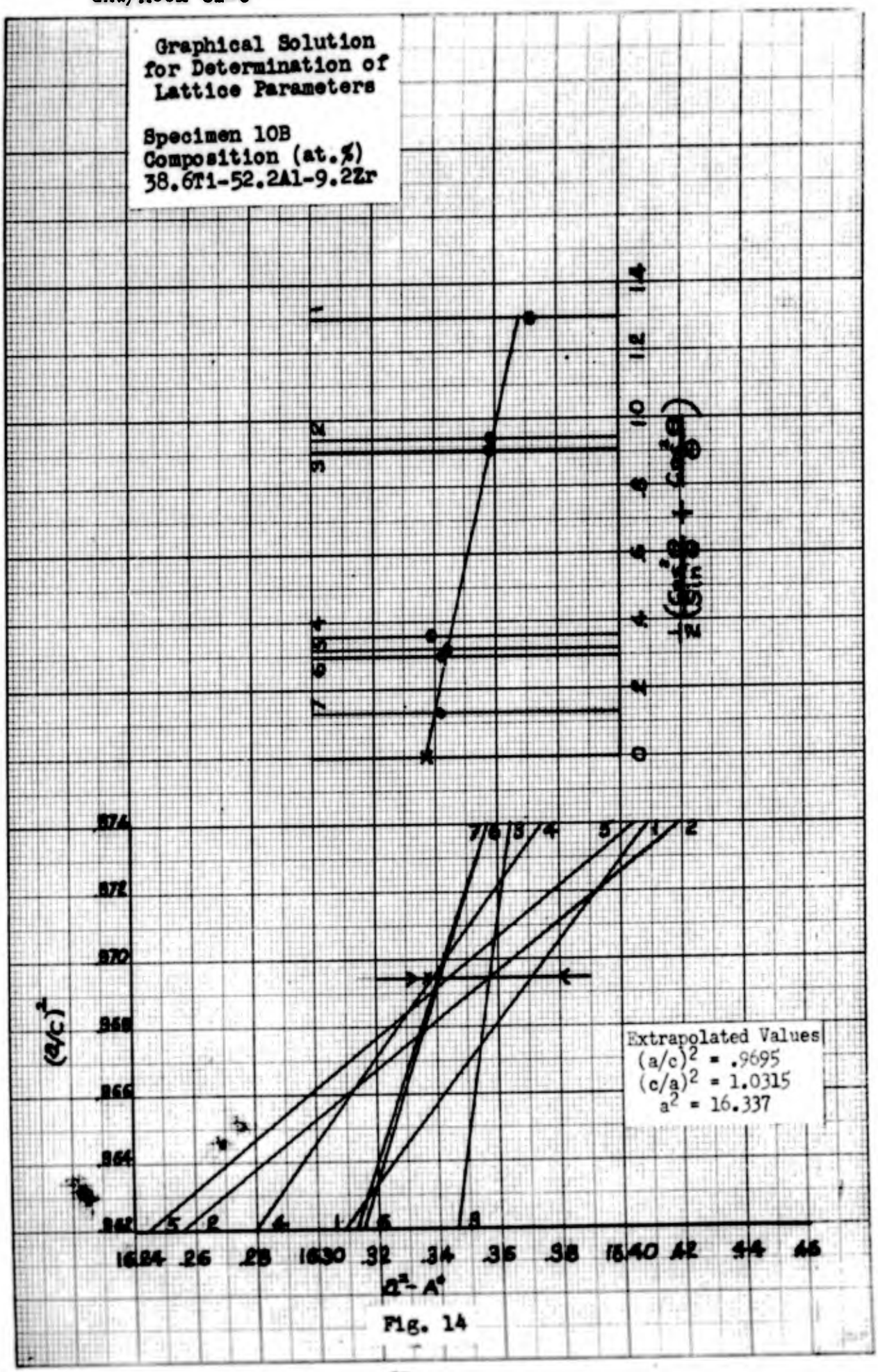
Graphical Solution
for Determination of
Lattice Parameters
Specimen 10B
Composition (at.%)
38.6Ti-52.2Al-9.2Zr
Extrapolated Values
(a/c)² = .9695
(c/a)² = 1.0315
a² = 16.337
(a/c)²
Θ²- A⁴

Fig. 14

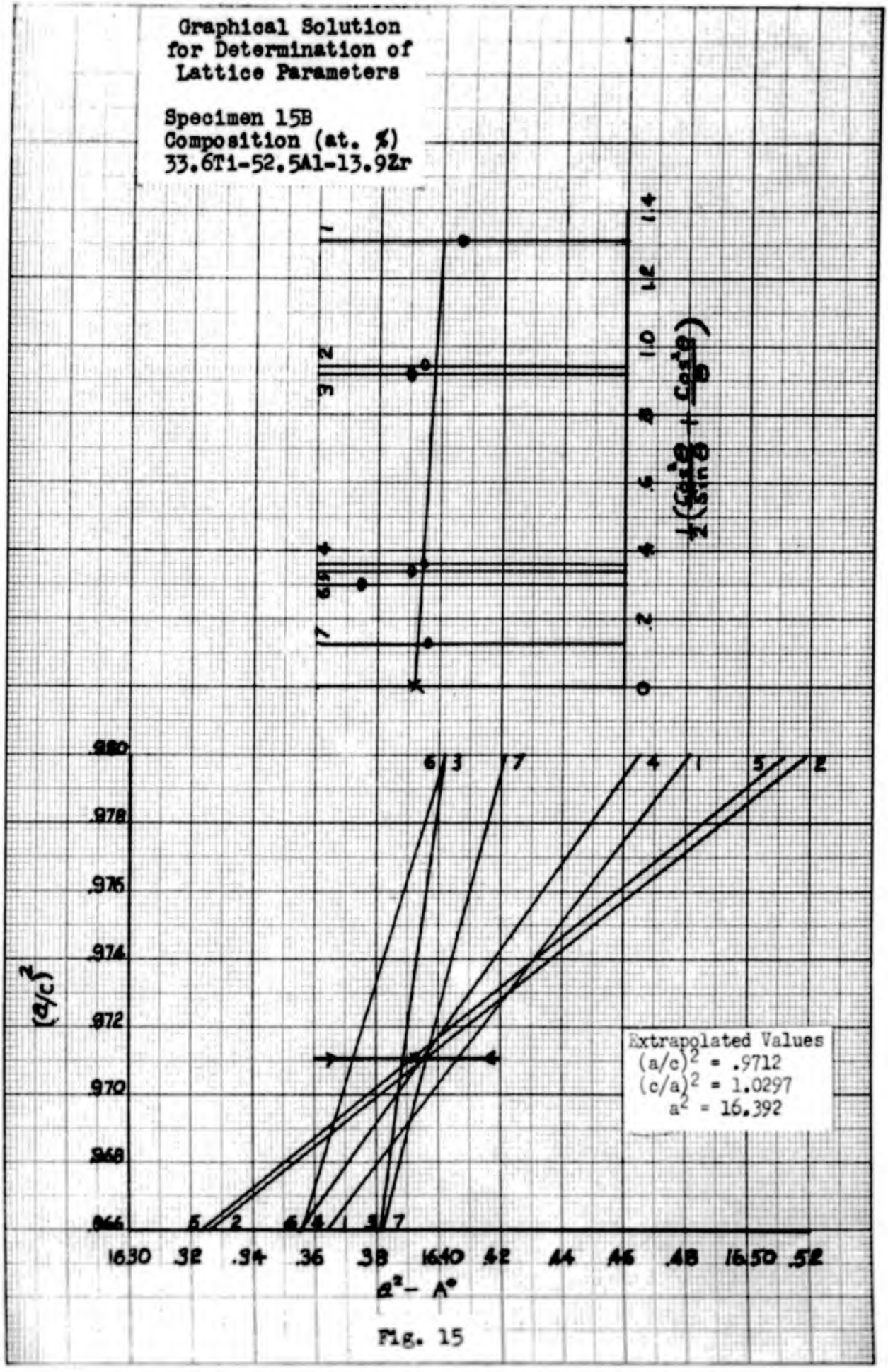
Graphical Solution
for Determination of
Lattice Parameters
Specimen 15B
Composition (at. %)
33.6Ti-52.5Al-13.9Zr
$\frac{1}{2}\left(\frac{\cos^2\theta}{\sin\theta}+\frac{\cos^2\theta}{\theta}\right)$
$(a/c)^2$
Extrapolated Values
$(a/c)^2$ = .9712
$(c/a)^2$ = 1.0297
a^2 = 16.392
a^2 - A°

Fig. 15

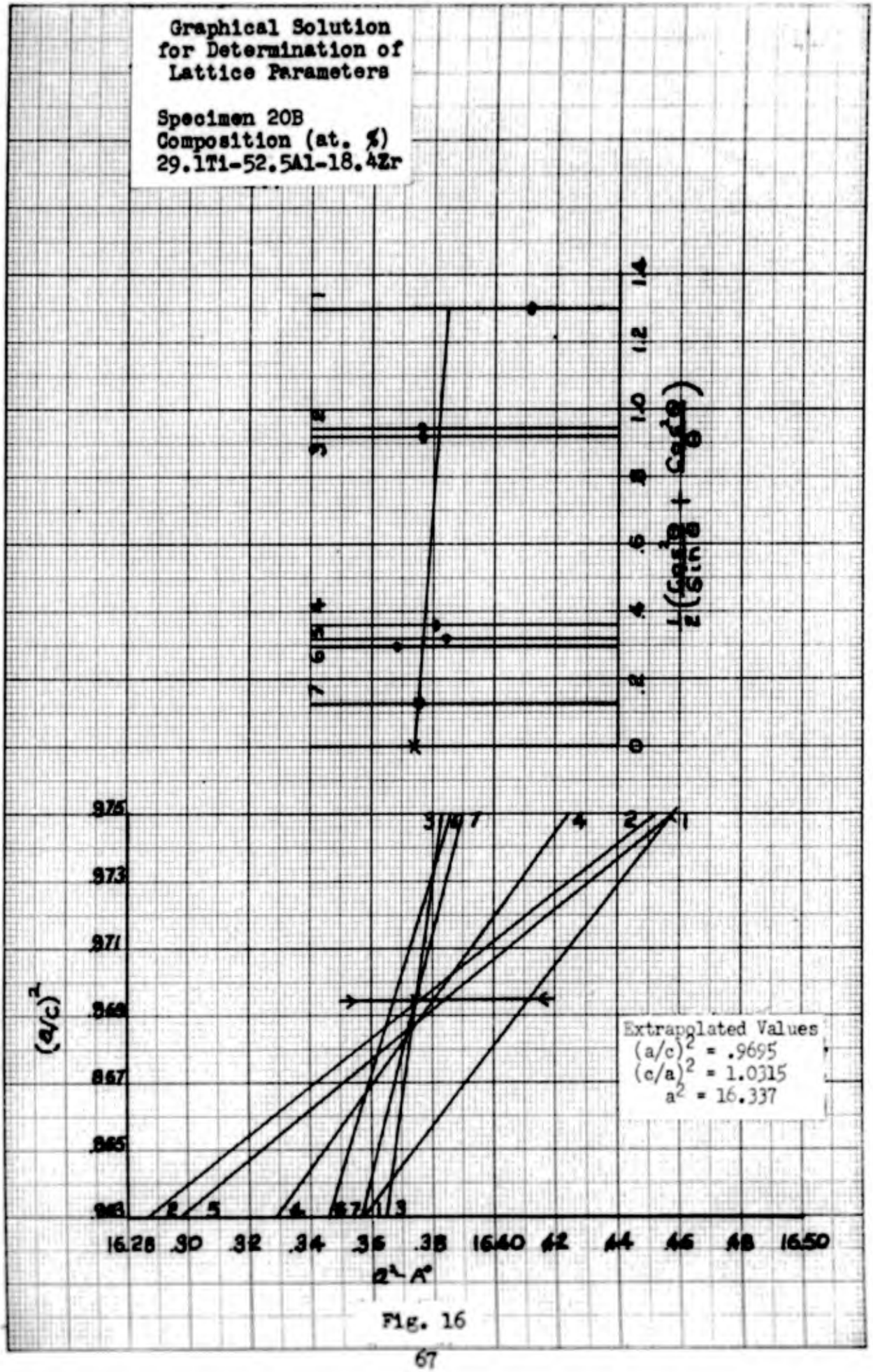
Graphical Solution
for Determination of
Lattice Parameters
Specimen 20B
Composition (at. %)
29.1Ti-52.5Al-18.4Zr
$\frac{1}{2}\left(\frac{\cos^2\theta}{\sin\theta} + \frac{\cos^2\theta}{\theta}\right)$
$(a/c)^2$
Extrapolated Values
$(a/c)^2$ = .9695
$(c/a)^2$ = 1.0315
a^2 = 16.337
a^2 A°

Fig. 16

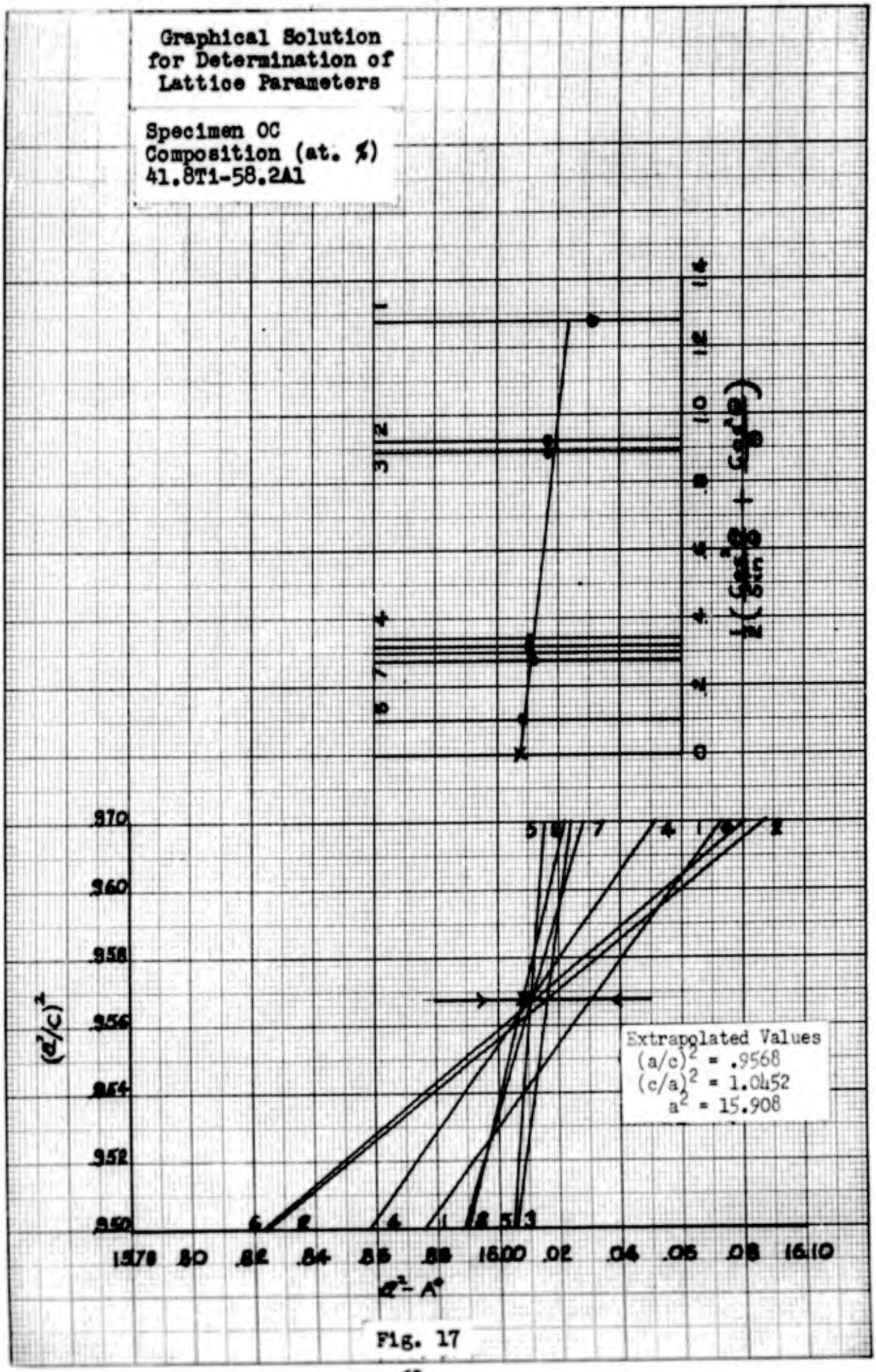
Graphical Solution
for Determination of
Lattice Parameters
Specimen OC
Composition (at. %)
41.8Ti-58.2Al
Extrapolated Values
(a/c)² = .9568
(c/a)² = 1.0452
a² = 15.908
(a²/c)²
α² - A²

Fig. 17

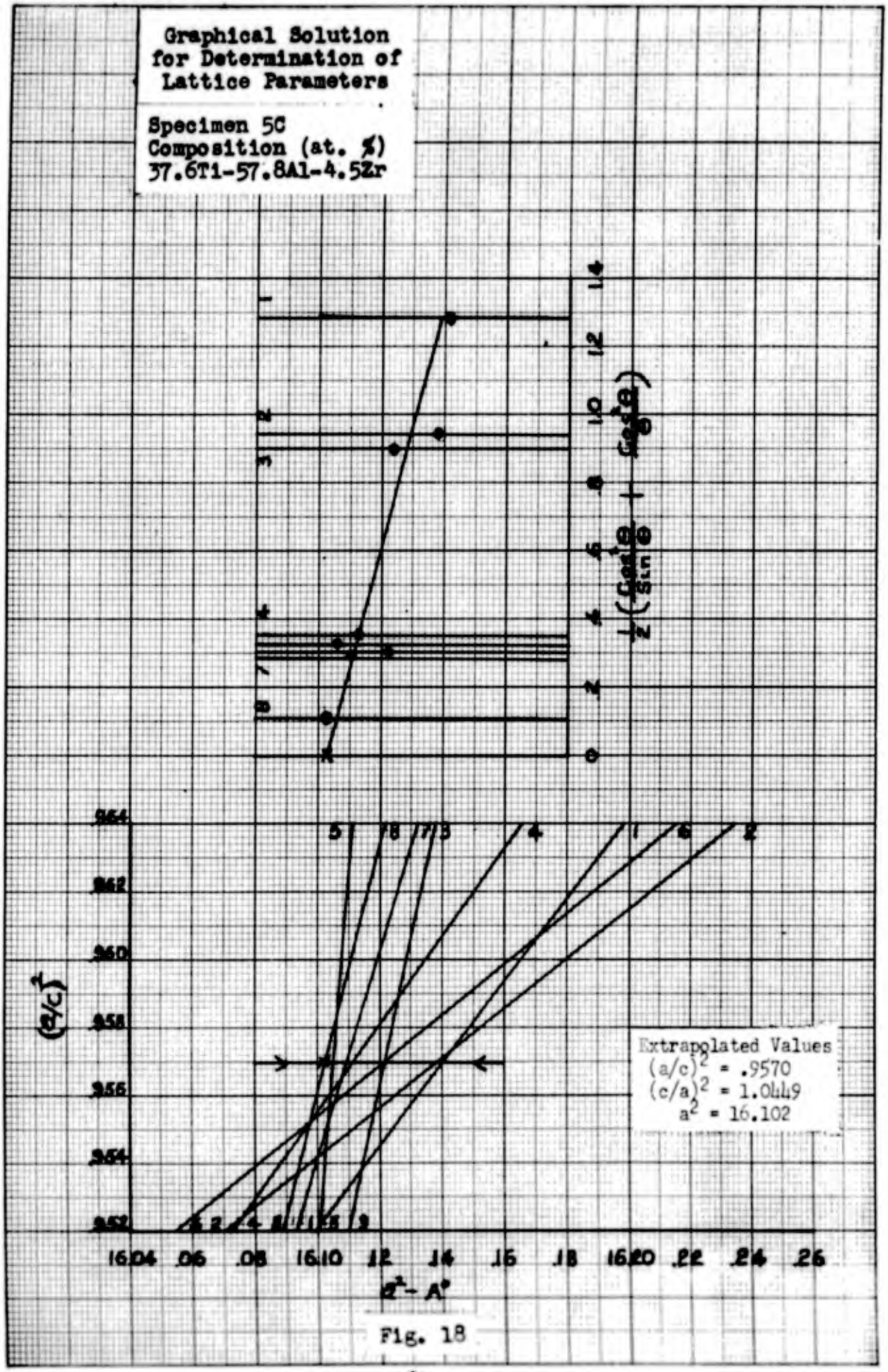
Graphical Solution
for Determination of
Lattice Parameters
Specimen 5C
Composition (at. %)
37.6Ti-57.8Al-4.5Zr
$\frac{1}{2}\left(\frac{\cos^2\theta}{\sin\theta} + \frac{\cos^2\theta}{\theta}\right)$
$(a/c)^2$
Extrapolated Values
$(a/c)^2$ = .9570
$(c/a)^2$ = 1.0449
a^2 = 16.102
$\theta^2 - A^2$

Fig. 18

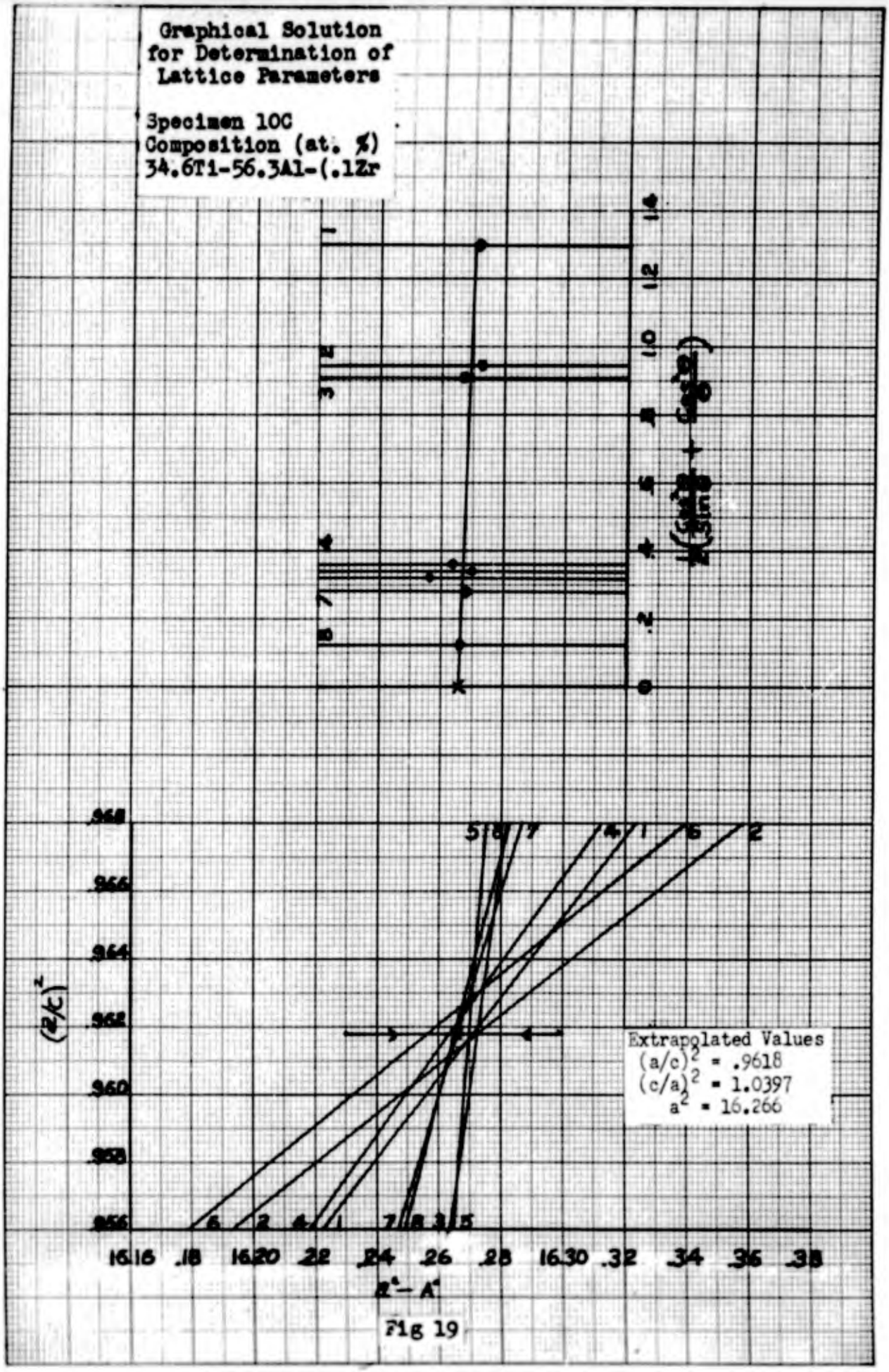
Graphical Solution
for Determination of
Lattice Parameters
Specimen 10C
Composition (at. %)
34.6Ti-56.3Al-(.1Zr
Extrapolated Values
$(a/c)^2$ = .9618
$(c/a)^2$ = 1.0397
a^2 = 16.266
$(2/c)^2$
$\lambda^2 - A^1$

Fig 19

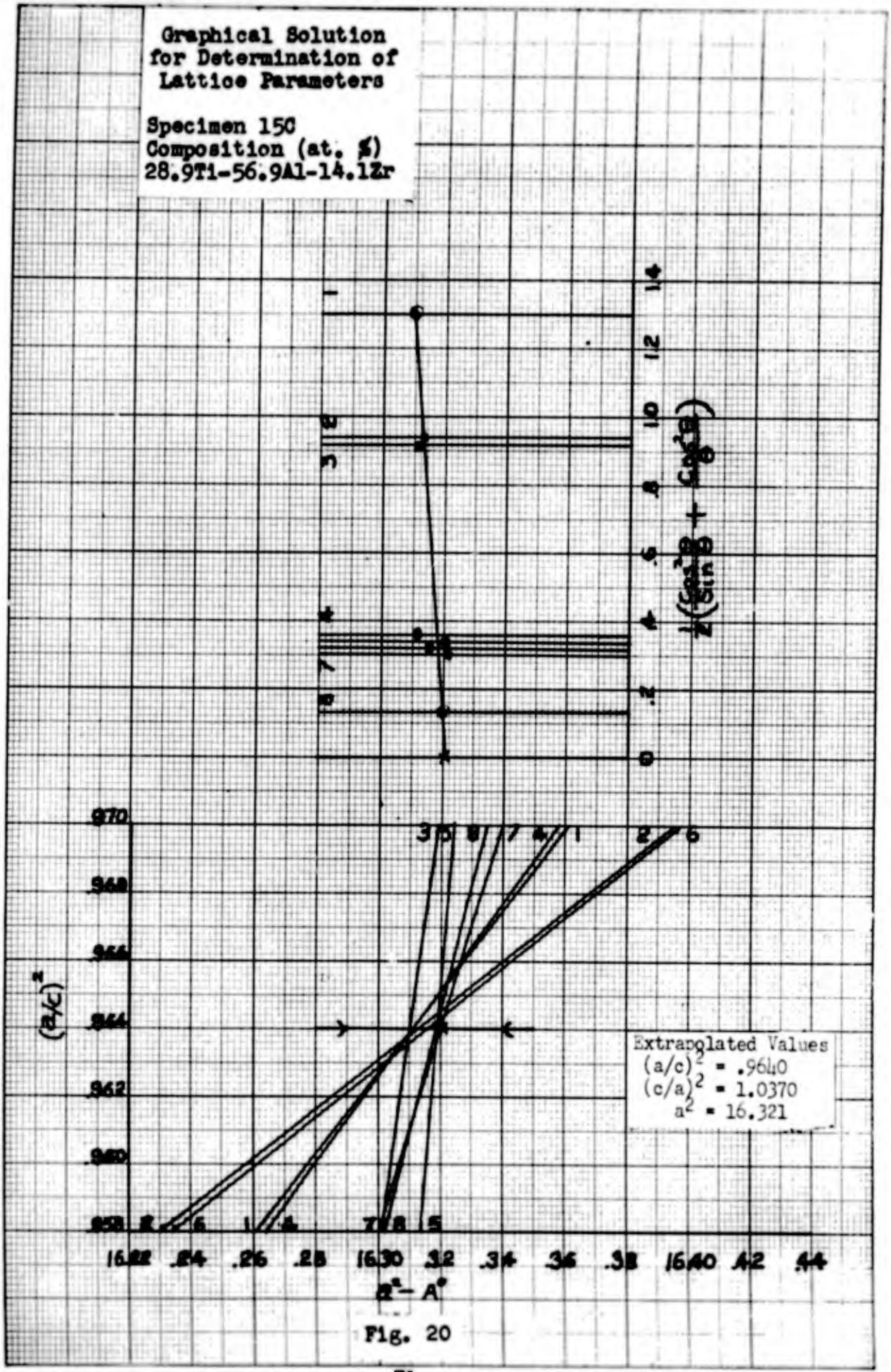
Graphical Solution
for Determination of
Lattice Parameters
Specimen 15C
Composition (at. %)
28.9Ti-56.9Al-14.1Zr
Extrapolated Values
(a/c)² = .9640
(c/a)² = 1.0370
a² = 16.321
(a/c)²
A²- A°

Fig. 20

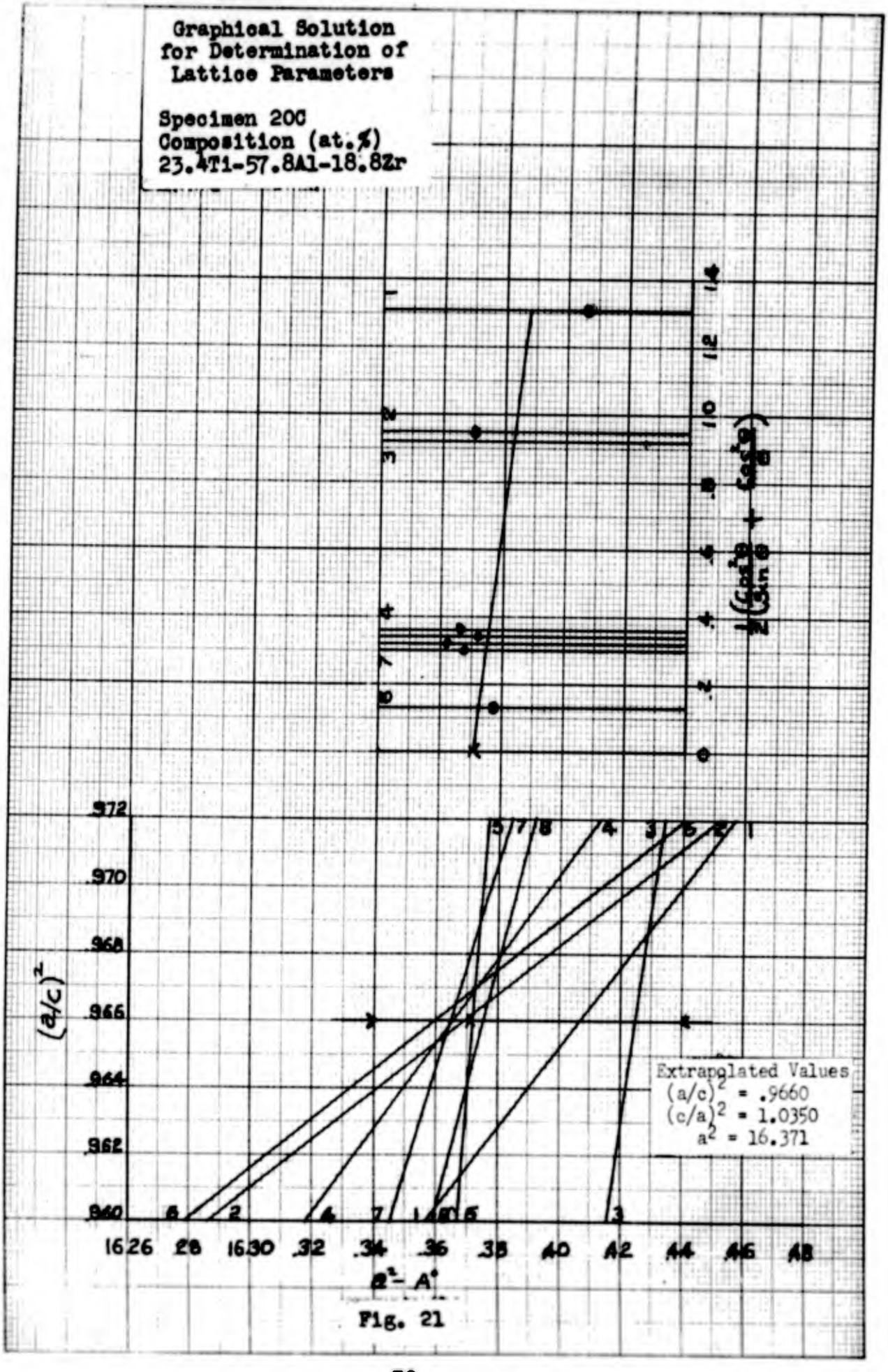
Graphical Solution
for Determination of
Lattice Parameters
Specimen 20C
Composition (at.%)
23.4Ti-57.8Al-18.8Zr
$\frac{1}{2}\left(\frac{\cos^2\theta}{\sin\theta} + \frac{\cos^2\theta}{\theta}\right)$
$(a/c)^2$
$\theta^2 - A^\circ$
Extrapolated Values
$(a/c)^2 = .9660$
$(c/a)^2 = 1.0350$
$a^2 = 16.371$

Fig. 21

Appendix E

Tabulation of 2θ Angles, Intensities, and Identities of Peaks Recorded From Diffractometer Patterns of Fifteen Titanium-Rich Specimens

Table	Specimen	Composition (Atomic %)	Page
XXIII	0A	51.4Ti - 48.6Al	74
	5A	47.8Ti - 47.6Al - 4.5Zr	
XXIV	10A	43.3Ti - 47.2Al - 9.5Zr	75
	15A	39.0Ti - 46.9Al - 14.1Zr	
XXV	20A	33.2Ti - 48.0Al - 18.8Zr	76
XXVI	0B	48.7Ti - 51.3Al	77
	5B	42.7Ti - 52.5Al - 4.8Zr	
XXVII	10B	38.6Ti - 52.2Al - 9.2Zr	78
	15B	33.6Ti - 52.5Al - 13.9Zr	
XXVIII	20B	29.1Ti - 52.5Al - 18.4Zr	79
XXIX	0C	41.8Ti - 58.2Al	80
	5C	37.6Ti - 57.8Al - 4.5Zr	
XXX	10C	34.6Ti - 56.3Al - 9.1Zr	81
	15C	28.9Ti - 56.9Al - 14.1Zr	
XXXI	20C	23.4Ti - 57.8Al - 18.8Zr	82

NOTE: 1) In the following tables, peaks with a dash in the identity column were not identified.

2) The intensity symbols have the following meanings:

VVS, most intense; VS, very strong; S, strong; M, medium; W, weak, VW, very weak.

TABLE XXIII

2θ Angles, Intensities, and Identities of Peaks for Specimens 0A and 5A

Specimen 0A				Specimen 5A			
Peak No.	2θ Value	Intensity	Identity	Peak No.	2θ Value	Intensity	Identity
1	21.80	W	γ(001)	1	21.70	M	γ(001)
2	31.65	W	γ(110)	2	31.40	W	γ(110)
3	35.95	M	α_2(200)	3	35.78	W	α_2(200)
4	38.75	VVS	γ(111)	4	38.40	VVS	γ(111)
5	41.00	VS	α_2(201)	5	40.80	VS	α_2(201)
6	44.50	M	γ(002)	6	44.30	M	γ(002)
7	45.40	S	γ(200)	7	44.98	S	γ(200)
8	50.80	W	γ(201)	8	50.40	W	γ(201)
9	54.80	M	α_2(202)	9	53.60	W	α_2(202)
10	64.40	W	α_2(220)	10	64.20	W	α_2(220)
11	65.30	M	γ(202)	11	64.85	M	γ(202)
12	66.35	M	γ(220)	12	65.40	M	γ(220)
13	74.40	M	α_2(203)	13	74.20	M	α_2(203)
14	76.80	M	γ(113)	14	77.48	M	γ(113)
15	79.30	M	γ(131)	15	78.40	M	γ(131)
16	83.10	W	γ(222)	16	82.30	W	γ(222)
17	98.23	W	γ(004)	17	97.50	W	γ(004)
18	100.00	M	γ(400)	18	99.70	W	γ(400)
19	104.55	W	α_2(403)	19	104.00	W	γ(403)
20	112.60	S	γ(313)	20	111.50	S	γ(313)
21	113.99	M	γ(331)	21	112.60	M	γ(331)
22	116.12	M	γ(204)	22	115.10	M	γ(204)
23	116.50	M	α_2(224)	23	115.80	M	α_2(224)
24	116.20	M	γ(402)	24	116.80	M	γ(402)
25	118.90	M	γ(420)	25	117.30	M	γ(420)
26	123.20	W	γ(422)	26	122.30	W	α_2(422)
27	123.70	W	-	27	123.30	W	-
28	124.00	W	-	28	124.00	W	-
29	137.33	M	γ(224)	29	136.90	M	γ(224)
30	140.30	S	γ(422)	30	138.00	S	γ(422)
31	145.25	M	α_2(423)	31	142.80	M	α_2(423)
32	158.20	W	γ(115)	32	156.30	W	γ(115)
33	159.30	M	α_2(602)	33	159.00	M	α_2(602)

TABLE XXIV

2θ Angles, Intensities, and Identities of Peaks for Specimens 10A and 15A

Specimen 10A				Specimen 15A			
Peak No.	2θ Value	Intensity	Identity	Peak No.	2θ Value	Intensity	Identity
1	21.70	W	γ(001)	1	21.60	M	γ(001)
2	26.00	W	-	2	27.75	M	∅
3	27.90	W	∅	3	31.05	M	γ(110)
4	31.30	W	γ(110)	4	33.00	W	∅
5	33.30	VW	∅	5	34.35	M	∅
6	34.50	M	∅	6	35.60	M	∅
7	35.70	M	∅	7	38.25	VVS	γ(111)
8	35.80	M	α_2(200)	8	39.10	W	∅
9	38.40	VS	γ(111)	9	40.20	M	∅
10	39.30	W	∅	10	40.65	W	α_2(201)
11	40.45	M	∅	11	44.20	M	γ(002)
12	40.75	S	α_2(201)	12	44.55	S	γ(200)
13	44.20	M	γ(002)	13	50.00	W	γ(201)
14	44.90	S	γ(200)	14	55.00	VW	-
15	50.30	W	γ(201)	15	57.35	VW	-
16	53.50	W	α_2(202)	16	62.50	VW	-
17	64.25	W	α_2(220)	17	63.90	VW	γ(220)
18	64.80	M	γ(202)	18	64.55	M	γ(202)
19	65.30	W	γ(220)	19	77.20	W	γ(113)
20	71.30	W	α_2(203)	20	77.80	M	γ(131)
21	77.35	W	γ(113)	21	81.80	VW	γ(220)
22	78.35	M	γ(131)	22	110.80	S	γ(313)
23	82.15	VW	γ(222)	23	111.25	S	-
24	103.90	W	α_2(403)	24	114.75	S	-
25	111.28	S	γ(313)	25	115.70	S	γ(420)
26	112.30	M	γ(331)	26	135.00	W	γ(224)
27	114.82	M	-	27	135.95	S	γ(422)
28	115.62	M	γ(204)				
29	116.50	M	α_2(224)				
30	117.00	M	γ(420)				
31	135.50	W	-				
32	137.50	M	γ(224)				
33	141.45	S	γ(422)				
34	143.49	M	α_2(423)				

TABLE XXV

2θ Angles, Intensities, and Identities of Peaks for Specimen 20A

Specimen 20A

Peak No.	2θ Value	Intensity	Identity
1	12.75	W	-
2	21.58	M	γ(001)
3	27.70	M	ø
4	31.00	M	γ(110)
5	33.00	M	ø
6	33.60	W	-
7	34.25	M	ø
8	35.55	M	ø
9	36.50	W	-
10	38.19	VVS	γ(111)
11	39.06	W	-
12	39.58	W	-
13	40.20	S	ø
14	44.10	M	γ(002)
15	44.50	S	γ(200)
16	57.30	W	-
17	57.40	W	-
18	61.50	W	-
19	62.35	W	-
20	62.50	W	-
21	63.85	W	-
22	64.40	W	-
23	64.70	W	γ(202)
24	77.20	W	γ(113)
25	77.75	W	γ(131)
26	110.60	M	γ(313)
27	113.00	M	-
28	114.55	W	-
29	135.90	W	γ(224)
30	136.60	M	γ(422)

TABLE XXVI

2θ Angles, Intensities, and Identities of Peaks for Specimens 0B and 5B

Specimen 0B				Specimen 5B			
Peak No.	2θ Value	Intensity	Identity	Peak No.	2θ Value	Intensity	Identity
1	12.90	W	-	1	21.66	M	γ(001)
2	21.75	M	γ(001)	2	31.43	M	γ(110)
3	31.65	M	γ(110)	3	38.51	VVS	γ(111)
4	38.75	VVS	γ(111)	4	44.19	M	γ(002)
5	40.10	M	-	5	45.06	S	γ(200)
6	44.35	S	γ(002)	6	50.54	W	γ(201)
7	45.35	S	γ(200)	7	55.20	W	γ(112)
8	50.90	W	γ(201)	8	64.93	S	γ(202)
9	55.55	W	γ(112)	9	65.60	M	γ(220)
10	65.32	S	γ(202)	10	77.47	M	γ(113)
11	66.08	M	γ(220)	11	78.72	M	γ(131)
12	66.25	W	-	12	82.53	W	γ(222)
13	77.92	M	γ(113)	13	91.10	VW	γ(312)
14	79.31	M	γ(131)	14	100.22	M	γ(400)
15	83.08	W	γ(222)	15	111.91	VS	γ(313)
16	100.86	M	γ(400)	16	113.26	M	γ(331)
17	112.46	VS	γ(313)	17	115.35	M	γ(204)
18	113.98	M	γ(331)	18	117.41	M	γ(402)
19	114.45	M	γ(204)	19	118.05	M	γ(420)
20	115.85	M	-	20	136.18	M	γ(224)
21	118.18	M	γ(420)	21	138.89	S	γ(422)
22	119.41	M	-	22	156.36	M	γ(115)
23	137.21	M	γ(224)				
24	140.32	S	γ(422)				

TABLE XXVII

2θ Angles, Intensities, and Identities of Peaks for Specimens 10B and 15B

Specimen 10B				Specimen 15B			
Peak No.	2θ Value	Intensity	Identity	Peak No.	2θ Value	Intensity	Identity
1	21.65	M	γ(001)	1	12.80	VW	-
2	31.28	M	γ(110)	2	21.65	M	γ(001)
3	34.56	VW	ø	3	27.85	W	ø
4	36.37	VVS	γ(111)	4	31.20	M	γ(110)
5	40.39	VW	ø	5	33.20	W	ø
6	44.12	M	γ(002)	6	33.80	M	ε
7	44.85	S	γ(200)	7	34.45	W	ø
8	50.35	VW	γ(201)	8	36.55	M	ε
9	55.05	VW	γ(112)	9	38.30	VS	γ(111)
10	64.60	S	γ(202)	10	39.75	M	ø
11	65.28	W	γ(220)	11	40.30	M	ε + ø
12	77.18	M	γ(113)	12	40.45	M	ø
13	78.21	M	γ(131)	13	44.00	M	γ(002)
14	82.15	W	γ(222)	14	44.75	S	γ(200)
15	90.48	W	γ(312)	15	50.15	Vw	γ(201)
16	97.20	W	γ(004)	16	64.60	M	γ(202)
17	99.35	W	γ(400)	17	65.10	W	γ(220)
18	111.08	S	γ(313)	18	77.15	W	γ(113)
19	112.25	M	γ(331)	19	78.10	W	γ(131)
20	114.58	M	γ(204)	20	82.00	W	γ(222)
21	116.30	M	γ(402)	21	99.10	W	γ(400)
22	134.95	M	γ(224)	22	110.90	S	γ(313)
23	137.29	S	γ(422)	23	112.00	M	γ(331)
24	154.70	W	γ(115)	24	114.50	M	γ(204)
				25	116.10	M	γ(402)
				26	116.60	M	γ(420)
				27	118.60	M	-
				28	134.70	W	γ(224)
				29	136.80	M	γ(422)

TABLE XXVIII

2θ Angles, Intensities and Identities of Peaks for Specimen 20B

Specimen 20B

Peak No.	2θ Value	Intensity	Identity
1	12.85	W	-
2	19.30	W	ϵ
3	20.38	W	ϵ
4	21.63	M	γ(001)
5	21.89	W	ϵ
6	27.87	W	ϕ
7	28.32	W	ϵ
8	31.25	M	γ(110)
9	33.20	W	ϕ
10	33.77	M	ϵ
11	34.45	W	ϕ
12	35.70	W	ϕ
13	36.59	S	ϵ
14	38.35	VS	γ(111)
15	39.20	W	ϕ
16	39.75	S	ϕ
17	40.35	S	ϵ or ϕ
18	40.55	W	ϕ
19	44.08	M	γ(002)
20	44.78	S	γ(200)
21	64.52	M	γ(202)
22	64.58	W	γ(220)
23	67.30	W	-
24	70.92	W	-
25	76.90	W	γ(113)
26	78.16	M	γ(131)
27	82.00	W	γ(222)
28	82.55	W	-
29	97.00	M	-
30	102.00	M	-
31	104.10	M	-
32	107.00	M	-
33	117.00	M	γ(313)
34	114.30	M	γ(204)
35	116.30	M	γ(402)
36	116.70	M	γ(420)
37	134.70	W	γ(224)
38	135.90	M	γ(422)

TABLE XXIX

2θ Angles, Intensities, and Identities of Peaks for Specimens 0C and 5C

Specimen 0C				Specimen 5C			
Peak No.	2θ Value	Intensity	Identity	Peak No.	2θ Value	Intensity	Identity
1	21.72	M	γ(001)	1	21.61	M	γ(001)
2	31.65	M	γ(110)	2	31.47	M	γ(110)
3	38.75	VVS	γ(111)	3	38.53	VVS	γ(111)
4	44.32	S	γ(002)	4	44.05	M	γ(002)
5	45.36	VS	γ(200)	5	45.09	S	γ(200)
6	50.85	VW	γ(201)	6	50.53	M	γ(201)
7	55.49	VW	γ(112)	7	55.15	VW	γ(112)
8	65.35	M	γ(202)	8	64.88	M	γ(202)
9	66.17	W	γ(220)	9	65.72	W	γ(220)
10	77.95	M	γ(113)	10	77.30	W	γ(113)
11	79.45	S	γ(131)	11	78.84	M	γ(131)
12	83.15	W	γ(222)	12	82.58	V	γ(222)
13	91.73	VW	γ(312)	13	91.05	VW	γ(312)
14	98.07	W	γ(004)	14	101.38	W	γ(400)
15	101.11	W	γ(400)	15	111.74	VS	γ(313)
16	112.78	VS	γ(313)	16	113.35	M	γ(331)
17	114.43	S	γ(331)	17	114.95	M	γ(204)
18	116.02	M	γ(204)	18	117.37	M	γ(402)
19	118.57	S	γ(402)	19	118.22	M	γ(420)
20	119.43	S	γ(420)	20	122.90	VW	-
21	124.26	VW	-	21	135.85	W	γ(224)
22	137.52	M	γ(224)	22	138.08	VS	γ(422)
23	141.01	VS	γ(422)	23	155.30	W	γ(115)
24	151.69	M					

TABLE XXX

2θ Angles, Intensities and Identities of Peaks for Specimens 10C and 15C

Specimen 10C				Specimen 15C			
Peak No.	2θ Value	Intensity	Identity	Peak No.	2θ Value	Intensity	Identity
1	21.62	M	γ(001)	1	19.31	W	ε
2	31.40	M	γ(110)	2	20.36	W	ε
3	33.90	W	ε	3	21.59	M	γ(001)
4	36.70	W	ε	4	21.87	W	ε
5	38.40	VVS	γ(111)	5	28.20	V	ε
6	39.90	W	ε	6	31.31	M	γ(110)
7	44.08	M	γ(002)	7	33.82	M	ε
8	44.95	S	γ(200)	8	36.56	S	ε
9	50.40	W	γ(201)	9	38.35	VS	γ(111)
10	55.05	W	γ(112)	10	39.22	VW	ε
11	64.68	M	γ(202)	11	39.80	S	ε
12	65.40	W	γ(220)	12	40.63	W	ε
13	77.12	W	γ(113)	13	41.35	VW	-
14	78.42	M	γ(131)	14	44.03	W	γ(002)
15	84.20	W	-	15	44.88	S	γ(200)
16	97.20	W	γ(004)	16	50.30	W	γ(201)
17	99.60	W	γ(400)	17	55.00	VW	γ(112)
18	111.20	S	γ(313)	18	62.27	W	-
19	112.55	M	γ(331)	19	64.62	M	γ(202)
20	114.60	M	γ(204)	20	65.36	W	γ(220)
21	116.60	M	γ(402)	21	67.35	W	-
22	117.30	M	γ(420)	22	77.05	W	γ(113)
23	135.00	M	γ(224)	23	78.32	W	γ(131)
24	137.72	S	γ(422)	24	82.06	W	γ(222)
25	154.45	M	γ(115)	25	96.88	W	γ(004)
26	161.30	M	-	26	99.45	M	γ(400)
				27	100.50	W	-
				28	102.10	M	-
				29	104.16	M	-
				30	106.90	W	-
				31	110.95	S	γ(313)
				32	112.25	M	γ(133)
				33	114.35	M	γ(204)
				34	116.45	M	γ(402)
				35	116.91	M	γ(420)
				36	126.32	W	-
				37	134.70	M	γ(224)
				38	137.28	S	γ(422)
				39	153.85	W	γ(115)

TABLE XXXI

2θ Angles, Intensities, and Identities of Peaks for Specimen 20C

Specimen 20C

Peak No.	2θ Value	Intensity	Identity	Peak No.	2θ Value	Intensity	Identity
1	19.30	M	ε	25	77.25	W	-
2	20.32	M	ε	26	77.65	W	-
3	21.58	M	γ(001)	27	78.20	W	γ(131)
4	21.85	V	ε	28	81.96	W	γ(222)
5	28.15	M	ε	29	82.60	W	-
6	31.30	M	γ(110)	30	96.90	W	-
7	33.78	VS	ε	31	97.20	W	-
8	36.55	VS	ε	32	99.45	M	γ(400)
9	38.32	VVS	γ(111)	33	100.35	M	-
10	39.20	W	ε	34	102.02	M	-
11	39.72	VS	ε	35	102.37	W	-
12	40.55	S	ε	36	104.02	S	-
13	41.42	W	-	37	110.88	S	γ(313)
14	44.00	W	γ(002)	38	112.07	M	γ(331)
15	44.80	S	γ(200)	39	113.00	M	-
16	56.35	W	-	40	114.32	M	γ(204)
17	60.35	W	-	41	116.17	M	γ(402)
18	62.18	M	-	42	116.85	M	γ(420)
19	64.38	M	-	43	117.22	W	-
20	64.55	M	γ(202)	44	120.14	M	-
21	65.18	M	γ(220)	45	121.60	W	-
22	67.30	W	-	46	126.04	M	-
23	70.97	W	-	47	134.51	W	γ(224)
24	77.00	W	γ(113)	48	136.40	M	γ(422)

Appendix F

Photomicrographs of Ti-Al-Zr Alloys

This appendix contains the photomicrographs of most of the alloys studied in this investigation.

Figure	Specimen	Composition (Atomic %)	Page
22	0A	51.4Ti-48.6Al	84
23	5A	47.8Ti-47.6Al- 4.5Zr	84
24	15A	39.0Ti-46.9Al-14.1Zr	85
25	20A	33.2Ti-48.0Al-18.8Zr	85
26	25A	30.2Ti-46.2Al-23.6Zr	86
27	35A	19.5Ti-46.1Al-34.4Zr	86
28	45A	9.0Ti-46.6Al-44.4Zr	87
29	50A	4.0Ti-46.4Al-49.6Zr	87
30	55A	46.2Al-53.8Zr	88
31	55AA	46.2Al-53.8Zr	88
32	0B	48.7Ti-51.3Al	89
33	5B	42.7Ti-52.5Al- 4.8Zr	89
34	10B	38.6Ti-52.2Al- 9.2Zr	90
35	15B	33.6Ti-52.5Al-13.9Zr	90
36	20B	29.1Ti-52.5Al-18.4Zr	91
37	25B	26.3Ti-50.9Al-22.8Zr	92
38	30B	19.6Ti-51.3Al-29.1Zr	92
39	35B	13.8Ti-51.6Al-34.6Zr	93
40	40B	9.3Ti-51.0Al-39.7Zr	93
41	50B	51.4Al-48.6Zr	94
42	50BH	51.4Al-48.6Zr	94
43	50BA	51.4Al-48.6Zr	95
44	50B	51.4Al-48.6Zr	96
45	50BA	51.4Al-48.6Zr	96
46	20C	23.4Ti-57.8Al-18.8Zr	97
47	20CA	23.4Ti-57.8Al-18.8Zr	97
48	25C	18.7Ti-56.6Al-24.7Zr	98
49	35C	9.6Ti-56.1Al-34.2Zr	98
50	45C	56.0Al-44.0Zr	99
51	45CA	56.0Al-44.0Zr	99

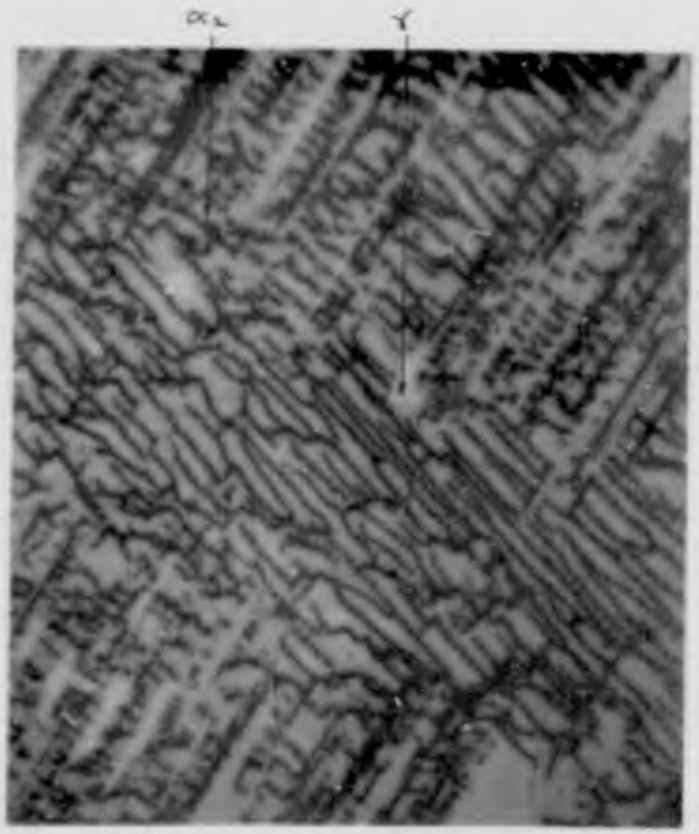

Fig. 22

0A(51.4Ti-48.6Al).2000°F for 39 hrs. Air cooled. X-ray patterns indicate α_2 and γ phases present. 1800x.

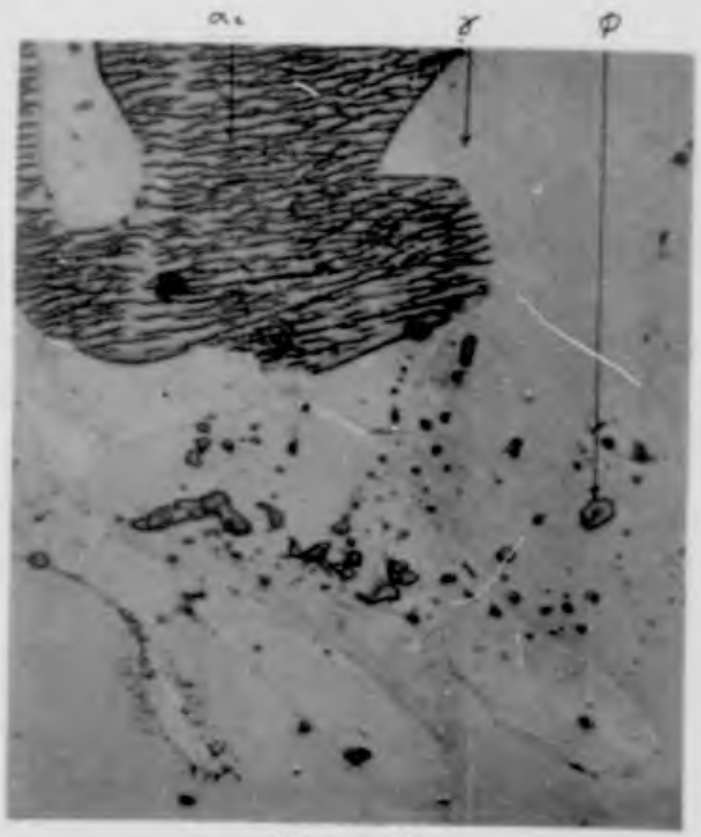

Fig. 23

5A(47.8Ti-47.6Al-4.5Zr). 2000°F for 39 hrs. Air cooled. X-ray patterns indicate α_2, γ, and ϕ phases present. 1325x.

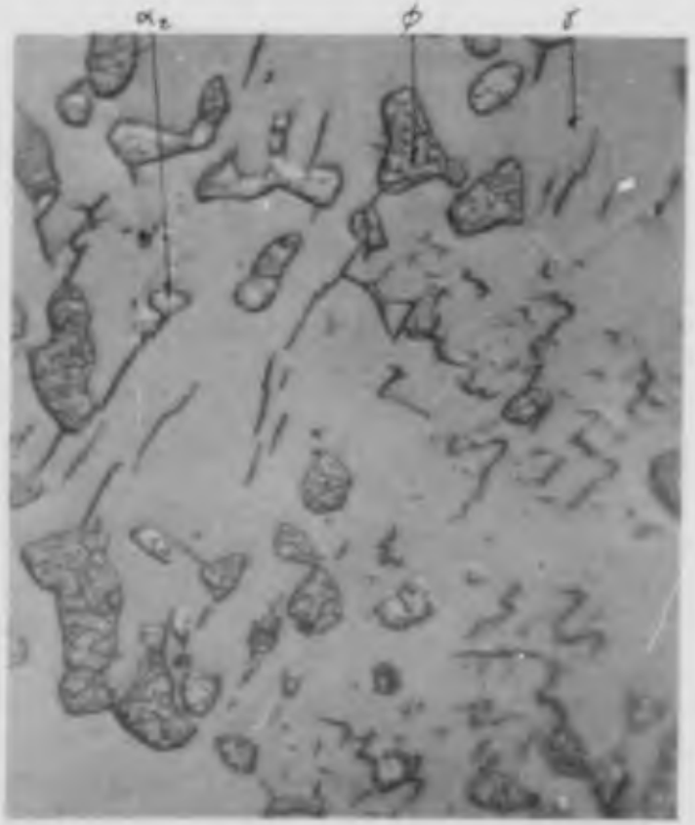

Fig. 24

15A(39.0Ti-46.9Al-14.1Zr). 2000°F for 39 hrs. Air cooled. X-ray patterns indicate α_2, γ, and ϕ phases present. 1800x.

Fig. 25

20A(33.2Ti-48.0Al-18.8Zr). 2000°F for 39 hrs. Air cooled. X-ray pattern indicates γ, ϕ, and ϵ phases present. 1800x.

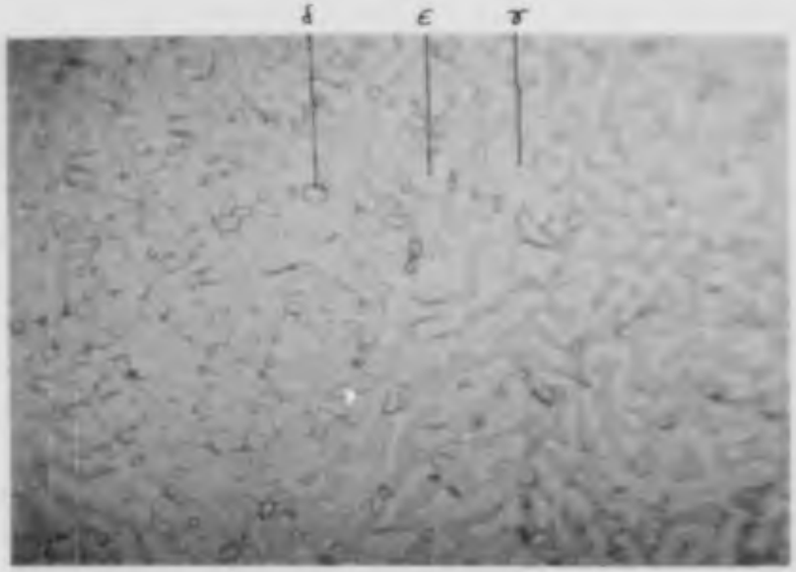

Fig. 26

25A(30.2Ti-46.2Al-23.6Zr). 2000°F for 48 hrs. Water quenched. X-ray pattern indicates γ, ϵ, and δ phases present. 750x.

Fig. 27

35A(19.5Ti-46.1Al-34.4Zr). 2000°F for 48 hrs. Water quenched. X-ray pattern indicates γ and ϵ phases present. 750x.

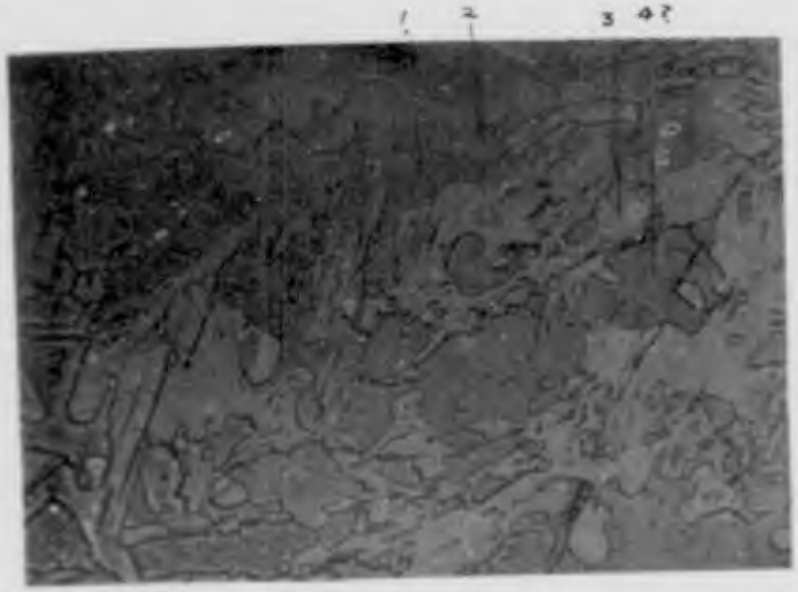

Fig. 28

45A(9.0Ti-46.6Al-44.4Zr). 2000°F for 48 hrs. Water quenched. X-ray pattern indicates Zr_4Al_3, ZrAl, and ϵ phases present. 2320x.

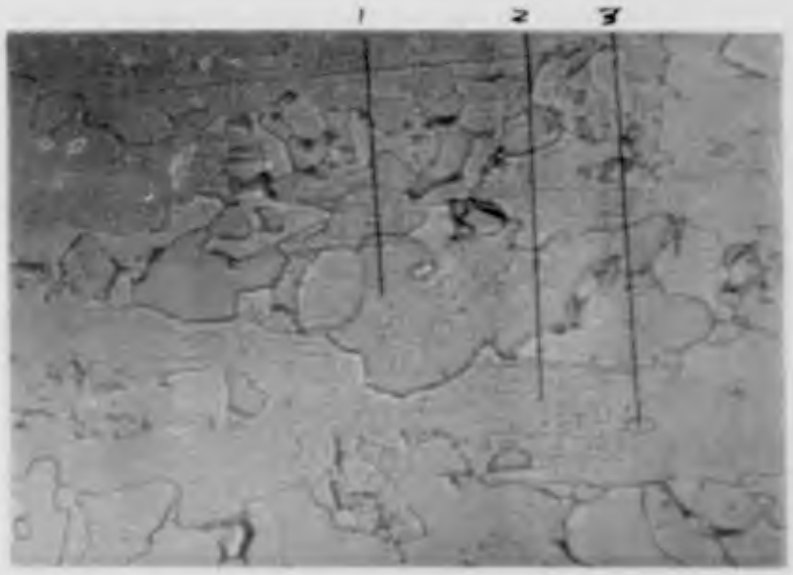

Fig. 29

50A(4.0Ti-46.4Al-49.6Zr). 2000°F for 48 hrs. Water quenched. X-ray pattern indicates Zr_4Al_3, Zr_2Al_3, and ZrAl present. 2000x.

The numbers in the borders of these and some of the following photomicrographs indicate the number of phases visually observed in the microstructures.

Fig. 30

55A(46.2Al-53.8Zr). 2000°F for 48 hrs. Water quenched. X-ray pattern indicates Zr_4Al_3 , Zr_2Al_3, and ZrAl present. 2000x.

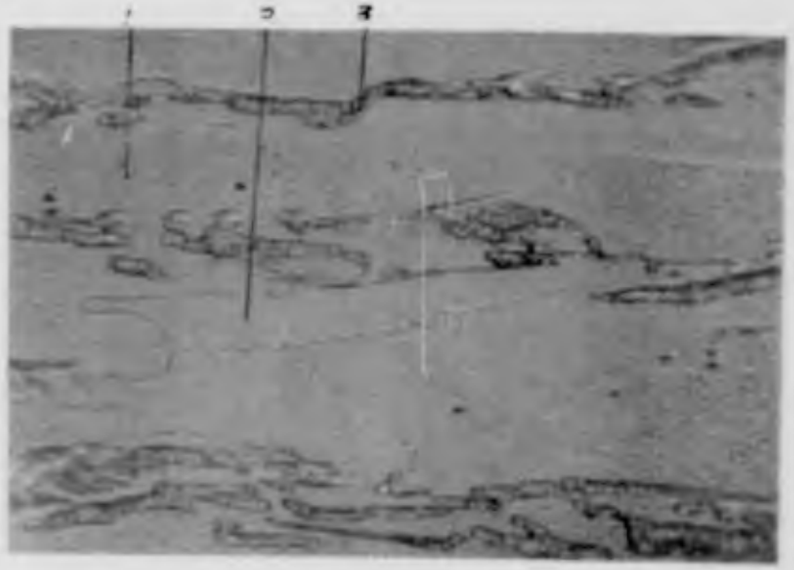

Fig. 31

55AA(46.2Al-53.8Zr). As-cast. X-ray pattern indicates Zr_4Al_3, Zr_2Al_3, Zr_3Al_2, and α-zirconium present. 2000x.

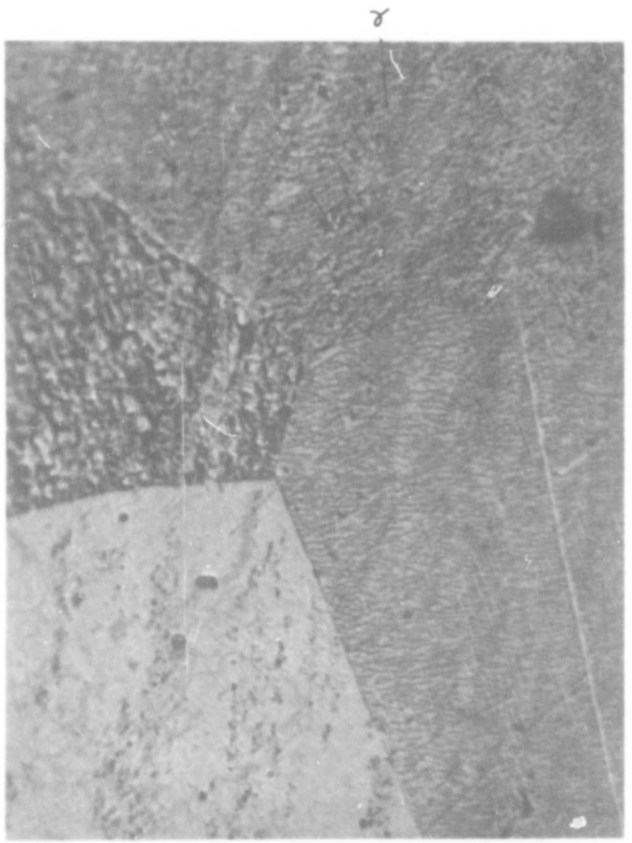

Fig 32

0B(48.7Ti-51.3Al). 2000°F for 39 hrs. Air cooled. X-ray pattern indicates Y phase present. 1800x.

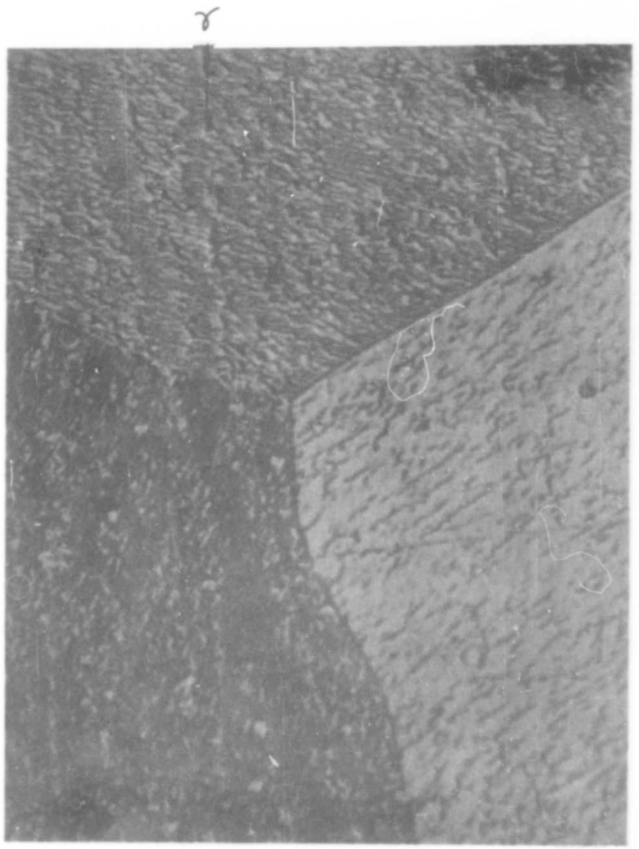

Fig. 33

5B(42.7Ti-52.5Al-4.8Zr). 2000°F for 39 hrs. Air cooled. X-ray pattern indicates Y phase present. 1800x.

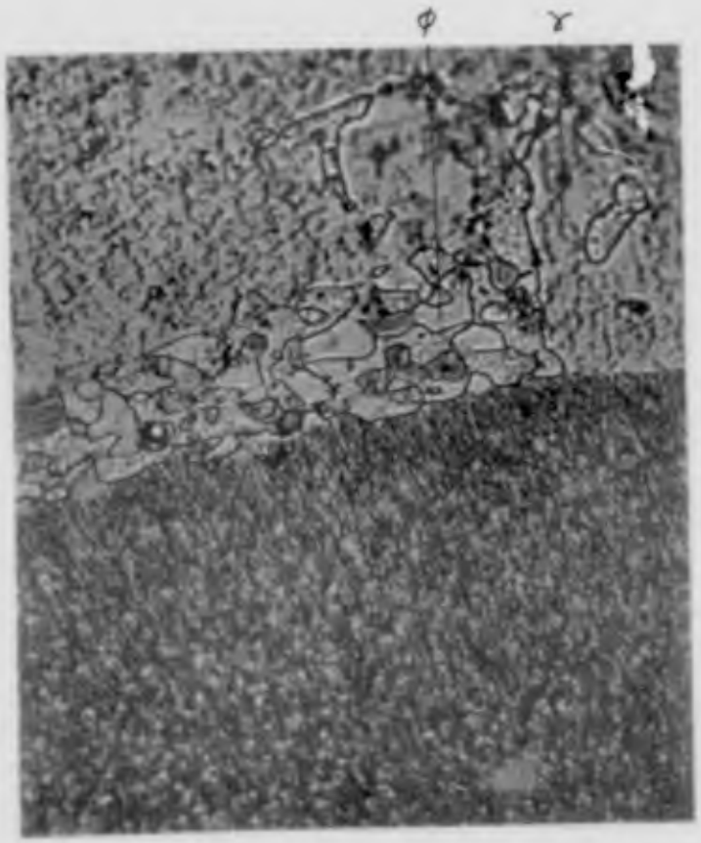

Fig. 34

10B(38.6Ti-52.2Al-9.2Zr). 2000°F for 40½ hrs. Air cooled. X-ray pattern indicates γ and ϕ phases present. 1800x.

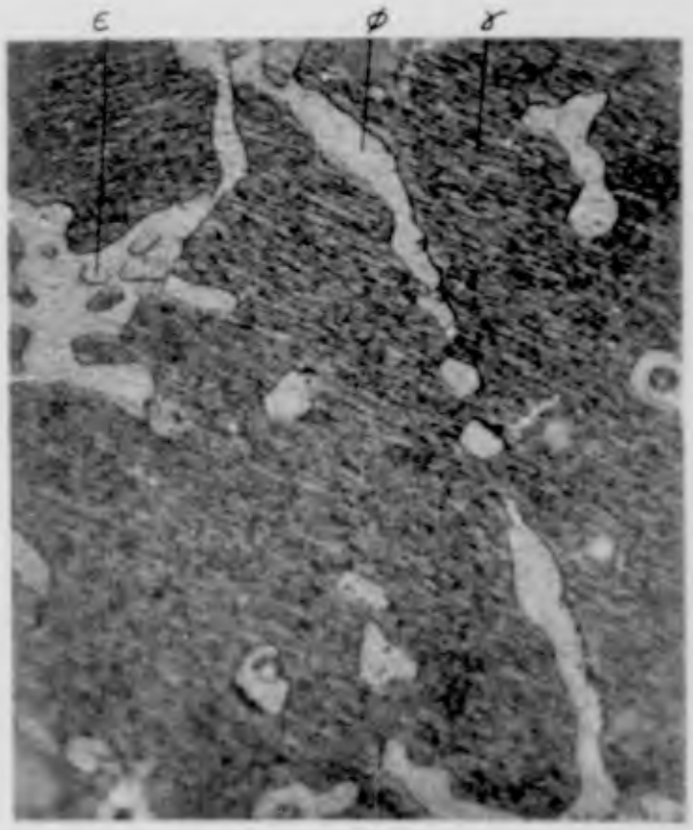

Fig. 35

15B(33.6Ti-52.5Al-13.9Zr). 2000°F for 40½ hrs. Air cooled. X-ray pattern indicates γ , ϕ , and ϵ phases present. 1800x.

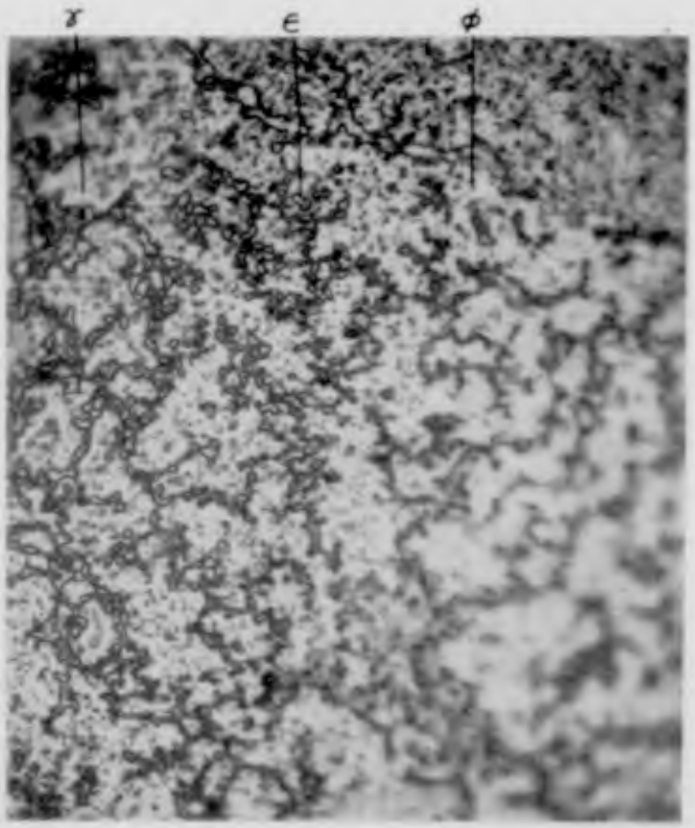

Fig. 36

20B(29.1Ti-52.5Al-18.4Zr). 2000°F for 40½ hrs. Air cooled. X-ray pattern indicates γ, ϕ, and ϵ phases present. 720x.

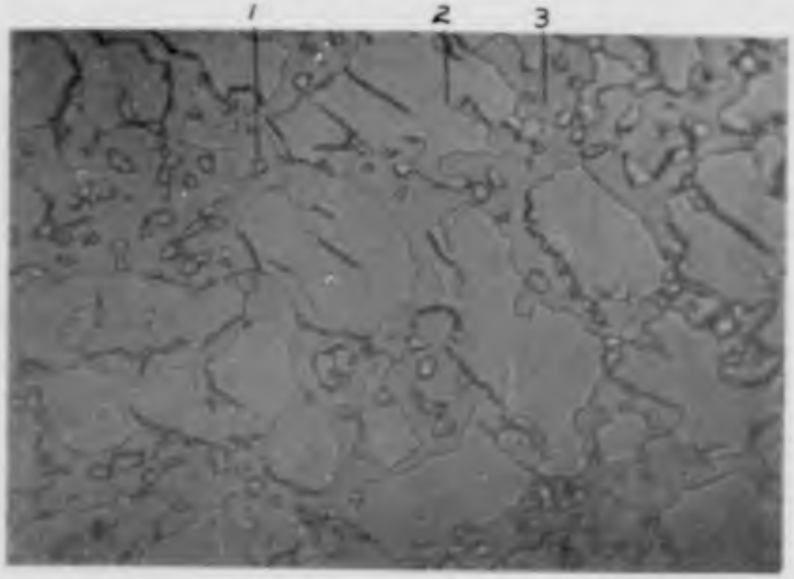

Fig. 37

25B(26.3Ti-50.9Al-22.8Zr). 2000°F for 48 hrs. Water quenched. X-ray pattern indicates γ, ϕ, and ϵ phases present. 2000x.

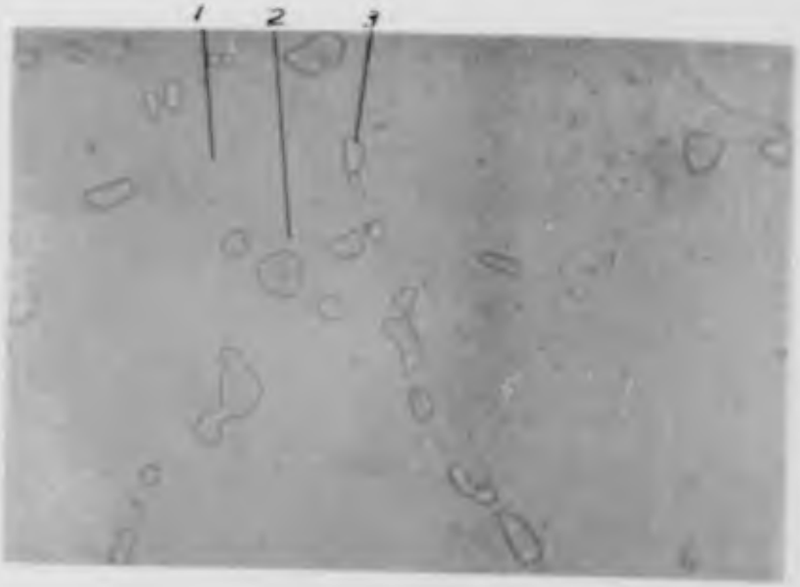

Fig. 38

30B(19.6Ti-51.3Al-29.1Zr). 2000°F for 48 hrs. Water quenched. X-ray pattern indicates γ and ϵ phases present. 2000x.

Fig. 39

35B(13.8Ti-51.6Al-34.6Zr). 2000°F for 48 hrs. Water quenched. X-ray pattern indicates ϵ phase and possibility of another unknown phase. 750x.

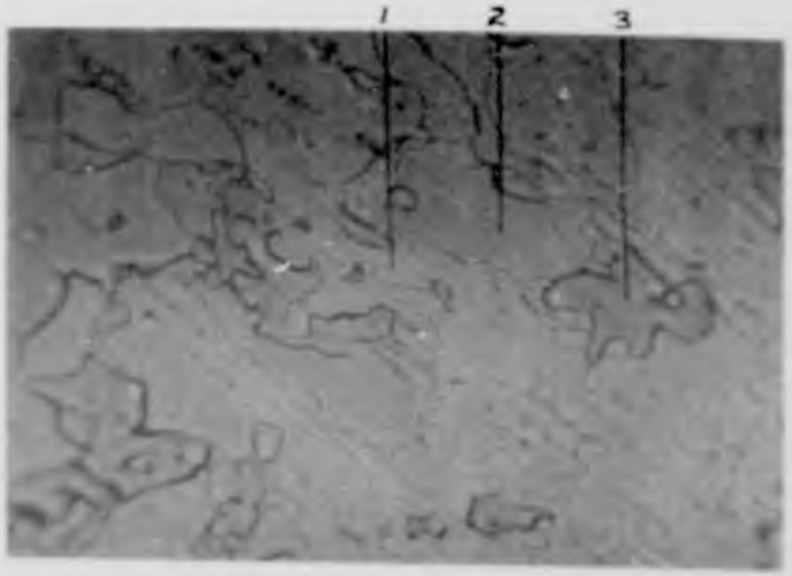

Fig. 40

40B(9.3Ti-51.0Al-39.7Zr). 2000°F for 48 hrs. Water quenched. X-ray pattern indicates ϵ, Zr_2Al_3, and ZrAl phases present. 2000x.

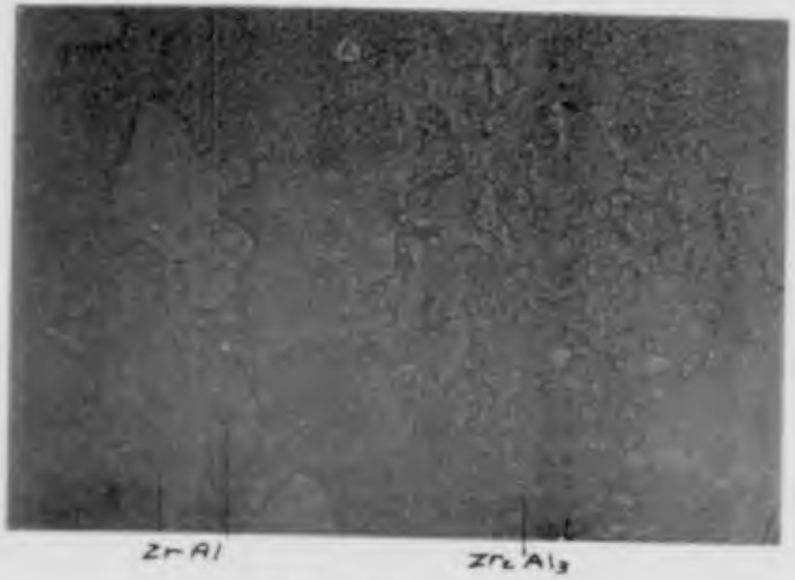

Fig. 41

50B(51.4Al-48.6Zr). 2000°F for 48 hrs. Water quenched. X-ray pattern indicates ZrAl and Zr_2Al_3 phases present. 2000x.

Fig. 42

50BH(51.4Al-48.6Zr). 2192°F for 6 hrs. Water quenched. X-ray pattern indicates ZrAl and Zr_2Al_3 phases present

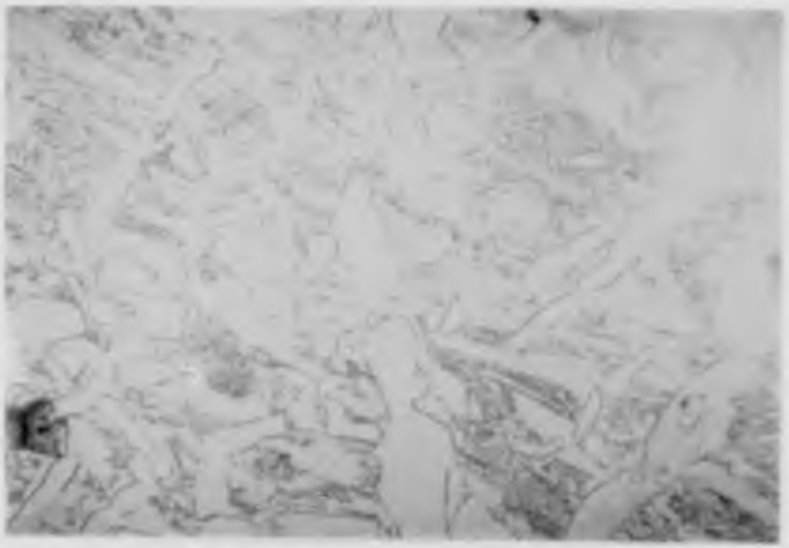

Fig. 43

50BA(51.4Al-48.6Zr). As-cast. X-ray pattern indicates Zr_2Al_3, Zr_3Al_2, and α-zirconium present. 750x.

Fig. 44

50B(51.4Al-48.6Zr). 2000°F for 48 hrs. Water quenched. X-ray pattern indicates ZrAl and Zr_2Al_3 present. Polarized light. 750x.

Fig. 45

50BA(51.4Al-48.6Zr). As-cast. X-ray pattern indicates Zr_2Al_3, Zr_3Al_2, and α-zirconium present. 750x.

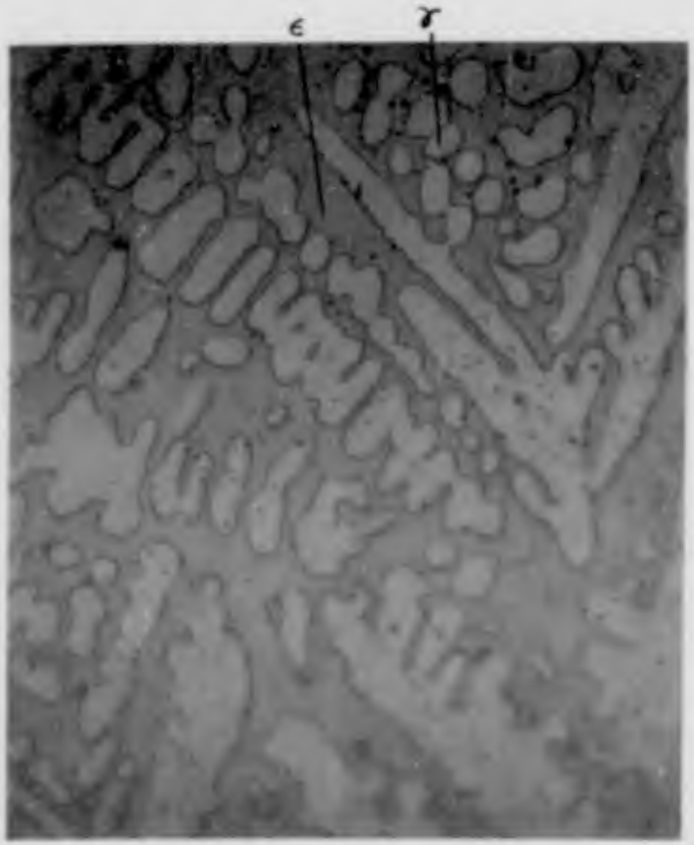

Fig. 46

20C(23.4Ti-57.8Al-18.8Zr). 2000°F for 39 hrs. Air cooled. X-ray pattern indicates γ, ϕ, and ϵ phases present. 720x.

Fig. 47

20CA(23.4Ti-57.8Al-18.8Zr). As-cast. No x-ray pattern. 1325x.

Fig. 48

25C(18.7Ti-56.6Al-24.7Zr). 2000°F for 48 hrs. Water quenched. X-ray pattern indicates γ and ϵ phases present. 750x.

Fig. 49

35C(9.6Ti-56.1Al-34.2Zr). 2000°F for 48 hrs. Water cooled. X-ray pattern indicates ϵ and Zr_2Al_3 phases present. 750x.

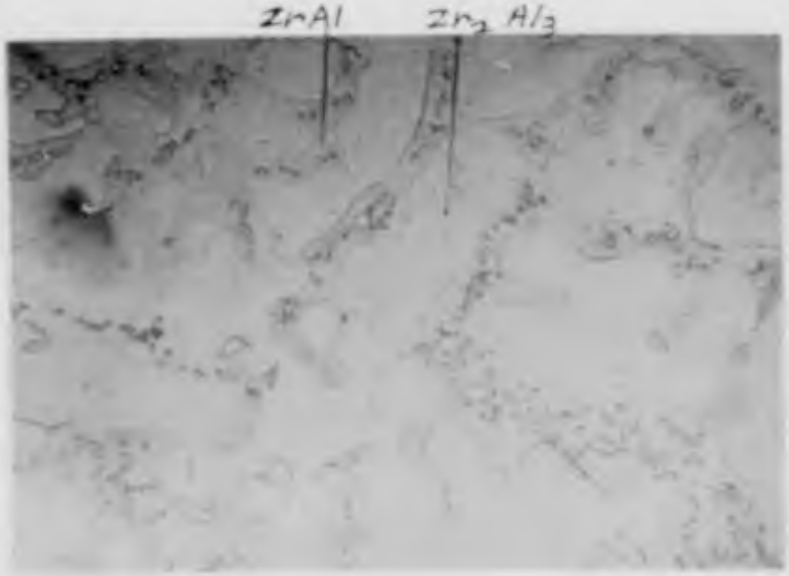

Fig. 50

45C(56.0Al-44.0Zr). 2000°F for 48 hrs. Water quenched. X-ray pattern indicates ZrAl and Zr_2Al_3 present. 750x.

Fig. 51

45CA(56.0Al-44.0Zr). As-cast. X-ray pattern indicates single phase Zr_2Al_3. 750x.

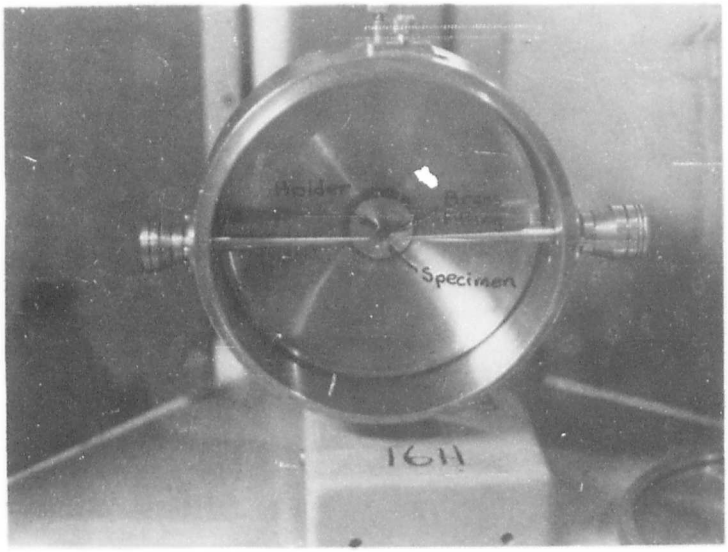

Fig. 52

Debye-Scherrer Camera

Appendix G

Debye-Scherrer Camera Techniques

The Camera

All of the alloys containing 25% or more zirconium were initially investigated by use of two 114.6 mm diameter Debye-Scherrer cameras. This type camera (Fig. 52), made by North American Philips as an accessory to their x-ray diffraction unit, employs the Straumanis film loading technique (Ref 1:154).

The initial step in the use of the cameras was to align them with the x-ray tube. The target of the x-ray tube is so arranged on the diffraction unit that four beams are emitted approximately in a plane perpendicular to the tube axis with right angles between beams. The goniometer was placed to utilize one beam while the cameras utilized two of the other beams. The two cameras were aligned with the x-ray tube in accordance with the manufacturer's instructions. Each camera was used only with a particular beam throughout the investigation in order to minimize necessary realignment. However, the alignment was checked periodically.

There are a number of suggested methods for mounting the powder specimens in the camera. After two methods proved unsuccessful (the method of rolling a mixture of the powder and collodion between two glass slides, and the method of extruding a mixture of the powder and collodion), it was decided to enclose

the powder in thin walled Pyrex capillary tubes. The thin walls were required so that the intensity of the reflected x-ray beam would not be significantly reduced by the glass. As ready-made tubing of this type was not available to the investigators, a handmade type of capillary was used. The procedure for making the capillaries will now be described.

Making the Thin Walled Capillaries.

The center of a piece of 16mm diameter standard wall Pyrex tubing about 10 inches long is held in a small gas flame. (This investigator used a hand torch, mounted on a work bench, employing natural gas and oxygen.) Satisfactory results were obtained with a flame height of about 4 inches with the intense part of the flame being about three fourths of an inch long. Both ends of the tubing are rotated at equal rates so that the center portion is evenly heated. A strong even pull on the ends of the tube, before it becomes too plastic, will cause the tube to neck slowly. When the diameter is about three fourths to one half of the original tube diameter, the pull on the ends of the tube is eased; and the rotation is continued until the neck becomes fairly plastic. (Great care must be exercised at this point to ensure even rotation of the tube ends. Uneven rotation of the ends causes twist which ruins the tube.) A very rapid pull on both ends

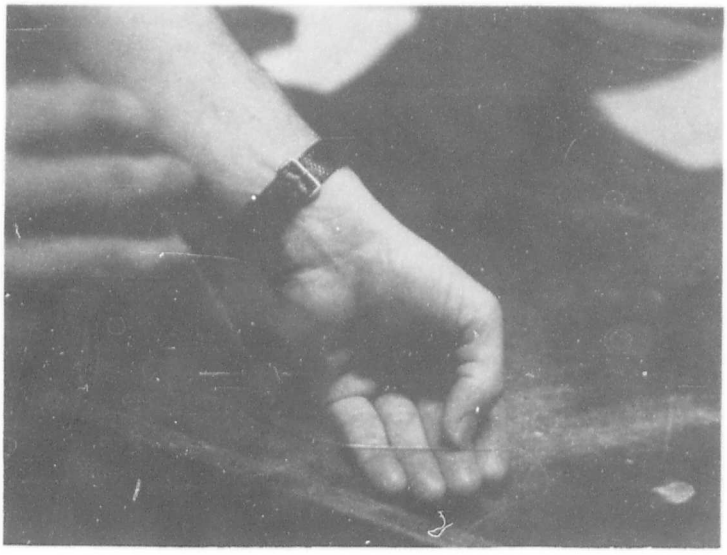

Fig. 53

Breaking Glass Tubing

of the tube will now draw the neck down to less than 0.5 mm in diameter and cause the tubing to break. Each of the halves may be used for a single specimen. A straight portion of the capillary, about one half inch long, is found and all excess glass on the flame end of the tube is broken off as shown in Fig 53. It is important that the fingers act as a cushion for the capillary to protect the tube from being shattered. (A knife edge may be used in place of a fingernail.) Insertion of the end of the capillary into a flame seals the end of the tube.

Mounting the Powder Specimen

A piece of copper wire, approximately the same diameter as the hole in the brass fitting of the camera, is placed in a vertical position in a vise so that about one eighth inch of the wire extends above the jaws. The brass fitting is then placed on this wire, and a small amount of beeswax is put on the top of the fitting.

The capillary is now filled with powder. (The large end of the tubing was not broken off previously so that it could act as a funnel for the capillary.) Tapping the larger end of the tube with the finger will settle the powder into the capillary. After it is filled, about one half inch of the capillary is broken off, as previously described. The specimen must be handled by fingers only. The capillaries are so weak that tweezers will collapse the tube. The powder may be sealed in the capillary by dipping it in the beeswax which is melted by use of a soldering iron. The tube

can now be inserted vertically into the fitting as the wax is being melted. (The reason that the copper wire was used was that it prevents the beeswax from running through the hole in the fitting.) The fitting is now removed from the wire.

The fitting containing the powder specimen is then placed in the holder in the center of the camera. By gently melting the wax around the specimen with the soldering iron while the fitting is in the camera, the specimen can be moved about until it is parallel to the axis of the camera. By following the manufacturer's directions, the axis of the tube can be made coincident with the camera axis. The camera is now ready to be loaded with film.

Taking the Exposures

After inserting the film, the cameras were placed on the diffraction unit. Twelve hour exposures were taken of each specimen at a power setting of 20 kv. and 15 ma. Higher settings were originally tried but the zirconium fluorescence fogged the film. During the exposures the specimen was rotated inside the camera by means of a rubber belt connection between the specimen holder shaft and an electric motor.

The film used was Kodak, Medical, No-screen, X-ray film. All patterns were developed with Kodak Liquid X-ray Developer and fixed with Kodak Liquid X-ray Fixer using the manufacturer's suggested developing and fixing times.

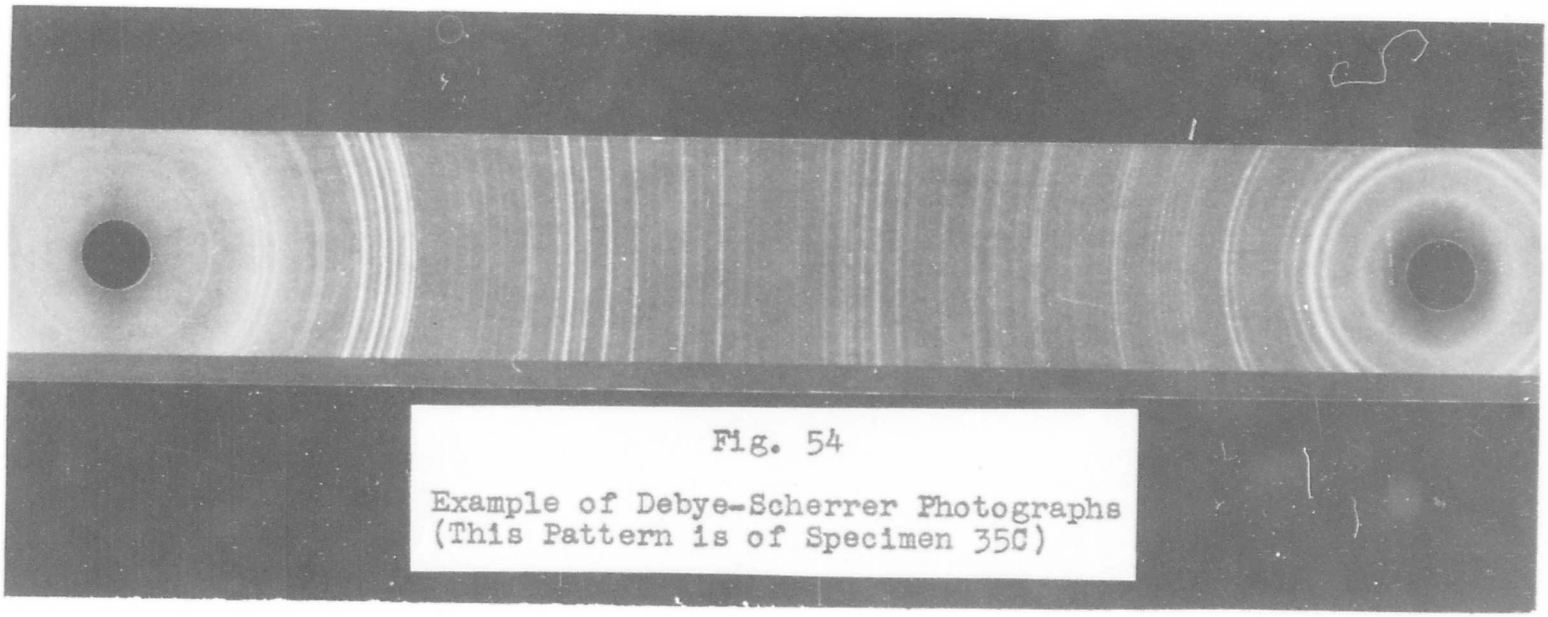

Fig. 54

Example of Debye-Scherrer Photographs
(This Pattern is of Specimen 35C)

After the film dried, the North American-Philips film reader was used to measure the position of all lines on each pattern. A correction factor, which averaged 1.003, was applied to correct for the shrinkage of the film in the developing process. The observed lines and intensities are listed in Appendix H.

Results of Camera Data

As can be noted from the data of Appendix H, many more lines were obtained from the camera patterns than from the diffractometer patterns. This was due to the long exposure times used for the photographs, and to the decreasing of the background level brought about by low x-ray tube power.

Since not only the angle and intensity of a reflection line are important but also the shape of the peak, it was difficult to trace lines between the different camera patterns as was done in Chapter VI of this report. This difficulty was compounded by the complexity of the film patterns. Attempts to correlate the camera film and diffractometer patterns proved to be difficult because of a shift in 2θ values of peaks. The shift in some cases was as much as 0.3 degrees but was not constant for different peaks of a single specimen or for the same peaks of different specimens. Also the relative intensities of lines did not match the relative intensities of peaks as can be seen by comparing for specimen 50B tabulated peak intensities in Table XXXVIII to observed values in Fig. 10(c). Because of these difficulties diffractometer patterns were taken of all specimens. These patterns yielded the information already

referred to in the body of the report.

If time had permitted the data obtained from these film patterns might have permitted the determination of the ϵ and β crystal structures.

Conclusions

The investigators reached some conclusions regarding the use of the x-ray equipment which may prove useful to later investigators.

1) For precise measurement of single phase lattice parameters, the camera techniques are probably more accurate than those of the diffractometer. More x-ray reflections from planes are recorded on film than on the diffractometer patterns and these reflections can be more accurately measured particularly at high 2θ angles. The alignment of the camera is simple, but the techniques for mounting the specimen, developing film, etc. are time consuming and sometimes tedious.

2) For phase determination study the diffractometer is recommended over the camera because diffractometer patterns for different specimens are easier to compare than are film patterns, relative intensities are easier to determine from diffractometer patterns and such useful information as peak size and shape can only be determined from diffractometer patterns.

Appendix H

Tabulated 2θ Angles and Intensities of Lines Recorded from Debye-Scherrer Photographs for Twelve Zirconium-Rich Alloys

The following tables list the diffraction lines observed on Debye-Scherrer photographs of selected Ti-Al-Zr alloys containing 25% or more zirconium. (For chemical analyses of these specimens, see Appendix A.) Table II indicates the initial homogenizing treatment given each of the specimens. The stress-relief treatment may be found in Table III.

Many lines which could not be accurately read on the film reader were not listed in this appendix. The omitted lines were of weak intensities (VVVW or weaker).

All of the patterns were obtained by use of 114.6mm diameter Debye-Scherrer cameras. Twelve hour exposures were required for nickel filtered copper radiation at a power setting of 20kv. and 15ma.

NOTE: The intensity symbols have the following meanings: VS, very strong; M, medium; W, weak; VW, very weak. Additional V's indicate decreasing intensities.

Table	Specimen No.	Composition		Page
XXXII	35A	19.5Ti-46.1Al-34.4Zr		108
	45A	9.0Ti-46.6Al-44.4Zr		
XXXIII	50A	4.0Ti-46.4Al-49.6Zr		109
	55A	46.2Al-53.8Zr		
XXXIV	55AA	46.2Al-53.8Zr	As-cast	111
XXXV	25B	26.3Ti-50.9Al-22.1Zr		112
	30B	19.6Ti-51.3Al-29.1Zr		
XXXVI	35B	13.8Ti-51.6Al-34.6Zr		114
	40B	9.3Ti-51.0Al-39.7Zr		
XXXVII	50B	51.4Al-48.6Zr		115
XXXVIII	50BH	51.4Al-48.6Zr	Special	116
	50BA	51.4Al-48.6ZR	As-cast	
XXXIX	25C	18.7Ti-56.6Al-24.7Zr		117
XL	35C	9.6Ti-56.1Al-34.2Zr		118
XLI	45C	56.9Al-44.0Zr		119
	45CA	56.9Al-44.0Zr	As-cast	

TABLE XXXII

2θ Angles and Intensities of Lines for Specimens 35A and 45A

Specimen 35A			Specimen 45A		
Line	2θ	Intensity	Line	2θ	Intensity
1	12.89	VVW	1	24.79	VVW
2	19.49	VW	2	25.62	VVW
3	20.57	W	3	26.52	VW
4	21.95	VW	4	27.60	VW
5	27.75	VW	5	32.72	VVW
6	28.28	VW	6	33.53	S
7	33.76	MS	7	34.11	W
8	34.29	VW	8	35.09	W
9	36.70	S	9	36.67	M
10	38.15	M	10	37.40	M
11	39.11	VW	11	37.87	VS
12	39.74	VS	12	38.58	M
13	40.54	M	13	39.66	M
14	41.49	VW	14	40.93	VVW
15	50.59	VW	15	41.98	VVW
16	56.46	VW	16	43.84	VVW
17	56.97	VVW	17	46.10	VVW
18	60.18	W	18	47.96	VVW
19	62.09	MS	19	50.42	VVW
20	63.50	VW	20	52.43	VW
21	64.20	M	21	54.39	VW
22	67.26	M	22	56.55	VW
23	70.68	M	23	59.71	VW
24	77.46	M	24	60.77	VW
25	79.77	W	25	61.67	W
26	82.18	M	26	62.98	M
27	84.65	VW	27	63.53	VW
28	85.25	VW	28	65.29	VVW
29	118.76	VW	29	68.00	M
30	119.51	W	30	70.16	W
31	123.83	W	31	72.37	VW
32	134.38	W	32	76.39	VW
33	135.53	W	33	77.50	VW
34	136.14	W	34	79.20	VW
35	141.38	M	35	106.30	VW
36	145.23	W	36	107.36	VW
37	146.70	M	37	126.41	VW
38	159.75	W			

TABLE XXXIII

2θ Angles and Intensities of Lines for Specimens 50A and 55A

Specimen 50A			Specimen 55A		
Line	2θ	Intensity	Line	2θ	Intensity
1	12.50	VVW	1	16.36	VW
2	19.68	VVW	2	19.52	VVVW
3	22.72	VVVW	3	21.88	VW
4	25.50	VW	4	22.58	VVW
5	26.80	M	5	25.28	VW
6	27.36	W	6	26.56	S
7	32.04	W	7	26.98	VW
8	33.10	W	8	27.82	VVW
9	33.82	M	9	31.78	W
10	34.78	M	10	32.98	M
11	35.16	M	11	33.60	M
12	36.74	W	12	34.20	M
13	37.56	VS	13	35.04	VS
14	38.48	W	14	36.54	M
15	39.28	MS	15	37.32	VS
16	39.84	M	16	38.26	VVVW
17	42.44	M	17	38.72	M
18	47.72	VW	18	39.28	W
19	49.76	VW	19	39.68	VVW
20	52.18	VW	20	42.36	MS
21	54.18	W	21	47.34	VVVW
22	55.04	W	22	49.84	VVVW
23	56.04	W	23	50.34	VVVW
24	57.30	M	24	54.76	M
25	60.46	W	25	55.50	VW
26	60.96	W	26	57.12	M
27	62.50	W	27	59.42	VVW
28	66.56	VW	28	60.17	M
29	71.88	W	29	61.86	M
30	75.74	W	30	65.38	VVVW
31	78.56	W	31	66.24	VW
32	80.00	VW	32	69.38	M
33	81.22	VVW	33	70.40	VW
34	81.76	VVW	34	71.54	M
35	132.86	VW	35	72.74	VVW

TABLE XXXIII Continued

Specimen 50A			Specimen 55A		
Line	2θ	Intensity	Line	2θ	Intensity
36	133.62	W	36	75.22	VW
37	137.74	VW	37	76.16	VVW
38	138.48	VVVW	38	77.76	VW
			39	79.96	VVVW
			40	80.02	VVVW
			41	81.12	VVW
			42	81.86	VW
			43	122.86	VVVW
			44	130.32	VVVW
			45	137.70	VW
			46	154.38	VW

TABLE XXXIV

2θ Angles and Intensities of Lines for Specimen 55AA

Specimen 55AA

Line	2θ	Intensity	Line	2θ	Intensity
1	17.53	VVVW	23	71.41	VVW
2	22.08	VVVW	24	72.86	VW
3	24.68	VVVW	25	75.21	VW
4	26.48	M	26	81.81	VVW
5	26.73	VVVW	27	85.31	VVW
6	33.09	VW	28	86.71	VVW
7	33.64	VVW	29	87.86	VVVW
8	34.24	S	30	88.56	VVW
9	35.14	VVW	31	90.17	VVW
10	36.59	VS	32	91.32	VW
11	37.29	M	33	92.52	VVVW
12	38.89	M	34	94.07	VW
13	39.39	M	35	95.17	W
14	42.44	M	36	97.27	W
15	54.70	VW	37	99.52	VW
16	55.55	M	38	103.57	VW
17	57.20	M	39	112.32	VVVW
18	60.05	W	40	122.58	VVW
19	61.90	VVW	41	136.70	VVW
20	66.20	VVW	42	137.44	M
21	69.40	VVW	43	154.00	M
22	70.36	VVW	44	155.25	W
			45	156.85	W

TABLE XXV

2θ Angles and Intensities of Lines for Specimens 25B and 30B

Specimen 25B			Specimen 30B		
Line	2θ	Intensity	Line	2θ	Intensity
1	19.42	VVW	1	13.00	VW
2	20.58	VW	2	19.47	VW
3	22.00	VW	3	20.63	VW
4	28.18	VW	4	21.98	VW
5	33.70	S	5	26.00	VVVW
6	34.60	VVVW	6	28.00	W
7	36.66	S	7	33.37	VVW
8	38.38	M	8	33.87	S
9	39.12	VS	9	34.47	W
10	39.72	M	10	35.78	VVW
11	40.42	VVVW	11	36.73	S
12	40.52	W	12	38.39	VS
13	44.48	VVW	13	39.19	VVW
14	50.46	W	14	39.84	S
15	56.52	VW	15	41.69	M
16	60.08	M	16	42.78	VVVW
17	62.04	M	17	48.67	VW
18	64.14	M	18	50.73	VVW
19	67.30	M	19	53.18	VVW
20	70.32	"	20	56.55	VVW
21	77.54	M	21	57.55	VVW
22	79.68	VVVW	22	60.36	VW
23	82.10	W	23	60.96	VVW
24	147.64	VVW	24	61.61	VVVW
25	148.74	VVVW	25	62.16	M
26	158.28	W	26	62.67	VW
27	159.82	VW	27	64.27	W

TABLE XXXV Continued

Specimen 308

Line	2θ	Intensity
28	67.43	W
29	70.89	VW
30	73.45	VVW
31	77.62	M
32	79.67	VW
33	80.63	VW
34	82.53	W
35	96.73	VW
36	99.94	VW
37	101.59	VW
38	103.60	W
39	106.51	VW
40	112.88	VVW
41	124.62	VVW
42	136.21	W
43	141.38	VW
44	145.29	VVW
45	150.15	M
46	161.59	S

TABLE XXXVI

2θ Angles and Intensities of Lines for Specimens 35B and 40B

Specimen 35B			Specimen 40B		
Line	2θ	Intensity	Line	2θ	Intensity
1	12.90	W	1	23.01	VVW
2	19.28	VVW	2	25.84	VVW
3	20.53	W	3	27.06	VW
4	21.78	VVW	4	27.76	VW
5	25.75	W	5	32.14	VW
6	27.75	M	6	33.75	MS
7	28.26	VVW	7	34.27	M
8	33.02	VVW	8	35.26	W
9	33.57	M	9	36.86	S
10	34.23	M	10	37.71	W
11	35.48	W	11	38.11	S
12	36.58	S	12	39.97	S
13	38.19	VS	13	48.17	VW
14	38.99	VVW	14	50.03	VW
15	39.54	S	15	50.88	VW
16	40.25	MS	16	52.73	VW
17	41.45	VVW	17	54.54	VW
18	46.02	VVW	18	55.39	VW
19	48.42	VW	19	56.69	W
20	50.38	VVW	20	57.49	W
21	52.79	VW	21	60.09	W
22	55.55	VVW	22	61.00	M
23	56.30	W	23	62.00	VW
24	57.10	W	24	63.30	W
25	58.01	VVW	25	64.20	VVW
26	58.77	VVW	26	67.40	M
27	60.62	VW	27	70.46	MS
28	61.22	VW	28	72.46	VW
29	61.87	M	29	74.36	VW
30	62.17	M	30	76.62	VW
31	63.78	M	31	78.11	VVW
32	67.84	M	32	79.47	VW
33	135.82	VW	33	80.12	VW
34	143.65	VW	34	81.37	VW
35	147.46	VW	35	82.12	M
36	157.90	VW	36	133.10	VW
37	159.55	M	37	133.80	VW
			38	135.15	VW
			39	136.09	VW
			40	138.00	VW

TABLE XXXVII

2θ Angles and Intensities of Lines for Specimen 50B

Specimen 50B

Line	2θ	Intensity	Line	2θ	Intensity
1	16.46	VVVW	26	57.22	VVW
2	19.62	VVW	27	57.92	MS
3	21.84	VVVW	28	59.38	VVVW
4	22.66	VVW	29	60.08	VVW
5	25.30	VVW	30	61.02	W
6	26.74	S	31	61.94	VVW
7	31.78	W	32	66.32	VW
8	33.00	M	33	67.50	VW
9	33.62	W	34	69.40	VW
10	34.28	W	35	70.42	VVW
11	34.92	M	36	71.36	VW
12	36.58	W	37	71.92	VVVW
13	37.34	VS	38	72.88	VVVW
14	37.84	VVVW	39	74.02	VVVW
15	38.30	VVVW	40	75.18	VVVW
16	38.70	W	41	76.48	VVVW
17	39.30	VVVW	42	79.94	VVW
18	39.76	W	43	81.03	VVW
19	42.42	W	44	81.96	VVW
20	49.78	VVVW	45	132.94	VVVW
21	50.44	VVW	46	133.58	VVW
22	54.10	VVVW	47	134.30	VVVW
23	54.66	VVVW	48	137.70	W
24	55.16	VW	49	138.50	VVVW
25	55.56	VVVW	50	149.60	VVW
			51	154.36	VVVW

TABLE XXXVIII

2θ Angles and Intensities of Lines for Specimens 50BH and 50BA

Specimen 50BH			Specimen 50BA		
Line	2θ	Intensity	Line	2θ	Intensity
1	16.61	VVVW	1	19.77	VVW
2	19.71	VVVW	2	22.81	VVW
3	20.56	VVVW	3	24.74	VVW
4	22.22	VVVW	4	26.45	VW
5	22.77	VVVW	5	27.00	VW
6	26.82	MS	6	32.07	VW
7	32.08	VVW	7	32.75	VVVW
8	33.18	M	8	33.23	W
9	34.13	VW	9	35.03	W
10	35.19	VS	10	36.26	VVW
11	36.79	S	11	37.22	VS
12	37.59	S	12	37.57	VS
13	38.04	VVW	13	38.09	M
14	38.94	VVVW	14	39.93	S
15	39.06	M	15	49.97	VVW
16	40.09	W	16	53.93	VW
17	41.05	VVW	17	54.39	VVW
18	42.50	M	18	55.34	VVVW
19	54.84	W	19	58.15	W
20	57.27	S	20	61.16	VVW
21	59.37	VVVW	21	67.08	VW
22	60.22	VVVW	22	67.64	VW
23	60.88	VVVW	23	70.40	VW
24	62.08	VVW	24	72.20	VW
25	62.68	VVW	25	74.31	VW
26	64.93	VVVW	26	76.67	W
27	66.44	VVW	27	80.13	VW
28	67.69	W	28	81.29	VVW
29	69.34	VW	29	82.14	VVVW
30	70.44	VW	30	124.80	VVVW
31	71.64	VW	31	125.30	VVVW
32	72.95	W	32	126.31	VVVW
33	74.15	VVVW	33	126.96	VVVW
34	75.35	VVW	34	132.98	VVW
35	76.65	VVW	35	133.64	VVW
36	77.80	VW	36	137.80	VVW
37	137.70	VVW	37	138.55	VVVW
38	154.03	M			
39	155.23	W			
40	167.40	M			

TABLE XXXIX

2θ Angles and Intensities of Lines for Specimen 25C

Specimen 25C

Line	2θ	Intensity
1	19.54	VW
2	20.70	VW
3	22.02	VW
4	28.44	VW
5	31.49	VVW
6	33.95	S
7	36.78	S
8	38.53	MS
9	39.36	VW
10	39.86	VS
11	40.70	M
12	41.65	VVW
13	44.41	VW
14	44.86	W
15	50.77	VW
16	56.58	W
17	57.04	VVW
18	60.44	W
19	62.30	M
20	64.45	M
21	67.56	M
22	70.97	M
23	77.63	M
24	78.28	W
25	79.79	VW
26	82.59	M
27	124.63	VW
28	125.13	VW
29	141.27	W
30	142.12	W
31	149.99	M
32	151.14	W

TABLE XI

2θ Angles and Intensities of Lines for Specimen 35C

Specimen 35C

Line	2θ	Intensity	Line	2θ	Intensity
1	12.81	W	31	71.12	M
2	19.41	M	32	77.54	M
3	20.41	M	33	79.75	M
4	21.97	M	34	82.61	VVW
5	25.73	VVW	35	92.99	VVW
6	27.66	W	36	96.80	VW
7	28.26	W	37	99.36	VW
8	30.42	VVW	38	100.26	VW
9	32.88	VVW	39	101.91	W
10	33.88	S	40	103.87	W
11	34.18	VVW	41	106.59	W
12	35.33	VW	42	112.70	VW
13	36.61	VS	43	116.96	W
14	38.07	M	44	119.87	W
15	39.87	VS	45	125.04	VW
16	40.63	M	46	125.69	VW
17	41.33	VW	47	135.22	VW
18	46.09	VVW	48	136.07	W
19	48.20	VW	49	136.77	W
20	50.66	W	50	140.79	VW
21	52.66	VW	51	141.89	VW
22	53.92	VVW	52	142.81	VVW
23	56.37	M	53	145.45	VW
24	56.98	W	54	146.35	VVW
25	60.39	M	55	150.97	MS
26	61.14	VVW	56	152.07	W
27	62.29	MS	57	158.69	W
28	63.40	VVW	58	160.40	M
29	64.45	M	59	162.60	S
30	67.41	M	60	164.56	M

TABLE XLI

2θ Angles and Intensities of Lines for Specimens 45CA and 45C

Specimen 45CA			Specimen 45C		
Line	2θ	Intensity	Line	2θ	Intensity
1	19.61	M	1	19.66	VW
2	22.62	M	2	22.74	VW
3	24.43	VVW	3	26.74	MS
4	26.25	VW	4	31.96	W
5	26.83	M	5	33.14	M
6	31.85	M	6	35.02	M
7	33.02	MS	7	36.60	W
8	34.83	M	8	37.50	VS
9	36.06	VW	9	37.94	W
10	37.04	VW	10	39.32	VW
11	37.44	VS	11	39.82	M
12	37.94	M	12	42.44	M
13	39.79	S	13	43.50	VVW
14	43.45	VVW	14	46.36	VVW
15	46.36	VVW	15	49.70	VW
16	49.72	W	16	54.20	VW
17	50.77	VW	17	54.84	VW
18	54.23	W	18	55.30	VW
19	55.13	W	19	57.18	S
20	57.19	M	20	57.86	VVW
21	57.94	VVW	21	59.36	VW
22	59.35	VW	22	60.06	VVW
23	61.00	VW	23	60.96	VW
24	63.41	VVW	24	61.92	VW
25	64.06	VVW	25	67.38	VW
26	124.74	VVW	26	67.74	W
27	125.34	VVW	27	69.34	VW
28	126.35	VVW	28	70.44	W
29	132.87	VVW	29	76.46	W
30	133.62	VW	30	79.98	W
31	137.73	VW	31	80.98	W
32	138.48	VVW	32	81.98	W
			33	87.80	VVW
			34	97.48	M
			35	132.90	VW
			36	133.60	W
			37	134.24	VW
			38	135.15	VW
			39	137.80	W
			40	139.56	VW

NOTE: The intensity symbols have the following meanings: VS, very strong; M, medium; W, weak; VW, very weak. Additional V's indicate decreasing intensities.

Vita

Doral R. Sandlin, the son of Mr. and Mrs. J.R. Sandlin, was born in [redacted]. The Sandlin family moved to west Texas, and Doral started to school at Levelland, Texas. During the years that he was in high school the family lived in Lubbock, Texas where he finished high school and attended Texas Technological College for two years. In 1950 he entered the United States Naval Academy and was graduated in June 1954 with a Bachelor of Science degree in engineering. Assignments prior to the Institute of Technology included pilot training and duty as a fighter pilot with the 456th Fighter Interceptor Squadron at Castle Air Force Base.

Permanent address: [redacted]

Henry Albaum Klung, Jr., the son of Henry A. and Margaret E. Klung, was born in [redacted]. After graduation from George Washington High School in San Francisco, he studied mechanical engineering for a year at the University of California. In 1951 he entered the United States Military Academy and graduated in June of 1955 with a Bachelor of Science degree. After completing pilot training, he was sent to the United States

GAW/Mech 61-6

Naval Air Station, Dallas, Texas, as a pilot for the Air Force Reserve Navigation Training Program. He entered the Graduate Air Weapons Program in August 1959.

Permanent address: [redacted]

This thesis was typed by Mrs. Nellie M. Weaver.

UNCLASSIFIED